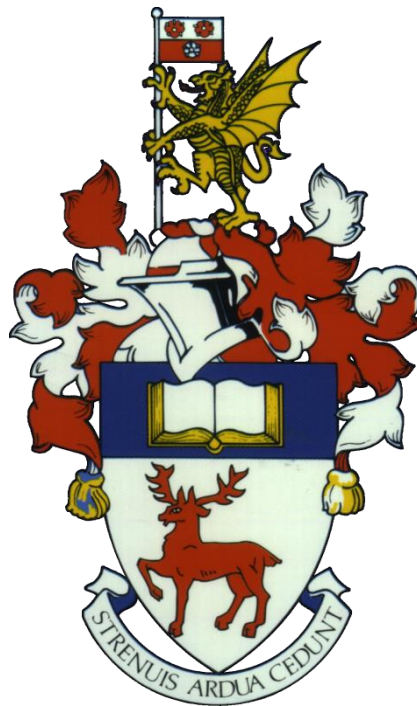# University of Southampton Research Repository

UNIVERSITY OF SOUTHAMPTON

Faculty of Medicine

Clinical and Experimental Sciences

Development of Acoustofluidic Devices for Bronchial Epithelial Cell Sheet Creation

By

Hayden George Tuckfield Foster BSc (Hons), MSc, MRes

Thesis for the degree of Master of Philosophy

August 2019

University of Southampton

<u>ABSTRACT</u>

FACULTY OF MEDICINE

Clinical and Experimental Sciences

Thesis for the degree of Master of Philosophy

Development of Acoustofluidic Devices

for the Creation of Epithelial Cell Sheets

Hayden George Tuckfield Foster

Epithelial cell (EC) sheet engineering is currently of interest for both regenerative medicine and drug research. Existing cell models for asthma research lack the complexity of heterogeneous tissue, while animal models provide complexity at the expense of molecular pathway accuracy via genetic drift. New models that are both complex and accurate are needed to improve efficacy testing and increase drug translation to the clinic.

Acoustofluidic (AF) levitation is the latest, non-invasive cell manipulation technique, that uses a piezoelectric transducer and resonator chamber to create an ultrasonic standing wave field (USWF) to trap cells within a pressure node. AF devices have previously been used to engineer 3D cartilage for transplant, create hepatocyte spheroids, and spatially organise cells within an extracellular matrix to create a vascular co-culture model. This project proposes novel microfluidic AF device designs for EC sheet engineering, utilising inexpensive glass capillaries as bioreactors, with potential for scalability by operating multiple devices in sequence. Levitated EC sheets could be used to engineer scaffold-free, autologous, multi-layered, retinal and myocardial constructs for transplant, or more replicative *in vitro* research models. Bronchial epithelial cells (BECs) were levitated to continue work by Dr Tait developing a direct-contact airway mucosa co-culture model using similar AF devices.

The final developed AF devices were able to levitate single BECs for one hour to create singular or multiple BEC sheets which satisfied morphological and functional requirements, such that they behave as cohesive sheet layers that move collectively via plithotaxis. The formation of BEC sheets within AF devices was visualised using immunofluorescence (IF); the surface area was then calculated using ImageJ software. Focal plane adjustments while levitating and IF adherens junction (AJ) staining post-seeding into collagen-coated wells confirmed that BEC sheets were sufficiently planar. Successful adhesion of BEC sheets to collagen before fixation was used as a blunt measure of viability. Transepithelial electrical resistance (TER) of long term BEC sheet cultures was measured using chopstick electrodes and voltohmmeter. TER readings after 11 – 13 days were indicative of tight junction and barrier formation.

This study presents the first successful application of an inexpensive, glass capillary-based AF device for EC sheet creation, with potential for higher EC sheet output and easier sheet handling and transfer via a microfluidic system. Further work is needed to confirm the morphology and functionality of successfully levitated EC sheets, as well as experimentation using additional cell types to demonstrate the versatility of AF devices.

Table of Contents

Table of Figures

Research Thesis: Declaration of Authorship

Print name   Hayden Foster

Title of thesis   Development of Acoustofluidic Devices for the Creation of
                                      Epithelial Cell Sheets

I declare that this thesis and the work presented in it are my own and has been generated by me as the result of my own original research.

I confirm that:

1. This work was done wholly or mainly while in candidature for a research degree at this University;

2. Where any part of this thesis has previously been submitted for a degree or any other qualification at this University or any other institution, this has been clearly stated;

3. Where I have consulted the published work of others, this is always clearly attributed;

4. Where I have quoted from the work of others, the source is always given. With the exception of such quotations, this thesis is entirely my own work;

5. I have acknowledged all main sources of help;

6. Where the thesis is based on work done by myself jointly with others, I have made clear exactly what was done by others and what I have contributed myself.

Signature   *Hayden Foster*   Date   22nd August 2019

Acknowledgements

Definitions and Abbreviations

16HBE   16-Human Bronchial Epithelial cell line 14-o

2D   Two-dimensional

3D   Three-dimensional

AC   Alternating Current

AF   Acoustofluidic

AJ   Adherens Junction

AMD   Age-related Macular Degeneration

APES   2-Aminopropylethoxysiline

BEC   Bronchial Epithelial Cell

BF channel   Bright Field channel

Ca^{2+} Calcium positive ion

CEA   Cultured Epithelial Autografts

CO_2 Carbon Dioxide

CVD   Cardiovascular Disease

DAPI   4', 6'-diamino-2-phenylindole

dH_2O Deionised water

DNA   Deoxyribose Nucleic Acid

EC   Epithelial Cell

E-cadherin   Epithelial cadherin

ECM   Extracellular Matrix

FAM   Focal Adhesion Molecule

FBS   Foetal Bovine Serum

FLUO beads   GFP-labelled microbeads

GFP   Green Fluorescent Protein

GM   Growth Media

HBSS   Hanks Balanced Salt Solution

ID   Internal dimensions

IF	Immunofluorescence
JAM	Junctional Adhesion Molecule
LT device	Large Transducer device
MALDI-MS	Matrix-Assisted Laser Desorption Ionisation Mass Spectrometry
MCL	Magnetite Cationic Liposomes
Mg^{2+}	Magnesium positive ion
NaN_3	Sodium Azide
NCD	Non-communicable Disease
NIPAM	Poly (N-Isopropyl acrylamide)
NKT	Natural Killer T Cell
OD	Outer dimensions
Pen-Strep	Penicillin Streptomycin
PZT volume	Piezoelectric Transducer covered volume
PZT	Piezoelectric Transducer
RD device	Reduced Dead volume device
RPE	Retinal Pigment Epithelium
RT	Room Temperature
ST device	Short Transduce device
TER	Transepithelial Electrical Resistance
TJ	Tight Junction
TW	Transwell
US	Ultrasound
USWF	Ultrasound Standing Wave Field

Chapter 1: Introduction

1.1   Epithelial cell tissues

1.1.1   Overview

Epithelial cells (ECs) pack tightly together as cohesive sheet layers, protect the external surface and internal cavities of the body. The apical surface of EC sheets face the air or fluid external environment, and the basolateral surface adheres to the internal basement membrane. Shared characteristics for all epithelial tissues include polarity, a plethora of contact adhesions, underlying basement membrane/connective tissue, and a robust regenerative capacity[1].

Epithelial tissues are specialised to provide additional functions ranging from gas exchange to regulating immune responses. Epithelial subtypes are classified by both their arrangement: simple, stratified or pseudostratified; and their morphology: squamous, cuboidal or columnar[1]. Simple epithelium is only one cell thick and creates a sheet monolayer. The stratified epithelium is multiple cell layers on top of each other, which protect against abrasion. Pseudostratified epithelial tissue is a mixture of concealed basal cells and taller columnar cells that comprise the apical surface[2].

Shared traits and specialisations enable ECs to function as a physical, chemical, and immunological barrier in their respective tissues[3]. During rapid growth and wound repair, the interplay of forces between the cytoskeleton, cell-cell contact, and basement membrane adhesions allow epithelial tissue to move collectively as a sheet layer via plithotaxis[4]. Recreating epithelial tissues in the lab which retain all of these adhesions, physiology and therefore functionality, is currently of interest for regenerative medicine and drug research.
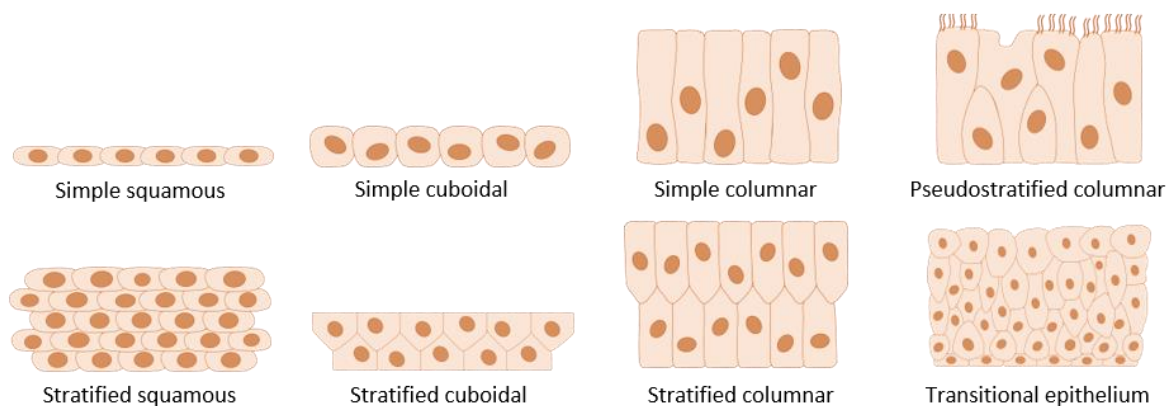
Figure 1.1.1.1 Image of epithelial cell arrangement and morphology.
Epithelial cells are classified by their arrangement: simple, stratified, or pseudostratified; and their morphology: squamous, cuboidal, and columnar, or a mix of all three in transitional epithelial tissue.

1

1.1.2 Cell cytoskeleton

The cell cytoskeleton is a complex network of filamentous polymers and regulatory proteins within the cytoplasm[5]. These polymer units assemble in a variety of ways to determine filament strength and elasticity, of which there are three main types: actin filaments, intermediate filaments, and microtubules[5]. All three are dynamic and can reassemble and disassemble in a matter of minutes or hours when needed[1]. The organisation of these filaments determines the morphology, strength, and internal framework of the cell.

Actin filaments are the smallest in diameter (7 nm) and least stiff. They are composed of repeating actin and myosin protein chains, which cross-link extensively to create large networks such as the cortex, which supports the cell membrane and maintain cell shape independent of the environment[6].

Intermediate filaments are slightly larger in diameter (10 nm) and are made from a heterogeneous family of proteins which twist together like a rope[1], and are consequently the most durable. One type of intermediate filament creates a network across the cell cytoplasm to provide mechanical strength, and another supports the nuclear membrane[1].

Microtubules are the largest in diameter (25 nm), most rigid, and consist of tubulin molecules organised into a cylindrical ultrastructure with a lumen[1]. Microtubules originate from an organelle called the centrosome and organise the interior of the cell. Motor proteins bind to and move along microtubules like highways while transporting cargo or organelles[1].
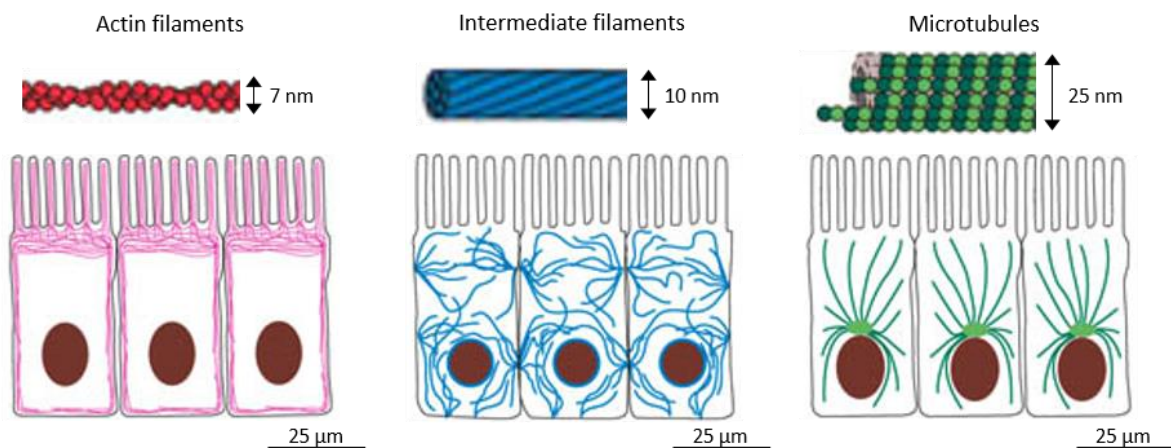
Figure 1.1.2.1 Diagram of the cell cytoskeleton filaments.
Actin filaments are 7 nm in diameter and composed of cross-linked actin/myosin protein chains; they support the cell membrane and initiate cell motility. Intermediate filaments are 10 nm in diameter and composed of multiple protein chains twisted together; they provide mechanical strength and support the cell nuclear membrane. Microtubules are 25 nm in diameter, composed tubulin molecules arranged into a cylindrical structure, and originate from a centrosome; they create a network which motor proteins can bind to, and help organise the cell interior.

1.1.3   Epithelial cell adhesions

To create a physical barrier, ECs form several junctional complexes. Adherens junctions (AJs) form first during growth and repair[7]; they join the actin cytoskeletons of two adjacent cells to allow cohesive sheet movement. Epithelial cadherin (E-cadherin) homophilically dimerises with an adjacent cell in the presence of Ca^{2+} ions which are required to stabilise five extracellular domains. The intracellular region of E-cadherin binds β-catenin which in turn binds α-catenin and associated F-actin filaments of the cytoskeleton[8].

Desmosomes are hyper-adhesive and much stronger than adherens junctions; they connect the intermediate cytoskeletons of adjoining ECs. The intercellular protein desmoplakin binds to intermediate filaments of the cytoskeleton[8] as well as two copies of the transmembrane proteins desmoglein and desmocollin, via plakophilin[9,10]. Extracellular regions of desmoglein and desmocollin bind homophilically to two copies from an adjacent cell.

ECs adhere to an underlying basement membrane composed of extracellular matrix (ECM) proteins via α-integrin and β-integrin heterodimers[11]. Most integrin heterodimer variants bind the actin cytoskeleton to the ECM via focal adhesion molecules (FAM)[12]. Hemi-desmosomes, which are much stronger, utilise a single integrin heterodimer variant to connect the intermediate cytoskeleton to the ECM via intracellular desmoplakin, similar to a desmosome[9].

Tight junctions (TJ) form last between ECs and are the largest, most apical complex; polarising the cell[13]. Each TJ complex contains three transmembrane glycoproteins that homophilically dimerise: occludin[14], which binds the actin cytoskeleton[15,16]; junctional adhesion molecule (JAM)[17]; and a claudin variant, that determines whether the TJ creates a seal or selective ionic/cationic pore[18]. Collectively this creates a selectively permeable macromolecular, and ionic barrier to the lumen[13]; which is considered a physical barrier in cell biology.

3
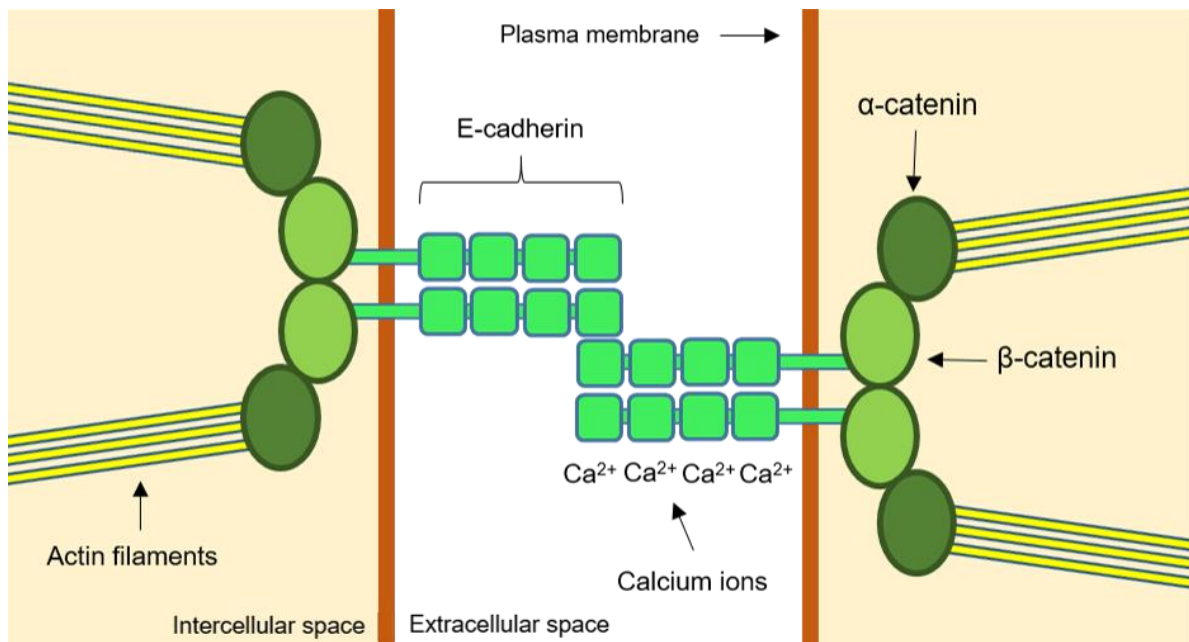
Figure 1.1.3.1 Schematic of the adherens junction complex between adjacent cells.
E-cadherin homophilically dimerises with an adjacent cell in the presence of Ca2+ ions which are required to stabilise five extracellular domains. The intracellular region of E-cadherin binds β-catenin which in turn binds α-catenin and associated F-actin filaments of the cytoskeleton. EC denotes shows E-cadherin extracellular regions. The intercellular space (pink) and extracellular space (white) is separated by each cell membrane (orange).
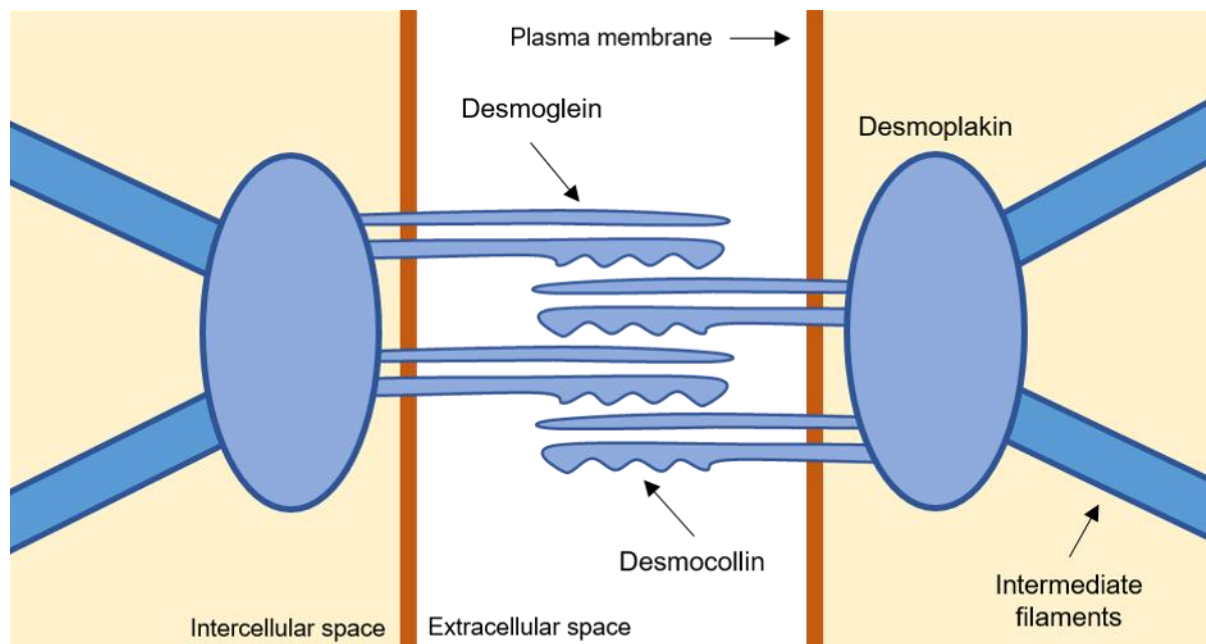
Figure 1.1.3.2 Schematic of the desmosome junction complex between adjacent cells.
Extracellular regions of desmoglein and desmocollin bind homophilically to two copies from an adjacent cell. The intercellular protein desmoplakin binds to intermediate filaments of the cytoskeleton as well as two copies of the transmembrane proteins desmoglein and desmocollin, via plakophilin. The intercellular space (pink) and extracellular space (white) is separated by each cell membrane (orange).

4
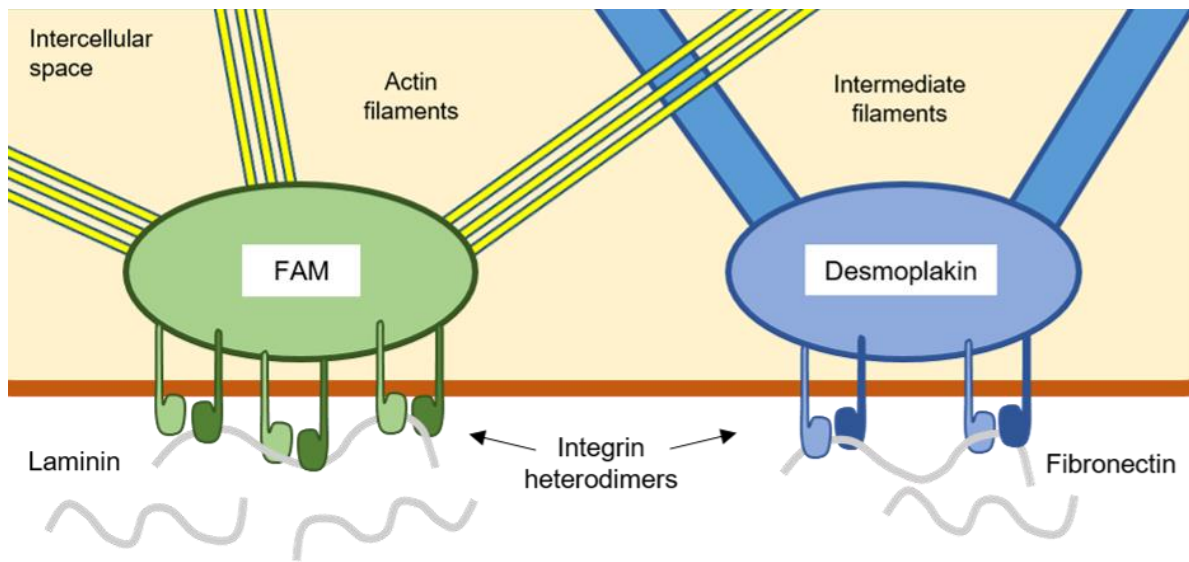
Figure 1.1.3.3 Schematic showing cell adhesion to a basement membrane via integrin junctions.
Transmembrane integrin protein heterodimers bind ECM linker proteins and intracellular complexes to tether cytoskeleton filaments to the basement membrane. To tether the actin cytoskeleton, multiple integrin heterodimers bind the laminin family of proteins and FAMs. Hemidesmosomes tether the intermediate cytoskeleton and are much stronger than FAMs: a single integrin heterodimer binds fibronectin and a desmoplakin plaque. The intercellular space (pink) and extracellular matrix (white) is separated by the plasma membrane (orange).
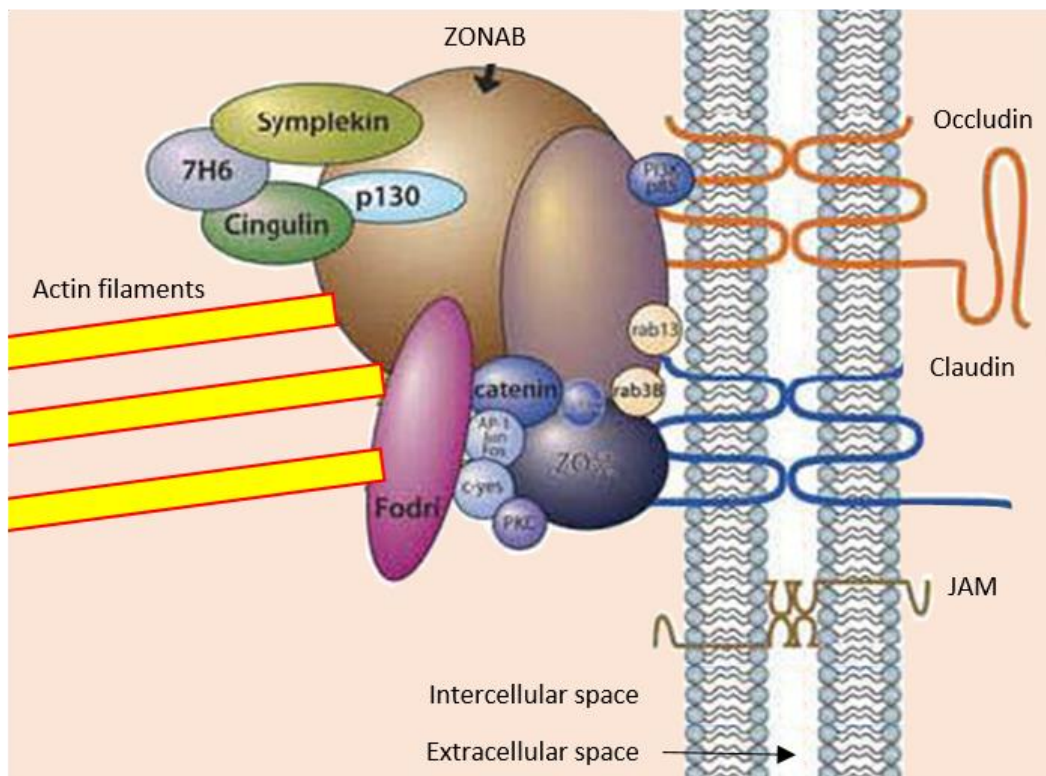
Figure 1.1.3.4 Schematic of the tight junction complex between adjacent cells.
The tight junction is made up of three transmembrane proteins: occludin (orange), claudin (blue) and JAM (brown). These interact with multiple cytosolic proteins and eventually, the actin cytoskeleton. The intercellular space (pink) and extracellular space (white) is separated by each cell membrane (blue).

1.1.4   Basement membrane

The epithelial basement membrane is a complex network of macromolecules separated into three layers: the lamina lucida, densa, and reticularis (connective tissue) in the airways. Each layer has a unique pattern of proteoglycans, structural and specialised proteins, and is collectively known as ECM. Binding and cross-linking of ECM fibres with each other and to ECs create a supportive migratory vehicle for cellular components[19].

The lamina densa and reticularis predominantly consists of collagen, of which there are four types (type I - IV). Within the basement membrane, type-IV is the most abundant. The collagen proteins are primarily synthesised by mesenchymal fibroblasts and by ECs to a lesser extent.

Collagen proteins are chain monomers, made up of 100s of repeating amino acid units, hydroxylated lysine residues and sugar monomers. These are attached along the chain allowing collagen proteins to twist on themselves to form a left-handed triple helical structure[20]. Collagen triple helices assemble and cross-link together via oxidation of hydroxyl-lysine residues to create fibril. Following cleavage of N- and C- terminal domains, fibrils cross-link to assemble collagen fibres.

A second repeat monomer fibre is elastin that is highly flexible and is responsible for the elasticity of ECM[21]. Elastin is tethered to cell membranes by cross-linked tropoelastin constructs and closely aligned with collagen elastin fibres via fibrillins and other glycoproteins[21].

Fibronectin is also a repeat monomer fibre protein, made of three repeating domains (FN I-III). Each domain is a pair of anti-parallel ß-sheets and a fibronectin subunit. The fibronectin subunit consists of twelve FN-I, two FN-II, and fifteen-seventeen FN-III domains. Two combined subunits create a functional fibronectin module, which can bind integrins, collagen and EC plasma membranes, and function as a cellular anchor[20].

Laminins are found in all basement membranes and bind to focal adhesion integrin heterodimers, collagen and numerous other receptors. These interactions are critical for cell movement, shape and survival. Laminins have a heterotrimeric structure and consist of a α-chain, ß-chain and a ɣ-chain: there are several variants for each which make a total of 15 different laminins[20].
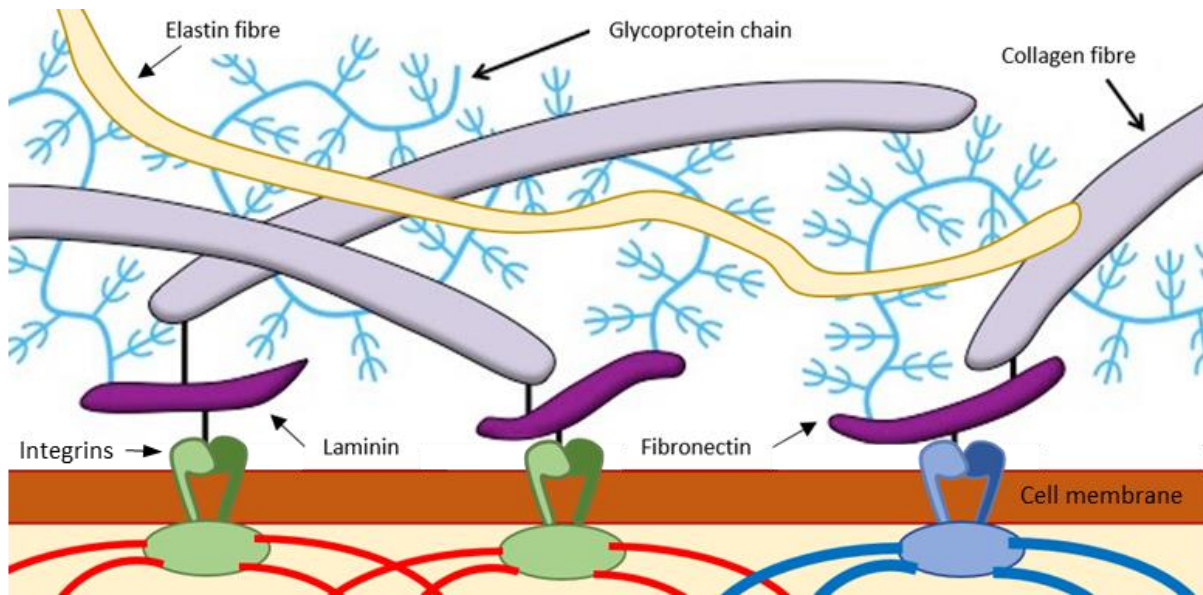
Figure 1.1.4.1 Diagram of extracellular matrix composition and linker proteins.
ECM consists primarily of collagen fibres which provide strength; intertwined with elastin fibres and glycoprotein chains which provide elasticity and biological activity: cross-linking of these fibres creates a cohesive matrix ultrastructure. ECM linker proteins such as laminin and fibronectin allow cells to adhere via transmembrane integrin heterodimers. The intercellular space (pink) and extracellular matrix (white) is separated by the plasma membrane (orange).

1.1.5 Collective movement via plithotaxis

Epithelial tissue requires collective cellular migration for growth, development, remodelling, and wound repair. Rather than moving individually, ECs tend to migrate collectively in sheets, ducts, strands or clusters[22]. Cell sheets exhibit a strong tendency to migrate in the direction of the stress ellipse, known as plithotaxis. The orientation of the stress ellipse is determined by the interplay of intracellular traction forces and intercellular stresses connected via the cytoskeleton. Intracellular traction forces include biochemical gradients, affinity to the basement membrane, and maintaining a polarised morphology. Extracellular stresses occur between all neighbouring cells across mutual cell-cell junctions as a consequence of individual traction forces[23]. EC sheet growth and migration are continuous until collective cell jamming is reached. As the density of a sheet increases due to proliferation and cells become increasingly crowded (appearing caged), groups of cells require larger amounts of co-operation from the monolayer to reaarange[24]. This is consequently more difficult, so the rate of migration and rearrangement becomes is decreased[25]. Ultimately, the cell sheet monolayer becomes static, and collective cell jamming has been reached.

Single cells without cell-cell adhesions, biochemical gradients, or other extracellular stresses display seemingly random motility: which was studied and quantitated to provide the random walk model[26]. Without sufficient cell density, epithelial cells exhibit 3D migration instead of planar when seeded onto collagen matrices[26].

1.1.6 The specialisation of epithelial tissue

ECs specialise in a multitude of ways to provide additional functions ranging from gas exchange to regulating immune responses. Simple squamous epithelia are laterally flat monolayers. They are found within diffusion and filtration tissues such as the alveoli, where the narrow thickness and large surface area maximises gas exchange. Stratified squamous epithelia are found within the oesophagus, mouth and uterus[27].

Cuboidal epithelia are more resistant to mechanical damage than squamous and adapted for secretion and absorption. Simple and stratified cuboid epithelia are typically found within secretory portions of small glands[27], such as the salivary, kidney tubules, and bronchi of the lower airways: where they secrete surfactant to trap fine particles.

Retinal pigment epithelium (RPE) are simple cuboidal cells which support light-sensitive photoreceptor cells and are essential for sight[28]. The main function of RPE is to regenerate bleached opsins from the photoreceptors, along with growth factor secretion, water regulation, and to prevent photo-oxidation[28]. Uniquely, RPE operates without support from underlying mesenchymal cells.

Columnar epithelia are the tallest, most damage resistant subtype. They also specialise in secretion and absorption and protect high-risk internal cavities such as the conducting airways (nasal cavity, trachea, bronchi, and bronchioles) or digestive tract.

The conducting airways are lined with ciliated, pseudostratified columnar epithelial tissue, interspersed with both mucus-secreting goblet cells[2,29] and basal progenitor cells[30]. Bronchial epithelial cells (BECs) provide a physical, chemical and immunological barrier against pathogens and particulates of the inhaled environment[31], and are pivotal in airway regulation[32].

As mentioned earlier, TJ complexes between BECs create a physical barrier. To create a chemical barrier, goblet cells secrete mucus: a viscoelastic gel that traps pathogens and particulates, and also contains anti-oxidants and anti-microbial peptides[33]. Known as the mucociliary escalator: the uniform beating of epithelial cilia then directs secreted mucus towards the oesophagus for removal via coughing or swallowing[3].

Both ciliated epithelium and goblet cells can secrete a wide range of cytokines, chemokines and growth factors[34], which contribute to the immunological barrier. BECs express pattern recognition receptors[35] for the pathogen and particulate response. They can also recruit innate immune cells such as granulocytes, natural killer T cells (NKTs), and alveolar macrophages[35] by releasing chemoattractants. BECs can release mediators to activate an inflammatory response by activating dendritic cells, then subsequently regulate this response[36].
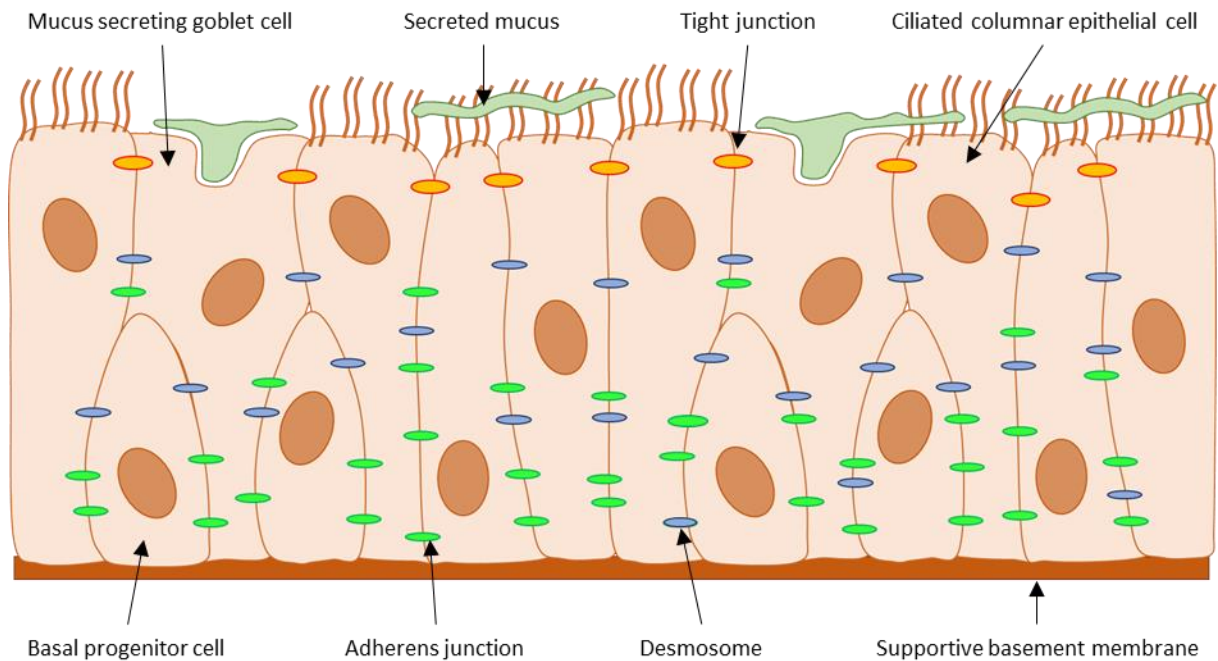
Figure 1.1.6.1 Specialisation of bronchial epithelial tissue
The bronchial and conducting airways are lined with ciliated columnar epithelium, interspersed with mucus producing goblet cells, and basal progenitor cells, to create a physical, chemical, and immunological barrier to the inhaled environment. TJs between columnar cells create a selectively permeable physical barrier. Secreted mucus traps and kills pathogens, and then directed by uniform beating of cilia towards the oesophagus for removal, creating a chemical barrier. Ciliated and goblet cells can also release multiple cytokines, chemokines, and growth factors to modulate innate and adaptive immune responses to create an immunological barrier. Basal progenitor cells accelerate wound repair and barrier recovery after injury or infection.
.

1.2 Evolution of cell-based therapies

The art of regenerative medicine is determining how to replace, repair, improve or regenerate various tissues and organs of the human body[37]. Historically, cell therapies were delivered to patients by injection, transfusion, or direct application of tissue grafts[38]. In the last two decades, a multitude of cell therapies and delivery techniques have emerged with no clear front-runner, which will be discussed later.

1.2.1 Injection and transfusion of cell therapies

The human body is filled with numerous planar epithelial membranes such as the skin, oesophagus, uterus, and bladder, which have proven impossible to treat with single cell suspensions[38]. When adherent cells are placed into a suspension, cell-cell interactions which may be critical to efficacy and modes of action are lost, potentially affecting viability and function[38]. Additionally, injection and transfusion are limited by a lack of control where cells go and non-homogeneous distribution within the affected area[39]. Delivering a graft or sheet of epithelial cells has been shown to negate these risks, and is the current aim of research[38].

1.2.2 Direct application of tissue grafts

Direct application of epithelial sheet layers has been of particular interest to western medicine since Bunger successfully grafted skin epidermis (outer squamous and basal layers of epithelium) from a patient's buttock to their nose in 1869[40], and Wolfe transplanted the first full-thickness skin graft in 1875[41]. In 1975, Reinwald and Green first demonstrated the isolation and serial culture of human epidermal keratinocytes *in vitro* with lethally irradiated mouse fibroblasts as a feeder layer[42]. Initial cell sheet technologies were developed, and cultured epithelial autographs (CEA) have been used for severe burn victims since 1981[43]. Transplanting skin epidermis, and other epithelial tissues have primarily been restricted by donor shortage, and high-rates of graft-rejection[44].

To overcome these obstacles, Professor Robert Langer, and Drs Joseph and Charles Vacanti proposed the concept of tissue engineering in 1988. They believed that organs and tissues could be engineered in the laboratory to meet the demand for transplantation, with increased acceptance by the host system[45-47].

1.3   The need for cell sheet engineering

1.3.1   Regenerative medicine

Increased understanding of specialised epithelial sheet structure and function has allowed more delicate tissues to be cultured and transplanted for disease treatment. Using acellular human dermis, cultured oral and urethral epithelial mucosa, have been transplanted to aid wound recovery after infection[48,49]. Additionally, the engineered corneal epithelium has successfully been used to treat limbal stem cell deficiency[50], in response to a worldwide shortage of donor corneas[44].

Age-related macular degeneration (AMD) is the leading cause of irreversible blindness in the developed world[51], and heightened clinical interest currently surrounds the engineering of RPE sheets for its treatment[52,53]. Also of interest, is the engineering myocardial epithelial cell sheets to treat cardiovascular disease (CVD)[54], responsible for over 17.7 million deaths globally each year[55]. Technologies able to construct multiple heterogeneous layers of myocardial tissue for transplant are still in their infancy[54].

1.3.2   Drug research

Epithelial sheet engineering is also needed to better research on new asthma and non-communicable disease (NCD) drug therapies. The current cost of translating a new drug candidate from the lab to the clinic ranges from 800 million US$ to 1.2 billion US$ and 8-12 years of development and testing[56].

Asthma currently affects 5.4 million people in the U.K, and the cost of treatment is £2.5 billion per annum[57]. The development of asthma therapies has stalled using existing airway mucosa models, despite massive pharmaceutical investment and over 30 years of research[58]. There is still no cure or preventative treatment for the disease, and current therapies can only manage symptoms of mild asthmatics, with little improvement since the discovery of dexamethasone in 1972[59].

For *in vitro* drug development, simple 2D cell mono-cultures or co-cultures (separated by a porous membrane) are the archetypes[60]. However, 2D cultures typically differ from their *in vivo* counterparts and have altered morphology, limited cell-cell or cell-ECM interactions, differentiation, and gene expression[61-64].

Animal models provide a 3D physiological environment, with complex molecular pathways for drug discovery. However, inconsistencies between gene ablation and chemogenic study results have led to opposing conclusions in the scientific community[65]. Unpredictable cytotoxicity/efficacy testing is also of concern[66]: divergent evolution of complex molecular

pathways in animals and humans mean that 50% of drugs which pass pre-clinical animal testing turn out to be toxic for humans, or drugs which fail pre-clinical tests would be non-toxic for humans[67]. Efficacy testing of therapeutics can also be impaired by these divergences, leading to significantly different clinical outcomes[68,69].

Fortunately, emerging technologies allow the creation of more complex 3D tissue and organ models with multiple epithelial, endothelial, or mesenchymal cell layers in direct-contact, or physiologically conditions more representative of *in vivo*[70,71]. Using novel healthy and aberrated 3D models to characterise the mechanisms of NCD development (such as airway mucosa responses to virus infection and asthma progression) could reveal potential new drug targets. Furthermore, developed 3D models would provide more accurate efficacy testing of new drug therapies, and potentially increase translation to the clinic.

1.4 Hydrogel and scaffold biomaterials for tissue engineering

The most commercialised approach to epithelial tissue engineering is the replication of ECM *in vitro,* using either a hydrogel or scaffold support to create 3D cell cultures for transplant or research[71]. Both technologies can be derived from natural sources or synthesised in the laboratory.

1.4.1 Natural hydrogel and scaffold technologies

Hydrogels primarily consist of a cross-linking protein or polymer units containing water and are therefore fluidic and permissive[72], while scaffolds are stiffer and provide more rigid support. Hydrogels contain, and scaffolds are treated with, growth factors and various proteins to influence cell growth and behaviour. Mesenchymal cells typically move freely within hydrogels or scaffolds, whereas epithelial cells have a lower affinity and remain supported on the surface.

Most 3D models comprise of tissues or isolated cells embedded within a hydrogel derived from natural ECM components[73]. The most widely used hydrogel products are reconstituted type I collagen gels such as Vitrogen™ and reconstituted basement membrane gels such as Matrigel™: which is 60% laminin, 30% type IV collagen, and contains unspecified growth factors[74].

Natural scaffolds were initially developed for tissue engineering and used as biodegradable vehicles for transplant. However, these scaffolds have recently been adapted for 3D cell culture studies. Available natural scaffolds include type I collagen, fibronectin, chitosan and, type-I collagen: fibronectin composite[74]. Both natural hydrogels and scaffolds have issues with batch variability and stability[74].

1.4.2 Synthetic hydrogel and scaffold technologies

Recent advances in materials science have led to the development of synthetic biomaterials with biophysical and biomechanical aspects of the ECM. Poly(ethylene glycol) polymer units, with added cross-linking agents to create a hydrophilic gel. Peptide substrates are added to the polymer chain to allow both the integrin-mediated binding of cells and enzymatic remodelling by them[73].

Synthetic scaffolds are more common than natural, and a variety of materials are available such as polystyrene, polyurethane, or poly(anhydrides). Many manufacturing methods are used to tailor the architecture, size, and distribution of scaffold pores. Conventional fabrication methods provide moderate control, such as gas foaming, thermal induced face separation, and electrospinning. Whereas, rapid prototyping methods using computer-aided design are more precise, such as 3D printing, selective laser sintering, and stereolithography[75].

1.4.3 Limitations of hydrogel and scaffold constructs

Suspension injections and "seed cells" combined with hydrogels or scaffolds or other tissue engineering methods have considerably advanced the field of regenerative medicine, such as CEAs for burn victims. However, there are many limitations to using the scaffold approach for tissue engineering or drug research.

Tissue constructs may not closely resemble denser cell tissues such as the heart or liver[54]. With scaffold degradation, a large amount of ECM is deposited and can even result in pathological fibrosis[44]. Despite the use of non-cytotoxic materials[76,77], the most substantial drawback is inflammation[78,79,] Additionally, without vascularisation, the centre of large scaffolds have limited access to nutrients or waste removal and can form a necrotic core[44].

Natural hydrogels and scaffold constructs primarily have issues with batch variability and stability[74].

Endemic problems with synthetic scaffold cultures include polymer cytotoxicity, rigidity, and inertness[80]. Specific problems with co-cultures Limited apical-basal cell layer interaction and apical epithelial sheet layer cohesiveness[80].

1.5 Scaffold-free cell sheet tissue engineering

To overcome the limitations of scaffold constructs, technologies that allow the direct application of cell sheet layers, without the use of a biodegradable scaffold, are being developed as an alternative tool for tissue engineering.

1.5.1 Scaffold-free cell sheet engineering technologies

1.5.1.1 Enzymatic detachment

The first cell sheet technology established was an enzymatic detachment of CEAs using the proteolytic enzyme dispase[81]. Cells were cultured with underlying ECM, which is cleaved by proteolytic enzymes to release cell-sheet layers partially intact. Though useful for burns treatment, a 10-year audit in 2006 reported a 45% clinical take for enzymatically released CEAs[82]. It is likely that proteolytic enzymes damage cell-cell junction proteins, ion channels, growth factor receptors, and other cell-surface proteins are damaged, in addition to ECM, and contribute to host-rejection[38]. Furthermore, enzymatically released sheets have no basement membrane and decrease graft viability[38].

1.5.1.2 Thermo-responsive polymers

In 1990 Professor Teru Okano developed the first thermo-responsive polymer to create cell sheets without enzymatic detachment[83]. Cells were cultured on poly (N-isopropyl acrylamide) (NIPAM), which is hydrophobic under standard culture conditions at 37°C. Decreasing the substrate temperature to 31°C induced a phase change of NIPAM, which becomes more hydrophilic and swells with later and leads to spontaneous detachment of the cultured cell-sheet[44]. Multiple thermo-responsive polymers have since been developed and are commercially available[37], along with biocompatible support layers used to ease the handling and transfer of the cell sheet[84,85]. Extensive cytotoxicity and functionality testing of cell sheets created using these products have so far been positive[84].

Current limitations of the technology are the mechanical strength, handling, and cost of the thermo-responsive and carrier layers[84]. Cell substrates with the properties of both layers are under development[86-89].

15

1.5.1.3   Magnetic force systems

Magnetic force was used for cell sheet engineering by Ito *et al.*[90] in 2004. Liposomes were first mixed with magnetic nanoparticles to create magnetite cationic liposomes (MCLs). Keratinocytes cultured on ultra-low attachment plates were then treated with MCLs used as a vehicle for magnetic nanoparticle adsorption. Magnetite labelled cells were then manipulated using an external magnet to release them. Ito *et al* used a similar technique to create hepatocyte-endothelial cell co-cultures[91]. Though successful, each cell layer required successful uptake of costly MCL particles, and two days culture under magnetic force for successful adherence. Endothelial cells seeded outside of the magnet radius did not adhere to underlying hepatocytes, and density of both cell layers increased toward the underlying magnet centre[91].

1.5.1.4   Electro-responsive and pH-responsive polyelectrolyte films

Orane Guillaume-Gentil *et al* first developed an electro-responsive system for cell sheet release in 2008[92]. Different cell lines were cultured on polyelectrolyte thin films, consisting of multiple cationic and anionic polymer layers, with highly tuneable properties. An electrical trigger was then used for instant cell sheet detachment. However, adherence to polyelectrolyte films was not consistent between cell types, some spontaneously detached upon confluence without electrical triggers, and others were released as small clusters or single cells when stimulated[92].

The same group later used polyelectrolyte films to develop a pH-responsive system[93]. Mesenchymal stem cells cultured on pH-treated polyelectrolyte films, were detached as intact cell sheets using electrochemical-induced reduction of environmental pH. Despite their high material/reagent cost (and lengthy manufacture), extensive degradation after just thirty minutes of electrochemical stimulus meant polyelectrolyte films could not be recovered or re-used for further sheet creation[93]. Additionally, the required deviations from physiological pH values may result in harm to other cell lines.

1.5.1.5 Photo-sensitive polymers

Hong *et al.* developed the first photo-sensitive system for cell sheet release in 2013[94]. Osteoblast cells were seeded onto titanium-oxide nano-dot coated films (TP), previously coated with desirable proteins, then released by illumination with 350nm UV radiation (350UV) for 20 minutes. Neither TP film culture or UV350 exposure reduced cell viability (>97%) or caused oxidative DNA damage. Instead, cell sheets readily reattached and retained high functionality. Despite this, both the mechanism of adsorbed protein release and radical oxide species suppression, are not yet understood. Other cell-specific protein coatings on TP films may be less successful.

1.5.2 Previous applications for regenerative medicine

Enzymatic release cell sheet engineering has not been limited to burn treatment. As early as 1999, autologous corneal cell sheets cultured on collagen were used to treat limbal cell deficiency[95]. Additionally, keratinocyte and fibroblast sheets cultured on the acellular epidermis, have been used to treat oral[48] and mucosal defects[49,96].

NIPAM and other thermo-responsive polymers have had the broadest range of publications and successful applications to date. Using the UpCell™ brand culture dish specifically, the following epithelial cell sheets have successfully been engineered and transplanted for clinical use: keratinocytes[97], retinal pigment[98], corneal[86], oral mucosal[99], urothelial[100,101], and kidney[102]. Success has also been achieved transplanting corneal[101] and aortic endothelial[102,103], periodontal ligament[104,105], and cardiac myocyte cell sheets[106,107].

1.5.3 Previous applications for disease research

Cell culture models have evolved exponentially in the last two decades. The shortfalls of established *in vitro* 2D monoculture and evolutionarily divergent animal tissue models can be overcome using 3D cell culture technologies[63,108]. Developed 3D tissue models remain sufficiently reductionist to model specific bio-molecular pathways for high-throughput disease research, but better represent the morphology, arrangement and chemical complexity of *in vivo* tissues[109]. An increasing number of publications agree that 3D models are superior to their 2D counterparts for mapping bimolecular pathways and therapeutic efficacy testing of specialised tissues; for example breast[110], intestinal[111], cerebral[112], as well as tumours of varying size and morphology[113]. Additionally, emergent cell sheet engineering technologies allows 3D culture creation without the associated limitations of hydrogel or scaffold materials.

1.5.4 Obstacles to scaffold-free cell sheet technologies

Research and investment in developing commercially available cell sheet engineering technology are increasing exponentially[71], yet there are still many obstacles to overcome before cell sheet engineering can meet the demand for tissue transplantation, and become a commercial reality for high-throughput disease research[38].

Logistical problems for tissue transplant include a lengthy production period of 2-4 weeks[114] and a narrow window of opportunity when both patient and autologous tissue graft are ready. This is further complicated by the transport of the graft from the laboratory bench to the clinic. Having a tissue culture laboratory on-site or near to the hospital would incur significant costs.

Biochemical challenges include cell sheet fragility due to its complexity, potential enzyme and xenobiotic material damage used during transport, and risk of infection from a variety of xenobiotic materials such as culture media and batch-batch variability[115].

Another limitation is the theoretical cost of autologous tissue construct manufacture, transport, and, transplant. Specialised workers, trained in the cell sheet engineering of choice, are required in the laboratory, and surgeons familiar with the technology are required at the hospital. Moreover, the proximity of these two locations would require paid drivers and specialised carrier vessels, exacerbating transport costs[38].

1.6   Acoustofluidic levitation for epithelial sheet engineering

Microfluidic systems and lab-on-a-chip devices were initially developed for analytical chemistry, but their scope is now much wider. Current microfluidic devices manipulate cells and particles using hydrodynamic, electric, dielectric, or magnetic forces. Using acoustic force within a static or microfluidic system, known as acoustofluidic (AF) levitation, is the most novel non-invasive technique for cell manipulation, with potential applications for analytical science, bioanalysis, cell biology, and cell sheet engineering[116].

1.6.1   Acoustofluidic levitation theory

AF devices use travelling or standing acoustic wave fields to exert acoustic radiation force on particles in a fluid medium. For planar levitation, an ultrasound standing wave field (USWF) is used, where acoustic force is generated from non-linear interaction between acoustic waves scattered by loaded particles, and the original wave field[117]. The respective density and compressibility of the object and fluid will decide if the object will move to the point of maximum or minimum acoustic potential. In standing waves, cells and particles with densities higher and compressibilities lower than the surrounding fluid will move to the point of lowest pressure amplitude, known as the pressure node[118].

Planar AF devices are typically composed of four specific layers. A piezoelectric material is utilised as a transducer (PZT), which can convert electrical signal into vibrational energy. The PZT of most planar devices is coupled to a fluid containing microchannel (Figure 1.6.1.1). The point of contact functions as a carrier layer: to isolate the PZT from the fluid layer but transmit a signal for particle manipulation. The opposite microchannel surface or reflector layer reflects acoustic waves within the fluid layer to create a USWF[117] (Figure 1.6.1.2). Considerations for the carrier layer material include bio-compatibility, ease of manufacture, cost, acoustic energy density and transmittance[119]. Desirable half wave acoustic frequencies for use within microfluidic channels are typically in the hundreds of kHz to tens of MHz region[117]. The shape of the planar USWF can be controlled by adjusting the position and intensity of the frequency sweep, and therefore, the geometric formation of cells within the acoustic trap[117].
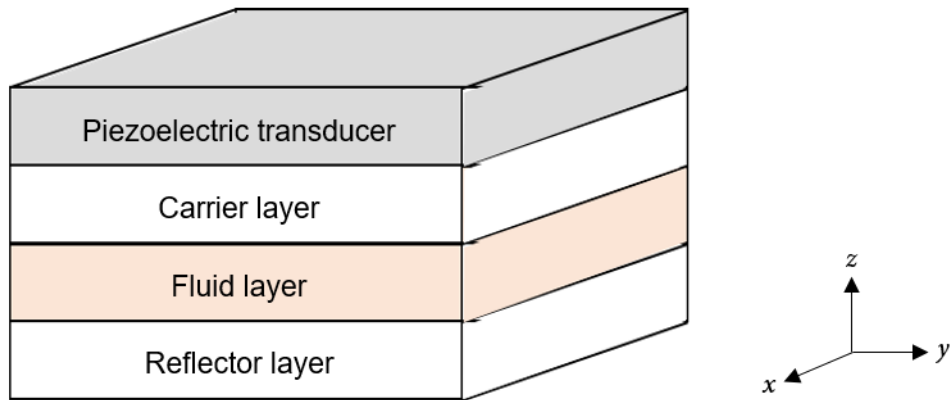
Figure 1.6.1.1 Schematic of required layers for typical planar acoustofluidic device.
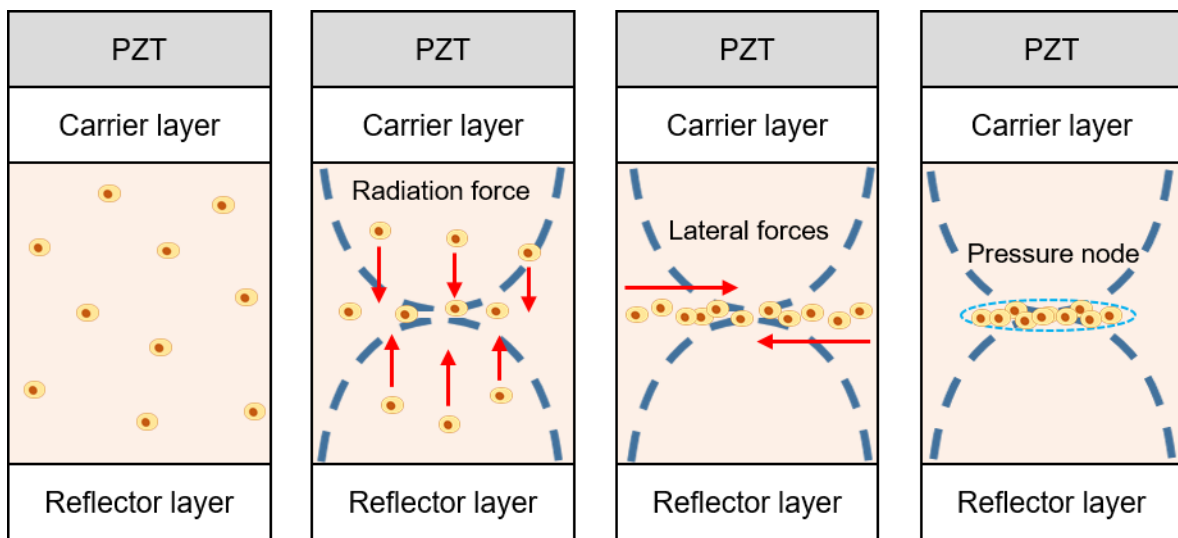
Figure 1.6.1.2 Schematic cross-section of planar acoustofluidic device showing the acoustic forces acting on cells within the fluid layer.
Without acoustic force the spatial organisation of cells loaded into a microchannel is random. Tailored acoustic signals create an USWF within the fluid layer (dashed blue line). Radiation force directs cells towards the centre axial plane where acoustic pressure is smallest, then subsequently directed towards the plane centre by lateral forces (red arrows). Cells are ultimately collected as a planar aggregate, within the area of least axial and lateral acoustic pressure known as the pressure node (cyan circle).

1.6.2 Maintaining cell viability under acoustic manipulation

To maximise the application potential for AF devices, the effects of low-frequency acoustic fields on mammalian cell viability and cell surface protein expression has been studied within microfluidic channels[120] and other standing wave systems[121-123]. A review by Professor Martin Wiklund in 2012[124] surmises over-heating and cavitation as the greatest damage risk during acoustic manipulation and provides guidelines on how to avoid them.

Levitated cells primarily convert acoustic energy into thermal energy within devices, and this is further exacerbated by heat-loss form surrounding device layers. Therefore, it is recommended that the fluid medium is kept at 37°C with a tolerance of ± 1°C to avoid heat-shock death of cells[124].

Cavitation within AF devices is the formation and harmful activity of gas/vapour bubbles within the fluid medium and typically occurs using lower frequencies in the 20-200 kHz range. Microbubbles create pores within lipid membranes of the cell[125], and their formation and collapse are either stable or transient (

Figure 1.6.2.1). With stable cavitation, microbubbles expand and oscillate in size until reaching an optimum resonance size[126], then oscillate symmetrically (gas influx and efflux are equal) over many cycles. With transient cavitation, size oscillation is unstable, so microbubbles expand rapidly, then implode after several cycles. Cavitation carries a high risk of cell shear stress and damage via membrane lysis[127,128], DNA strand breaks[129], or necrosis[130], and should be avoided by using higher frequencies in the 1-10 MHz range[124].
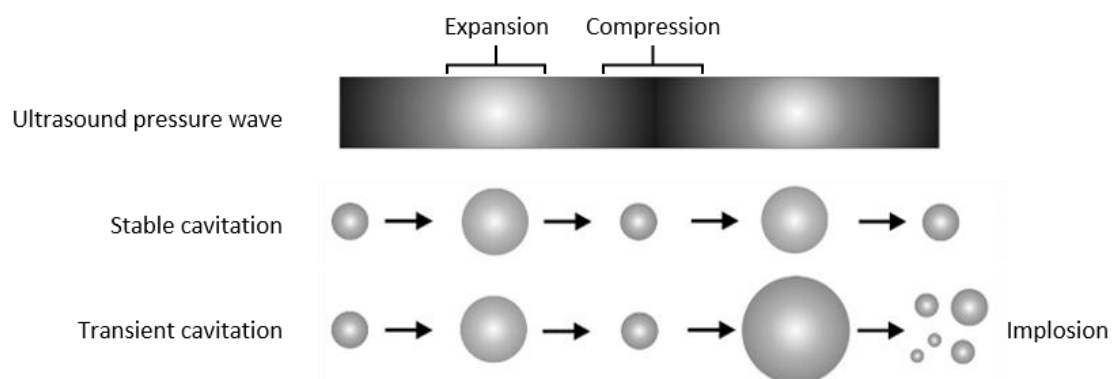
Figure 1.6.2.1 Stable and transient microbubble cavitation.
(A) Schematic representation of an acoustic pressure wave. (B) Stable cavitation of microbubble with symmetrical oscillation and net gain of zero after one gas influx/efflux cycle. (C) Transient cavitation of microbubble with linear gas influx oscillation leading to implosion. Adapted from Lentacker at al 2014.

The biophysical effects of stable cavitation include: localised shear stresses, liquid microstreams, and microbubble displacement; all of which can create pores in the cell membrane (

Figure 1.6.2.2A, B, C). The biophysical effects of transient cavitation are more damaging. Imploding microbubbles create a shock-wave, that increases medium temperature and pressure[124]; as well as a high velocity liquid jet directed towards the cell[131], able to perforate the lipid membrane, (

Figure 1.6.2.2D, E).
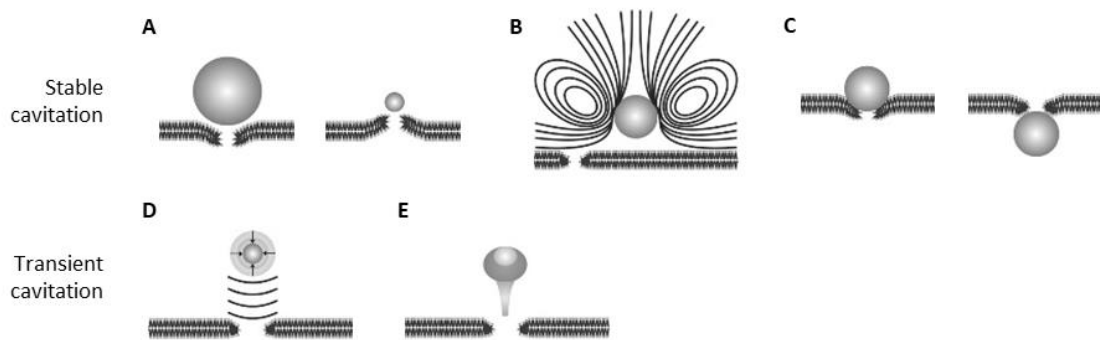
Figure 1.6.2.2 Biophysical effects of stable and transient microbubble cavitation.
(A), (B), and (C) show the biophysical effects of stable cavitation, while (D) and (E) show the effects of transient cavitation. (A) Pushing (left) and pulling (right) forces of a stably oscillating microbubble during expansion and compression phases respectively, thereby disrupting the adjacent membrane. (B) Stable oscillation of a microbubble creates microstreaming in the surrounding fluid, which exert mechanical stress on the cell membrane, causing pore formation. (C) Acoustic radiation force causes displacement of the microbubble which is compressed against the cell membrane, resulting in disruption, and may even push through the lipid bilayer and enter the cell. (D) Shock waves produced by microbubble implosion generate high temperature and pressure stresses on adjacent cell membranes, resulting in disruption. (E) When a microbubble implodes near a surface or cell membrane, the collapse is asymmetrical, leading to the formation of a liquid jet towards said membrane, which it is able to perforate, thereby creating a pore. Adapted from Lentacker et al 2014.

1.6.3 Previous applications of acoustofluidic devices

1.6.3.1 Sonoporation of cells for drug delivery

Despite the risks, the cavitation phenomenon of ultrasound (US) frequencies has been used to reversibly increase transmembrane permeability of cells, known as sonoporation, to enhance the delivery of macromolecules[128,132,133]. Sonoporation has significantly increased uptake of fluorescent dyes[134,135], therapeutic drugs[136], and gene transfer[137] in healthy tissue models, as well as delivery of cancer therapies to tumour models[138-141].

1.6.3.2 Structural organisation of engineered tissue

Recreating the complex structural organisation of cells and proteins found in native tissue poses a great challenge for tissue engineering[142], moreover that spatial organisation of cells within, and signals from their environment, directly influence behaviours critical for tissue regeneration[142]. Natural and synthetic hydrogels/scaffolds mimic proteins of the ECM and allow the creation of three-dimensional tissue, but with little control over the structural organisation and none over cellular arrangement within them.

A research group at the University of Rochester utilised acoustic force to address these issues with fabricated tissue. Using acoustic force, Garvin *et al.*[143] controlled the spatial patterning of fibroblasts within a collagen hydrogel without reducing viability and also shown not to directly influence the arrangement of the pre-polymerised hydrogel. Fibroblasts were organised loosely into planar bands which significantly increased collagen-mediated gel contraction and collagen fibre re-organisation. The same technique was used to arrange endothelial cells within a hydrogel and promote vascularisation[144]. As before, endothelial cells were organised into planar bands after fifteen minutes of acoustic force. Subsequently, levitated cells formed capillary-like sprouts within the hydrogel[144]. In a subsequent publication, cultures ultimately formed a network of branching vessels with an arteriole-sized lumen, throughout the collagen hydrogel[145]. Lymphatic cells exposed to acoustic force showed the same spatial patterning and micro-vessel outgrowth[142]. Dalecki *et al.*[142] created a composite hydrogel of one endothelial cell-containing collagen layer, exposed to ten minutes of acoustic force, overlaid by a duplicate second layer. The initial layer, exposed to acoustic force twice, had a distinct micro-vessel morphology after only three days.

The effect of acoustic force on the collagen fibril arrangement itself was also studied[146]. The acoustic force applied to an un-polymerised collagen hydrogel influenced fibril microstructure: which became short, narrow, and dense within pressure nodes and anti-nodes, instead of long and thick like non-treated counterparts. Fibroblasts subsequently seeded onto the hydrogel rapidly migrated towards treated regions and formed circular aggregates.

1.6.3.3 Spheroids for drug research

Stationary AF devices have also been used for the creation of spheroid cell constructs. Bazou *et al.*[122] levitated hepatocytes for five minutes, to form spheroid aggregates 0.4 – 2.6 mm in diameter, which were then pipetted into a 96-well plate containing hydrogel to create multiple 3D liver tissue models. Further study confirmed that levitated spheroids remained viable, maintained specific biomarker expression, and had relatively increased enzyme activity than non-levitated counter-parts[123].

1.6.3.4 Wound healing

Dalecki *et al.* also employed US technology as a treatment *in vivo* for wound repair and regeneration[142]. US force was applied to the wound site of mice with full-thickness epidermal excisions for ten minutes per day, for two weeks. Interestingly, treated mice had significantly increased granulation tissue thickness, collagen deposition, ECM remodelling and revascularization over the wound site.

1.6.3.5 Bioanalytical and biomedical assays

Non-invasive cell and particle manipulation, separation, and trapping techniques are highly sought after for bioanalytical and biomedical assays. An increasing number of research groups have developed microfluidic AF devices, and successfully demonstrated their potential use for research assays. Evander at al[147] developed an AF device which successfully manipulated particles as small as 1.8 µM in diameter, and found that acoustic trapping force increased linearly with particle volume. Thus, acoustic trapping could be a tool for mass-associated particle sorting or assays. Live-cell experiments were performed using the device trapping yeast for 6 hours, rat liver cells, and neuronal stem cells for 15 minutes, which remained viable. Using a similar AF device, Hammarstrom and Evander *et al.*[148] separated erythrocytes from whole blood plasma, and published work outlining the benefits of utilising a borosilicate glass capillary as a fluid microchannel for AF devices. Hammarstrom *et al.*[149] later demonstrated successful acoustic trapping to remove unspecific immuno-background during a matrix-assisted laser desorption ionisation, mass spectrometry (MALDI-MS) assays. The AF device trapped antigen-labelled beads, allowing them to be washed while levitating, then released onto an integrated selective enrichment target. Immuno-background from detergent was higher with the magnetic washing system. Using a unique acoustofluidic system containing bio-functionalised polymer layers, Gupta *et al.*[150] isolated infected erythrocytes from healthy erythrocytes within whole blood plasma. The microfluidic channel contained a pair of antibody-coated polystyrene layers strategically placed within the fluid channel. Healthy levitated erythrocytes passed between the polystyrene layers, whereas infected cells were captured either side.

24

1.6.3.6   Creation of 3D tissue grafts

The first successful application of AF technology for scaffold-free engineering of cartilage grafts was in 2014 by Siwei Li *et al.*[151]. Their developed AF device utilised a rectangular glass capillary as a resonator chamber, 5 cm in length with internal dimensions 8 x 0.8 mm^3. The device was operated using a 10 V peak-peak signal, and 890 – 810 kHz frequency sweep, which created a large, central pressure node in the capillary lumen. To create autologous hyaline cartilage grafts for transplant, chondrocyte cells were isolated from an osteoarthritic patient then fed into the AF device at 1 mL/min. Cells were levitated for 21 days with media perfusion and formed 3D aggregates approximately 2.5 x 2.5 x 0.2 mm^3 in size. Histological analysis of two grafts revealed hyaline-cartilage specific ECM expression. Three grafts used for mechanical analysis had elasticity reading comparable to *ex-vivo* cartilage samples. Two cartilage grafts were successfully transplanted into chondral defect sites of *ex-vivo* patient cartilage samples approximately 10 x 10 x 1 mm^3 in size. After sixteen weeks, histological analysis of the implant site analysis showed continuous repair tissue from the neo-graft to the *ex-vivo* patient tissue, containing dense, proteoglycan-rich ECM found *in vivo*.

1.6.3.7   Bronchial epithelial cell sheet creation

Using a static AF device with a planar pressure node, Dr Angela Tait levitated BEC s to create planar sheets (BEC sheets)[152] to develop direct-contact *in vitro* models of the airway mucosa. Single epithelial cells were pipetted into the acoustic trap and levitated for two hours, previously determined as sufficient for adherens formation. Epithelial cells levitated for five days became 3D spheroid aggregates. A single, planar BEC sheet created after two hours of levitation was then pipetted by hand onto fibroblasts within a transwell to create a direct-contact co-culture, which was maintained for three days[153]. The BEC sheet successfully expanded across the fibroblast layer before fixation and staining. Confocal microscopy revealed that cell layers remained as two distinct layers.

1.6.4   Newly developed acoustofluidic devices for epithelial sheet creation

A plethora of cell sheet engineering technologies is under development[71], with relative levels of interest and endemic limitations[38]. Static AF devices have already proven useful for enhancing the spatial and structural organisation of hydrogel/scaffold engineered tissue constructs[142] and preliminary work with another device successfully created a bronchial epithelial sheet for direct-contact co-culture with fibroblasts[152]. Combining microfluidic and AF technology has allowed the creation of high-output AF devices for non-invasive cell manipulation[117], with potential applications for bioanalytical/biomedical research[148,149,154], and the creation of 3D tissue grafts for transplant[151].

This project proposes a novel technique for the creation of epithelial cell sheets using microfluidic AF devices based on initial designs by Hammarstrom *et al.*[154], utilising low-cost glass capillaries as bioreactors[148], and with potential for scalability and increased output using multiple AF devices in sequence. Levitated epithelial sheets could potentially be used for scaffold-free engineering of autologous multi-layered tissue constructs for myocardial[54], retinal[53], and corneal transplant[155], or the creation of more replicative *in vitro* models for disease research[60]. Following on from Dr Tait's work, developing a direct-contact co-culture of the airway mucosa[152], BECs will be levitated for the duration of this project.

1.7   Hypothesis

Developed microfluidic AF devices can levitate BECs to create multiple large BEC sheets with sufficient adherens junctions to be transferred onto collagen-coated surfaces intact, and subsequently behave as cohesive sheet layers.

1.8   Aims

Aim 1. Use small transducer AF devices to demonstrate scale-up capability for increased output of BEC sheet formation.

Aim 2. Use large transducer AF devices to visualise and optimise BEC sheet formation.

Aim 3. Use reduced dead volume AF devices to create and release BEC sheets without single BECs present.

Chapter 2: Materials and methods

2.1   Cell culture methods

2.1.1   Recovering cell lines from liquid nitrogen storage

The 16-human bronchial epithelial 14-o (16HBE) cell line was used for this project. 16HBE cells were kept in cryovials as 1.0×10^6 cell aliquots in cryopreservation media and stored in liquid nitrogen. To thaw the frozen pellets within each cryovial, pre-warmed 16HBE growth media (GM) (described in 2.1.2) from a 25 mL tube was washed over the pellet using a pipette (1 mL), and the thawed cells transferred to the 25 mL tube. After centrifugation (200 x g, 5 minutes, room temperature (RT)) pellets were resuspended in 13 mL GM then seeded into T75cm^2 flasks pre-treated with collagen (described in 2.1.2). Flasks were labelled with cell-line, name, passage number and date then transferred to an incubator for continuous culture (37°C, 5% carbon dioxide (CO_2)).

2.1.2   Continuous culture of cell lines

The 16HBE cells were seeded onto T25cm^2 flasks for experimentation or T75cm^2 flasks for continuous culture. Flasks were pre-treated with 30 μg/mL collagen-I solution (37°C, 30 minutes) (Advanced BioMatrix, USA), and cultures were maintained in 16HBE cell growth medium (GM): MEM and Glutamax™ (Thermofisher, UK), supplemented with 10% Fetal bovine serum (FBS) (Life Technologies, UK) and 1% Penicillin-Streptomycin (Pen/strep) (Sigma Aldrich, UK).

16HBE cells were passaged at 70-90% confluence by rinsing with Hanks Balanced Salt Solution (HBSS) (without magnesium (Mg^{2+}) or calcium (Ca^{2+}) ions) (Life Technologies, UK), then incubating with 1 mL of 1X Trypsin solution (details of components!, Life Technologies) (37°C, 5 minutes). Trypsin was neutralised with 10 mL GM followed by centrifugation (20°C, 300 x g, 5 minutes). The cell pellet was resuspended in 1mL GM, and cell counts determined using the Trypan blue exclusion method (10 μL cell suspension diluted with 40 μL GM and 50 μL of 0.4% Trypan blue solution (Sigma)) using a 10 μL aliquot and haemocytometer.

2.1.3 Transfection of cell lines

To aid with visualisation of BEC and fibroblast monocultures or direct-contact co-culture models, 16HBE cells were stably transfected with a green fluorescent plasmid (GFP). Stocks of GFP-16HBE cells had previously been prepared by Dr Tait using the TransIT-2020 transfection reagent method[152].

The 16HBE cells were seeded onto a six well plate (0.12 x 10^6 cells/well) and maintained in GM until cells reached 40 - 50% confluence. TransIT-2020 GFP transfection solution (250 µL OptiMEM reduced serum media, 5 µL GFP plasmid (Clontech California, USA) and 7.5 µL TransIT-2020 reagent (Mirus Bio, Madison, USA)) was added dropwise to each well. After 2-3 days, the GM was replaced with 3 mL of G-418 antibiotic (Sigma Aldrich, UK) selection media (600 µg/mL of GM). Once GFP-16HBE cells were a majority (3-4 days), transfected populations were maintained with 200 µg/ml G-418 media.
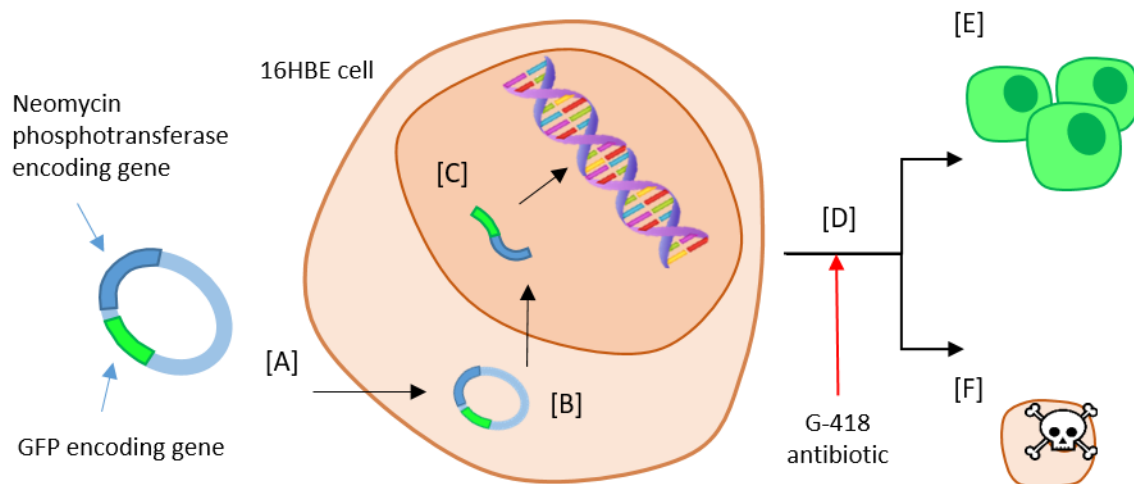
Figure 2.1.3.1 Transfection of 16HBE cells with green fluorescent protein plasmid and selection of cells stably transfected.
[A] The plasmid encoding both Neomycin phosphotransferase and GFP passes through the cell membrane using Trans-IT-2020 transfection reagent. [B] The plasmid is introduced to the cell nucleus. [C] The plasmid is cleaved and integrated into the chromosomal DNA by enzymes. [D] G-418 antibiotic is added to the cell culture. [E] Stably transfected cells express both GFP for imaging and Neomycin phosphotransferase: which confers protection against G-418 antibiotic; and therefore proliferate. [F] Cells which have not integrated the plasmid are susceptible to G-418 antibiotic and perish.

2.1.4   Seeding cell lines onto Transwell^{TM} inserts

For initial monoculture levitation experiments, 24-well transwell^{TM} (TW) plates containing 0.4 μm pore, 6.5 mm polyester inserts (Corning Costar, UK) were pre-coated apically with 200 μL of 30 μg/mL collagen-I solution (37°C, 30 minutes). Wells were seeded with levitated GFP-16HBE cell sheets or 20,000 single GFP-16HBE cells as a control. Empty TW inserts were seeded with 20,000 or 150,000 GFP-16HBE cells in duplicate, as further controls. Cultures were then maintained with 200 μL/500 μL 16HBE cell GM in the apical/basolateral compartments.
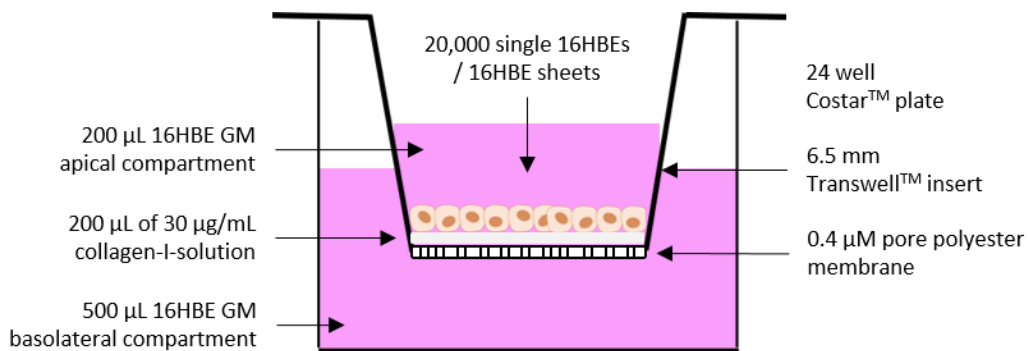
Figure 2.1.4.1 Maintaining BEC cultures seeded into transwell^{TM} inserts.
The 0.4 μM pore, 6.5 mm, polyester Transwell^{TM} inserts were pre-coated with 200 μL of 30 μg/mL collagen-I-solution (37°C, 30 minutes). Equilibrated 16HBE GM (37°C, overnight) was then added to the apical (200 μL) and basolateral compartments (500 μL). Single 16HBEs (50/150,000) or 16HBE cell sheets created using AF devices were seeded into the apical compartment and kept at 37°C, 5% CO_2. With long term 16HBE cell cultures 200/500 μL apical/basolateral GM was replaced every 2-3 days.

2.1.5 Seeding BECs onto glass coverslips

For immunofluorescence staining and further levitation experiments, 24-well plates (Corning, costar, UK) containing 13 mm round glass coverslips (CSs) (Thermofisher, UK) were used. For viable cell-dependant adherence, CSs were first washed using pure ethanol (EtOH) (40 minutes), rinsed with sterile dH$_2$O, then air-dried within a petri-dish (20 minutes). CSs were transferred to plates and treated with 200 µL of 30 µg/mL collagen-1 solution (37°C, 30 minutes). For non-specific adherence, CSs were instead rinsed with dry acetone (10 minutes), followed by sterile dH$_2$O (10 minutes), and then air-dried overnight. CSs were then pre-coated with a 2% 3-aminopropyltriethoxysilane (APES) (Sigma, UK) solution in dry acetone (Sigma, UK) for 10 minutes.

For staining experiments CSs were seeded with 150,000 single 16HBE cells in 1 mL GM then maintained with GM until confluent. For levitation experiments, 24-well plates were loaded with 1.4 mL of GM and equilibrated (30 minutes, 37°C, 5% CO$_2$) before seeding with levitated 16HBE cell sheets, or 20,000 single 16HBE cells in 100 µL GM as controls.

2.1.6 Alcohol fixation of BEC cultures

After experimental completion, 24-well plate 16HBE cell sheet cultures were fixed with alcohol to allow for subsequent adherens junction and cell cytoskeleton staining. To avoid disturbing any BEC sheets, GM was carefully removed by tilting the plate and drawing slowly from the bottom edge of the well using a 200 µL pipette tip. Cells were then fixed with 200 µL of ice-cold acetone: methanol (1:1) (Sigma Aldrich, UK) solution pipetted slowly into the side of each well. Plates were then covered in foil and incubated (-20°C, 20 minutes). Each well was then rinsed with 500 µL of 1X PBS and stored in 1 mL 0.05% sodium-azide solution (NaN$_3$) in 1X PBS (Sigma Aldrich, UK), covered in foil and stored at 4°C for immunofluorescence (IF) staining.

2.2 Acoustofluidic levitation for BEC sheet creation

2.2.1 Small transducer (ST) device preparation

Acoustofluidic devices developed by engineer's Dr Bjorn Hammarstrom and Dr Peter Glynne-Jones, with help from Professor Martyn Hill, were used to levitate GFP-16HBE cells within glass capillaries used as bioreactors, each contained a piezoelectric transducer connected to a signal generator (Figure 3.2.1.1). Internal capillary dimensions were: 50 × 6 × 0.3 mm. Resonance at a specific drive frequency created an USWF within the capillary that directed GFP-16HBE cells toward a pressure node in the centre, trapping them. Dr Tait previously demonstrated that cell-cell adherens junctions formed over a two-hour incubation period[156], so GFP-16HBE cells aggregates were levitated for a minimum of two hours. For triplicate AF device experiments, the signal generator used a 2.35-2.45 MHz sweep over 20 m/s period, with a peak-to-peak voltage of 6.00 V. For experiments using six AF devices 3.7-4.7 MHz sweep over 20 m/s period was used.

2.2.2 ST device loading protocol

Before levitation 16HBE GM was incubated overnight at 37°C, 5% CO_2 to equilibrate. On the day of levitation, the syringe, capillaries, and capillary tubing were flushed with 1 ml 70% IsOH followed by 1 ml equilibrated 16HBE GM. For capillary loading, a 2.0×10^6 cells/mL GFP-16HBE cell suspension was prepared, and 600 μL added in triplicate to a 24-well plate. The tips of each capillary were submerged in 2.0×10^6 cell suspension and 30 μL aspirated over six seconds (300 μL/min).

The total internal volume of each glass capillary was 90 μL, of which 9 μL (ST1) or 14.4 μL (ST2+3) was covered by the PZT, with a 21 μL (ST1) or 15.6 μL (ST2+3) volume between the opening and PZT volume. Thus, when 30 μL of 2.0×10^6 cells/mL loading solution was aspirated, we assume the cells fill the PZT-volume and are held there.

AF devices were calculated as holding: 9 μL × $(2.0 \times 10^6$ cells/mL) = 18,000 cells (ST1),

or 14.4 μL × $(2.0 \times 10^6$ cells/mL) = 28,800 cells (ST2+3).

2.2.3 ST device levitation protocol

Loaded capillaries were transferred to a 37°C incubator for perfusion, to pass loaded cells through the ultrasonic trap and to feed the cells caught within the trap. The syringe pump and capillary tube carousel (via the control-box) were operated using a laptop. Cells were levitated for at least two hours or more, to develop cell-cell adherens junctions. Multiple perfusion and loading protocols were used; which will be discussed later. To dispense BEC sheets after levitation with perfusion, capillary tips were submerged in 150 µL 16HBE GM of TW-insert apical compartments and 50 µL perfused at 300 µL/min.

Time (minutes)	Levitation step	Syringe pump instruction			
		Action	Flow rate (µL/min)	Length (minutes)	Device sequence
-1	loading	aspirate	300	0.1	ST1, ST2, ST3
0	static phase	perfuse	-	-	-
30	feeding #1	perfuse	2	10	ST1, ST2, ST3
60	feeding #2	perfuse	2	10	ST1, ST2, ST3
90	feeding #3	perfuse	2	10	ST1, ST2, ST3
120	seeding	perfuse	300	0.1	ST1, ST2, ST3

Table 1 Syringe pump instructions for triplicate ST device levitation experiments.

2.3   Analytical methods

2.3.1   CyQuant assay for determination of cell number of created BEC sheets

To quantify cells expelled from AF devices after levitation, the CyQuant NF dye assay kit was used (ThermoFisher, UK). CyQuant fluorescent dye was diluted with 1X buffer reagent at either 1:500 or 1:1,000 ratio, supplemented with 1:1,000 reacting agent. To produce a ten point standard curve for 16HBE cell quantitation, ten serial dilutions of a 2.0×10^6 cells/mL solution were performed in 1.5 mL eppendorf tubes and kept at 37°C, 5% CO_2 during levitation. After levitation with perfusion, BEC sheets were dispensed into 0.5 mL eppendorf tubes. BEC sheet and standard curve tubes were then spun down (300 g, 4°C, 7 minutes). BEC sheet pellets were next resuspended in 100 μL of desired dye solution and standard curve pellets in 250 μL dye solution. To produce a standard curve of 80,000 to 156 cells, 100 μL of each standard dye solution was added in duplicate, followed by singular 100 μL aliquots of experimental cell sheet dye solution. The plate was covered in foil then incubated (37°C, 60 minutes). Fluorescence intensity of the plate was measured using a Fluoroskan Ascent FL plate reader (excitation ~485 nm, emission ~530 nm) after 30, 45, and 60 minutes. Empty wells were measured as background fluorescence control (blank). Using the Fluoroskan Ascent software, fluorescence intensity values were blank subtracted, then a standard curve (either linear or quadratic polynomial) was created, which the software utilised to calculate cell number of experimental wells.

2.3.2   Measuring BEC culture barrier formation

Barrier formation of the GFP-16HBE cell sheet and single cell TW cultures was monitored over time. Transepithelial electrical resistance (TER) was measured using an EVOM RS2 voltohmmeter with 4 mm chopstick electrodes (WPI, United Kingdom) which can measure the resistance between the apical and basolateral compartment[157]. Readings were taken from 4-18 days post-seeding. To increase accuracy: 24-well plates were kept on an eppendorf tube block to retain heat, and the chopstick electrode was washed with HBSS between each reading. Resistance measurements >1,000 ohms was considered indicative of TJ formation, and a physical barrier,[158].
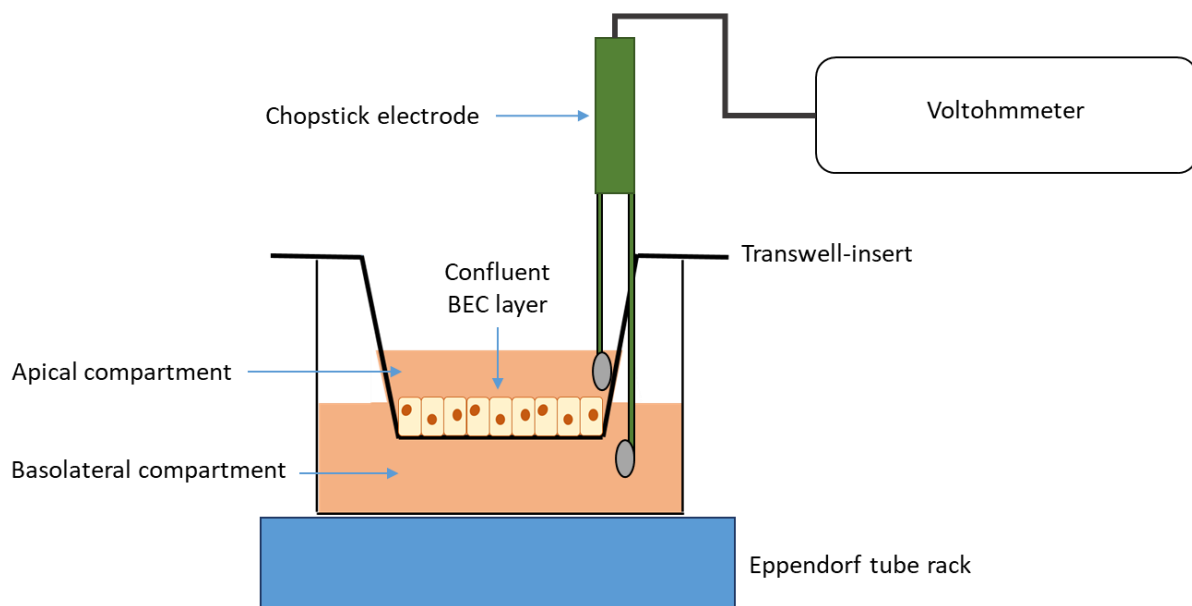
Figure 2.3.2.1 Measuring transepithelial electrical resistance of BEC cultures using a chop-stick electrode and voltohmmeter.
BEC sheet and single BEC cultures were seeded into the apical compartment of 0.4 μm pore polyester TW-inserts, within a 24-well plate. To measure physical barrier formation, the plate was first transferred to a cell-culture hood with an eppendorf tube below to retain heat. Using a chop-stick electrode connected to a voltohmmeter, the electrical resistance between the apical and basolateral compartments was measured. Resistance greater than 1,000 ohms was indicative of tight junction formation and development of a selectively permeable physical barrier.

2.3.3 LIVE/DEAD nuclear staining of BEC cultures

To visualise BEC sheet formation and quantify BEC sheet viability while levitating within developed AF devices: the LIVE/DEAD BLUE/GREEN nuclear staining kit was used (Invitrogen, USA). 16HBE flasks were passaged when 70-90% confluent and 1.5×10^6 cells/mL suspensions prepared in GM. Two drops of membrane permeable, Hoechst33342 LIVE nuclear stain were added to 1 mL of cell suspension in a 15 mL falcon tube. BECs were then incubated at 37°C for 15 minutes with agitation every 2-3 minutes and centrifuged (20°C, 300 g, 5 minutes). Pellets were resuspended in 1 mL of GM containing membrane impermeable, NucGreen DEAD nuclear stain, ready for AF device loading. Whilst levitating GM containing NucGreen was perfused through the device at 2 µL/min.

2.3.4 Viability calculations

Non-viable BEC nuclei were imaged using the GFP-FLUO channel of a Leica DMI6000 microscope (Leica microsystems, UK) then counted manually. Total levitated nuclei were imaged using the DAPI-FLUO channel, then exported to ImageJ software (National Institute for Health, USA) for quantitation. The image was first converted to greyscale, and the threshold adjusted to capture all nuclei. Next, the image was converted to binary, and the total area measured using the software. The area was divided by the average nuclei size; previously calculated using ImageJ and smaller BEC sheets of known cell number.
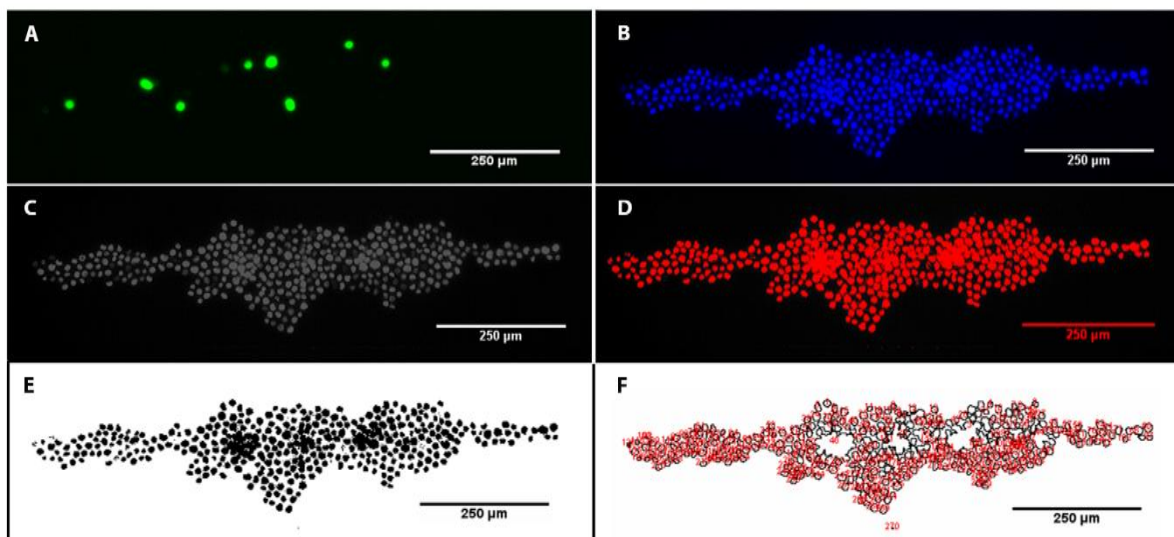
Figure 2.3.4.1 Calculating BEC sheet cell number using ImageJ software for viability analysis. To visualise BEC sheet formation, BECs were pre-loaded with membrane-permeable Hoechst33342 (blue). For viability analysis, BECs were also suspended in GM containing membrane-impermeable NucGreen dye (green). [A] Non-viable NucGreen +ve BEC sheet nuclei. [B] Total Hoechst33342 +ve BEC sheet nuclei. [C] Greyscale image of BEC sheet nuclei. [D] Threshold adjusted image of BEC sheet nuclei. [E] Binary image of total levitated BEC sheet nuclei. [F] Measured total area of BEC sheet nuclei. The total nuclei area was then divided by average nuclei size, previously calculated using BEC sheet images of countable cell number.

2.3.5 Size analysis of Levitated BEC sheets

Fluorescence tilescan images of Hoechst-loaded, levitated cell sheets were exported into the ImageJ software for size analysis. The image was first converted to greyscale, then threshold adjusted to visualise all nuclei clearly. After setting the scale for each image, the Measure tool was used to measure individual cell sheet length, width, and area. Total levitated sheet area for each image was then calculated using Microsoft Excel.

2.3.6 Immunofluorescence staining of BEC cultures

Following fixation with alcohol and storage in 0.05% NaN_3 solution, levitated BEC sheet and non-levitated single BEC cultures were washed three times in 1X PBS (5 minutes) and permeabilised with 1 mL of 0.1% Triton-X 100 (Sigma Aldrich, UK) in 1X PBS for 30 minutes. BECs were washed with 1X PBS another three times, and subsequently blocked with 1X PBS containing 1% bovine serum albumin (BSA) and 0.1% Tween20 for a further 60 minutes. Cells were then incubated with E-cadherin (clone 4A2) mouse monoclonal IgG antibody (Cell Signalling, UK,) at a 1:100 dilution in blocking solution at 4°C overnight. Following primary antibody incubation, cells were washed with 1X PBS three times then incubated for one hour at room temperature with goat anti-mouse IgG antibody, conjugated to Alexa Fluor-647 (Abcam, UK) at a dilution of 1:100 in blocking solution. For all monoclonal primary antibodies, an isotype control was performed. A secondary antibody control was performed for every secondary antibody used in this project.

For all staining experiments, 1 µg/mL of 4',6'-diamino-2-phenylindole (DAPI) was used to visualise cell nuclei (Sigma Aldrich, UK). BEC cultures were washed three times with 1X PBS before incubation with DAPI for 15 minutes, then a further three times with 1X PBS after. Plated BEC cultures were then ready for visualisation. Coverslip seeded BEC cultures were mounted onto glass slides using Mowiol (Harlow Chemical Company LTD, UK). Finally, images were acquired at 10x, 20x, and 40x magnification using a Leica DMI6000B microscope (Leica microsystems, UK); with sequential scanning and system optimised settings.

Chapter 3: Results

3.1   Acoustofluidic device requirements for BEC sheet creation

For BEC sheet creation, either research or clinical, developed AF devices must be able to fill the following criteria:

1. Create multicellular BEC sheets greater than 50 µM in length and width able to move collectively via plithotaxis instead of independently.
2. Levitate BECs within a narrow plane so that BEC sheets are sufficiently planar and only 1-2 cells deep across the whole surface.
3. Maintain viability of BECs while levitating inside the device, at the same level expected of BECs passaged without levitation: which should be >95%.
4. Levitate BECs steadily enough to create adhesions; and long enough for sufficient adhesion formation to allow BEC sheets to be seeded intact.
5. Finally, AF devices must be able to release created BEC sheets without unwanted single cells; resulting from BEC sheet fragmentation or otherwise.

Experimental design of the project is to investigate each requirement for developed AF devices in the order listed and make appropriate modifications to the design until they are all met.

3.2 Small transducer device development

Initial levitation experiments were conducted using the small transducer (ST) AF devices, as part of a short research project for the completion of my MRes Biomedical science degree. Consequently, all ST device data shown was acquired before the official start of my MPhil project.

3.2.1 ST device design allows operation in triplicate for BEC sheet creation

ST devices were held in triplicate by a capillary rack (ST1-3) (Figure 3.2.1.1A) and operated using an oscillating 2.3 – 2.4 MHz frequency sweep from the signal generator. Multiple devices were connected to a single syringe via 0.1 mm diameter capillary tubing and a carousel. The system was cleaned using 75% IsOH then conditioned with equilibrated 16HBE growth media (GM) before levitation. To load 30,000 single BECs, the open ends were submerged in a 2.0 x 10^6 cells/mL suspension and 30 μL aspirated in sequence at 300 μL/min. Devices were then transferred to a cell-hood located incubator (37°C, 5% CO_2) with a waste dish to catch GM (Figure 3.2.1.1B).
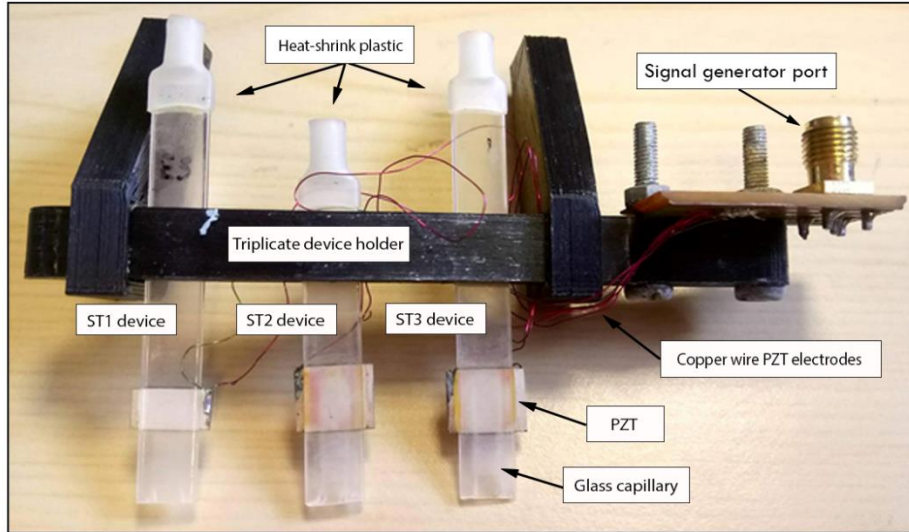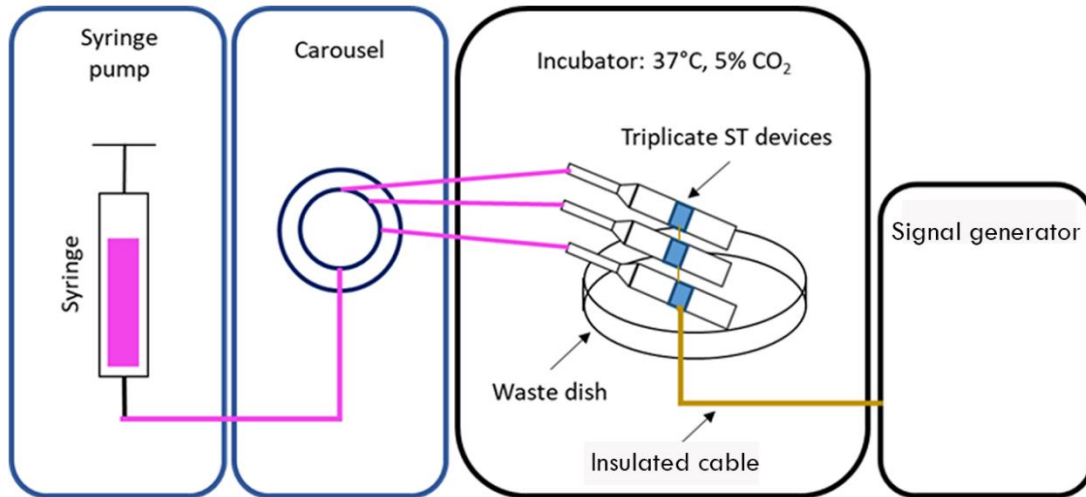
Figure 3.2.1.1 Newly developed ST device design allows BEC sheet creation in triplicate.
[A] Labelled image of triplicate ST devices. Each device consisted of a PZT and glass capillary used as a resonator chamber. Devices were held within a plastic rack, and PZTs connected to the signal generator port via copper wire electrodes. One end of each device was attached to 0.1 mm capillary tubing and sealed with heat-shrink plastic. [B] Schematic of the experimental set-up. Devices were connected to a syringe of GM (held within a pump) via capillary tubing and a carousel, and to the signal generator via an insulated cable. Single BECs were aspirated through the open loading-end of each device, which were then transferred to a portable cell-hood located incubator (37°C, 5% CO2), with a petri-dish below to catch perfused GM.

3.2.2   Variable BEC sheet creation using ST devices

Dr Tait previously established two hours levitation as sufficient for adherens junction formation, and therefore BEC sheet creation, using a similar AF device that levitated BECs within a well of a culture plate[152]. Using the developed capillary-based ST devices, single BECs stably transfected with GFP were levitated for two hours to create cohesive cell sheet monolayers (BEC sheets). After a 30 minute static phase, GM was perfused at 2 µL/min through each device in sequence: this was to prevent cell starvation and remove cells outside of the PZT volume pressure nodes. BEC sheets were then released into collagen-coated 6.5 mm diameter TW-inserts for analysis.

To determine optimal visualisation technique to monitor BEC sheet growth and migration, the TW-insert containing the largest cell sheet was imaged at 10x magnification using both bright-field (BF) and GFP-fluorescence (GFP-FLUO) channels. GFP-FLUO images provided greater resolution and definition of BEC sheet edges than BF images and was used for further image analysis (Figure 3.2.2.1).
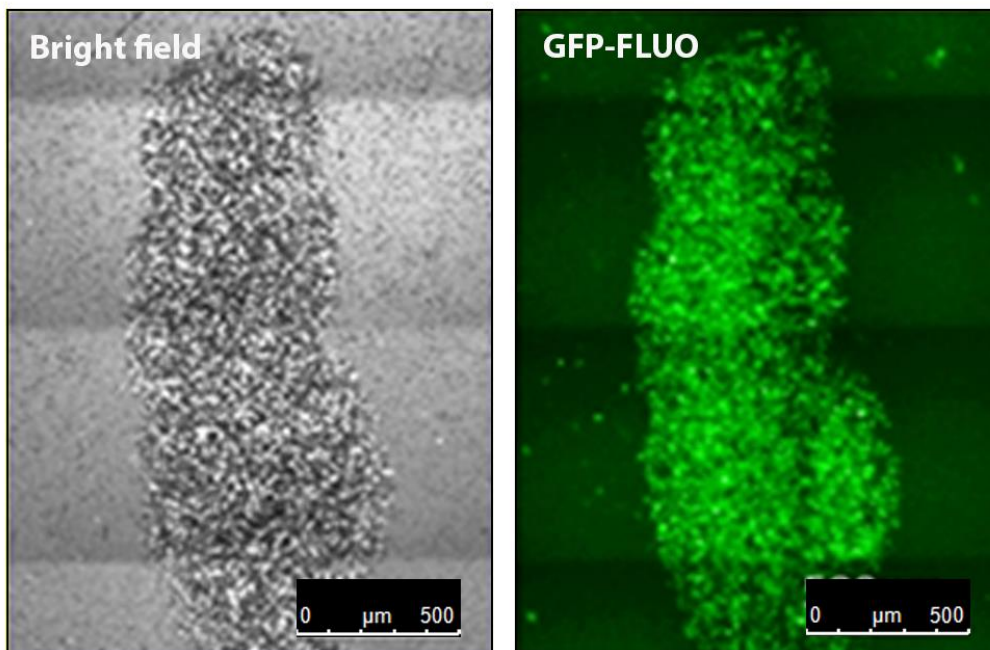
Figure 3.2.2.1 Fluorescence microscopy improves visualisation of seeded BEC sheets.
GFP-transfected BECs were levitated for two hours with GM perfusion using ST devices. Created BEC sheets were then seeded onto collagen-coated TW inserts and visualised at 10x magnification using both the Bright-field and GFP-FLUO channels. The resolution and definition of seeded BEC sheets was greater with GFP-FLUO images.

Consistency of BEC sheet creation was next investigated. Three levitation experiments were performed, using triplicate devices (ST1-3). As previous, single BECs were levitated for two hours with flow, dispensed into collagen-coated TW-inserts, and tile-scan images taken immediately after seeding (Figure 3.2.2.2). For one experiment, ST1 provided the single largest BEC sheet without any single BECs present but subsequently yielded smaller BEC sheets with increasing single BEC presence. The ST2 device performed poorest and had the largest single BEC presence. Fortunately, the ST3 device provided 2-3 BEC sheets of sufficient size each experiment with visibly fewer single BECs and BEC sheet fragments (Figure 3.2.2.2). The disparity between ST device performance would require further exploration.
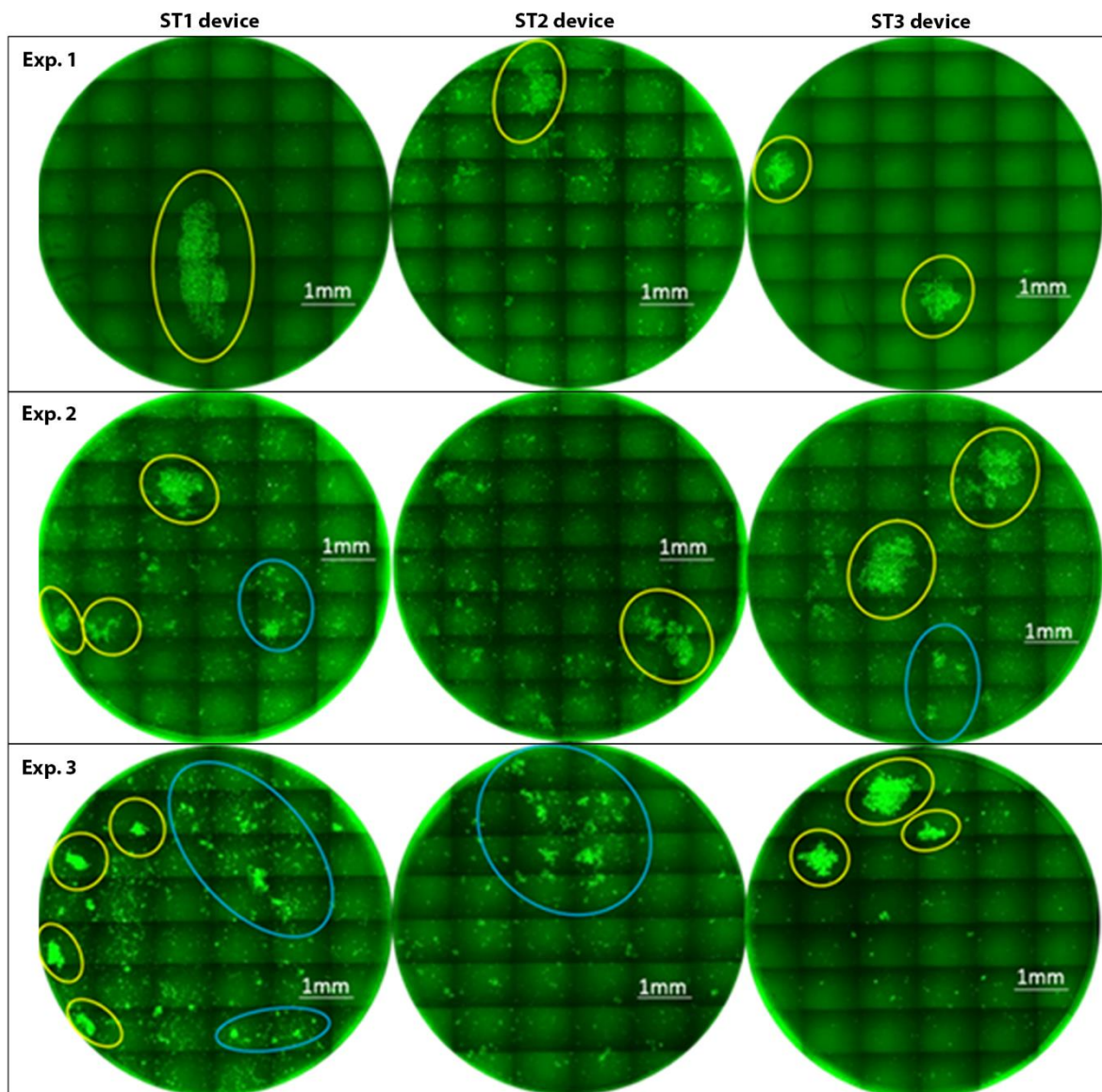
Figure 3.2.2.2 Fluorescence images show BEC sheet creation is variable using ST-devices.
For three replicate experiments, using triplicate ST-devices (ST1-3): GFP-BECs were levitated for two hours with 2 µL/min GM perfusion, then seeded onto collagen-coated TW-inserts by perfusing 100 µL GM at 300 µL/min. Tile scan images were acquired immediately after sheet seeding using the GFP-FLUO channel. The number and size of seeded BEC sheets is not consistent between devices or experiments. A variable number of single BECs are also present with seeded sheets. Desired BEC sheets are circled yellow, and non-desirable cell clusters circled blue.

3.2.3 Quantitation of BEC number held within each ST device

The number of BECs levitated, then dispensed from each device required quantitation. Total BECs levitated was a measure of device acoustic strength and resistance to GM perfusion. Variability between devices would need to be addressed but potentially lead to levitation protocol or device development. Data was also needed to provide more accurate single BEC controls.

The CyQuant NF dye kit (Thermofisher) was selected but required protocol optimisation. First, a standard curve of known cell number was needed using the kit. To determine optimal incubation time with the dye: fluorescence intensity was measured at three time-points and was greatest after 60 minutes (Figure 3.2.3.1A). No considerable change of fluorescence intensity was seen using a clear-bottom 96-well plate, as opposed to a black-bottom plate (Figure 3.2.3.1B). Therefore, clear-bottom plates of lower cost were preferable. Optimal CyQuant dye dilution was determined as 1:1000. Only a marginal drop in fluorescence intensity was seen against the recommended dilution of 1:500 (Figure 3.2.3.1C).
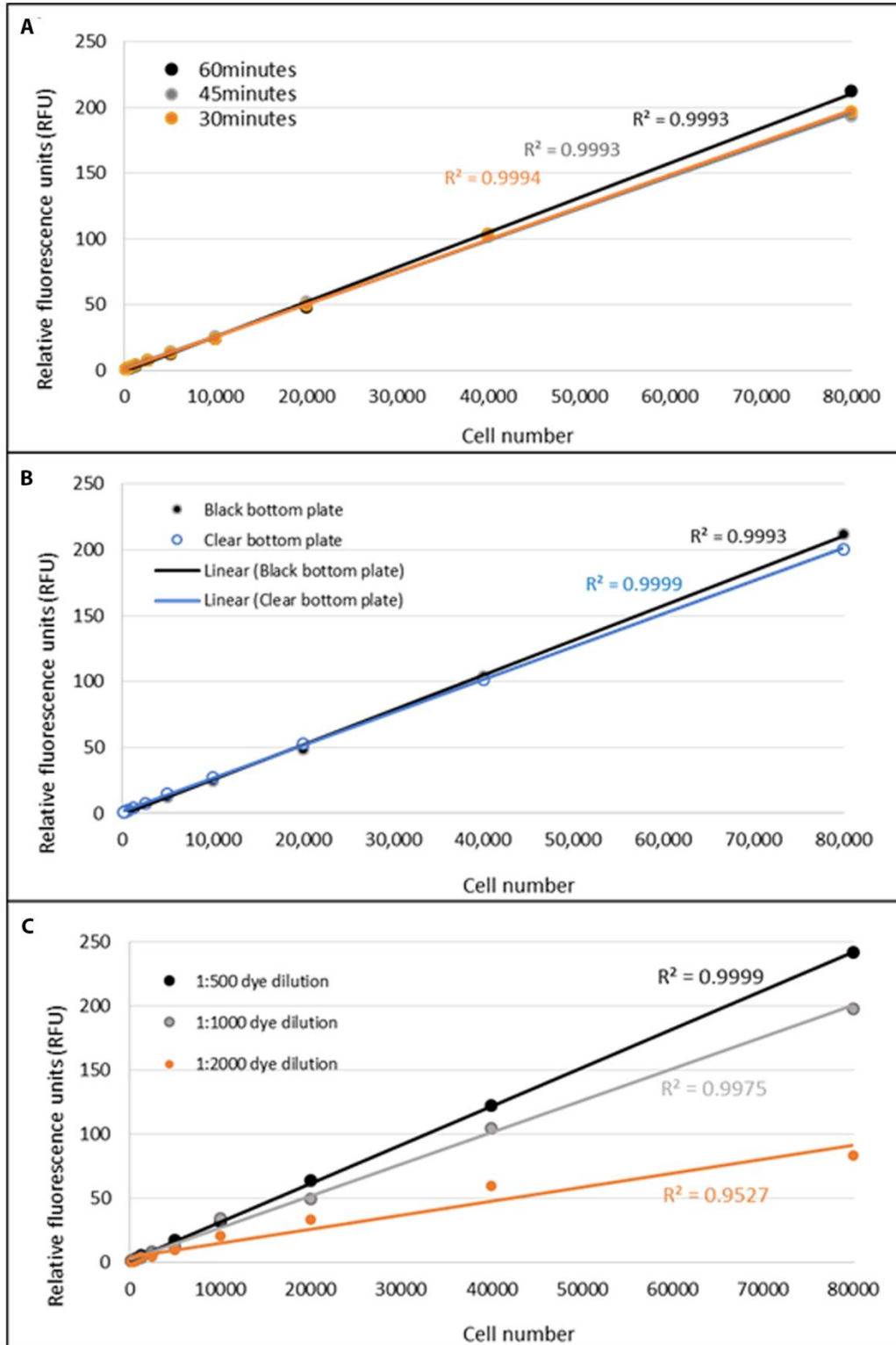
Figure 3.2.3.1 Optimisation of CyQuant dye protocol to produce standard curve of BEC number. Single BEC suspension were prepared in eppendorf tubes, then incubated with CyQuant dye. Aliquots of known BEC number (500 – 80,000) were then loaded onto 96-well plates in duplicate, and fluorescence intensity measured using a plate reader. [A] Optimal dye incubation time was 60 minutes for maximum fluorescence (n=1). [B] Relative fluorescence was not reduced using lower cost clear-bottom plates instead of black (n=2). [C] The 1:1000 dye dilution provided an R^2 value >0.99 and was optimal (n=1). R^2 values are shown adjacent to trend-line.

Two racks of triplicate ST devices were loaded with single BECs by aspirating 30 µL of a single 2.0×10^6 cells/mL solution. Expected cell number levitated was derived from their PZT volumes: 18,000 ST1, 28,000 ST2-3, 26,000 ST4-5, and 14,000 ST6. Single BECs were levitated for two hours with perfusion after a 30-minute static phase then dispensed and quantitated using the optimised CyQuant dye protocol. For all six devices, levitated BEC number was higher than expected. However, the standard deviation each device was considerable, such that the positive relationship between PZT volume and levitated BEC number was not clear (Figure 3.2.3.2).

Considerably lower values of 4,418 and 3,228 levitated BECs, from ST5 and ST6 devices respectively, could be attributed to dispensing error when ejecting cells into eppendorf tubes. If these values are excluded, all six devices levitated >20,000 BECs each experiment. Considerably higher BEC counts of 41,390 or 40,754 could be attributed to settled single cells, acquired during the loading or removed from the pressure node via perfusion; or increased loading solution density, due to cell count inaccuracy and non-homogeneous distribution in the loading wells.

Device	Experiment			Mean	StDev
	1	2	3		
ST1	36,316	36,410	28,585	33,770	4,491
ST2	18,801	25,671	36,344	26,939	8,840
ST3	24,207	32,420	40,754	32,460	8,274
ST4	10,671	41,390	30,046	27,369	15,533
ST5	4,418	34,960	41,931	27,103	19,953
ST6	3,228	27,306	34,626	21,720	16,427
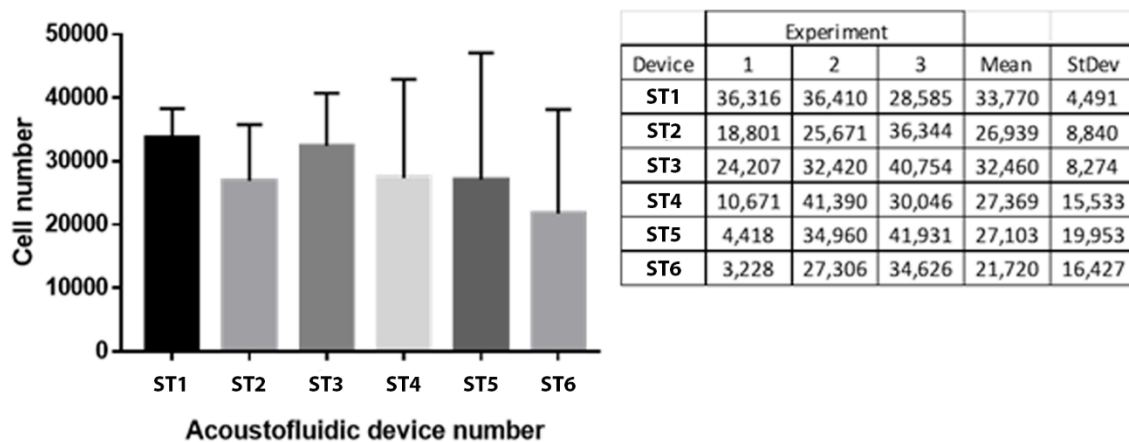
Figure 3.2.3.2 Quantitation of BECs expelled from each ST device after two hours levitation with growth media perfusion.
Using the optimised perfusion and CyQuant NF dye quantitation protocols (1: 1000 dye dilution with RA, using clear bottom plate, and plate read after 60 minutes) average BEC sheet cell number was calculated for 6 small transducer devices across 3 levitation experiments. Devices held 21-34,000 cells with high variability. ST1-3 devices performed more consistent than ST4-6. Results are mean +/- standard deviation for each device, n=3 biological replicates. To the right is the data table showing individual cell number each experiment with mean and standard deviation.

3.2.4   BEC sheet culture physical barrier development

Before exploring levitated BEC number further, it was critical that the functionality of all BECs (cohesive sheet or singular) to be measured and maintained after two hours levitation. Seeded BEC sheet cultures created using the ST1-3 devices were maintained for 18 days, along with non-levitated controls of equivalent BEC number (20,000) and the established TW-insert model (150,000). Physical barrier formation was monitored using fluorescence microscopy and by reading TER: which measured the resistance of ions moving through the BEC layer. TER readings greater than 1,000 ohms were indicative of TJ formation, and therefore a physical barrier.

BEC sheets typically developed a barrier day 13 whereas 150,000 single BEC controls peaked day 4 then steadily decreased due to over-confluence. The 20,000 single BEC control developed a barrier much faster than the levitated equivalent (day 5) (Figure 3.2.4.1), which could be attributed to greater dispersal within TW inserts, and unrestricted growth and proliferation.

BEC sheet cultures became confluent day 11 (ST3) or day 13 (ST1, ST2). Growth and expansion were relatively slow and limited by co-ordinated sheet movement. By comparison, 150,000 and 20,000 single BEC control cultures became confluent day 4, and day 6 respectively (Figure 3.2.4.2). With successful barrier formation established, AF device design could be further developed for BEC sheet creation.
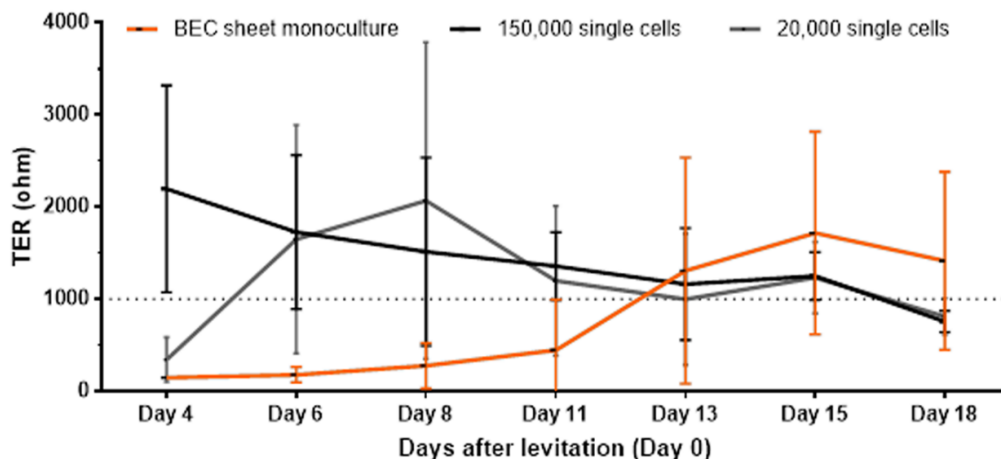
Figure 3.2.4.1 Physical barrier development of BEC sheet cultures over time.
To create BEC sheets, GFP-BECs were levitated for two hours with flow using triplicate ST devices. BEC sheets were seeded onto collagen-coated TW-inserts with non-levitated 150,000, and 20,000 single BECs seeded as controls. TER was measured using chopstick electrodes with a voltohmmeter over 18 days, with values >1000 ohm indicative of a physical barrier. The 150,000 and 20,000 single BEC control wells develop a barrier day 4 and day 6 respectively, whereas collective BEC sheet cultures develop a barrier day 13. Results are mean +/- standard deviation from: n=3 (BEC sheet) or n=2 (single BEC) technical replicates, and n=3 biological replicates.

46
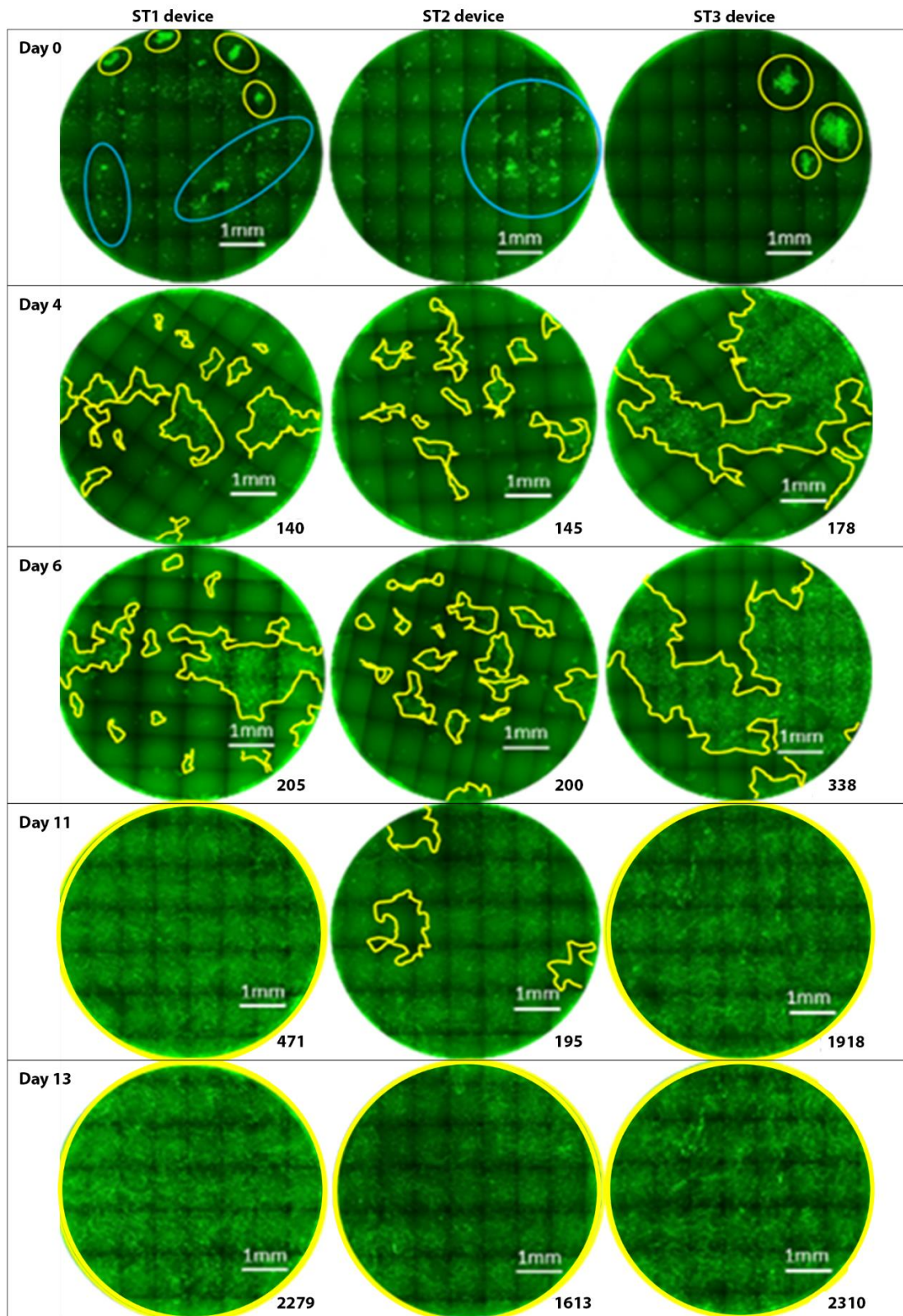
Figure 3.2.4.2 Fluorescence images show barrier development of BEC sheet cultures.
To create BEC sheets, GFP-BECs were levitated for two hours with flow using triplicate ST devices. BEC sheets were seeded onto collagen-coated TW-inserts, with TER readings and GFP-FLUO tile scan images acquired over 13 days. Average BEC sheet cultures reached confluence 11-13 days post-levitation. Large BEC sheet edges are circled yellow, and clusters of smaller BEC sheets are circled blue. TER is shown bottom right for each image.

3.3 Tubing-tipped large transducer device development

The prototype large transducer device (LT1) was created to address issues with BEC sheet size, single BEC presence, and to allow visualisation of BECs while levitating.

3.3.1 Modified LT1 design allows visualisation of improved BEC sheet creation

To increase the size and number of levitated BEC sheets, LT1 utilised a 25 × 6 mm PZT poly-cemented to a glass capillary (50 × 6 × 0.3 mm) and subjected an increased 45 µL volume to acoustic force (PZT volume). It was possible that settled BECs were later released during BEC sheet seeding, so the volume where single BECs might settle after loading (the loading volume) was reduced by to 22.5 µL by PZT placement (Figure 3.3.1.1A).

To allow BECs to be visualised using fluorescence microscopy while levitating, the capillary was adhered to a glass slide and microscope stage-fitted plastic holder with a PZT volume viewing window. To aspirate cells/perfuse GM without contaminating the microscope hood, either end of the capillary was attached to 0.3 mm outer diameter (OD) tubing and sealed with heat-shrink plastic. The signal generator was kept outside of the microscope hood and a signal conducted via clippers to copper wire electrodes. The hood environment was sealed and maintained at 37C, 5% CO_2 using heating and control units (Figure 3.3.1.1B).
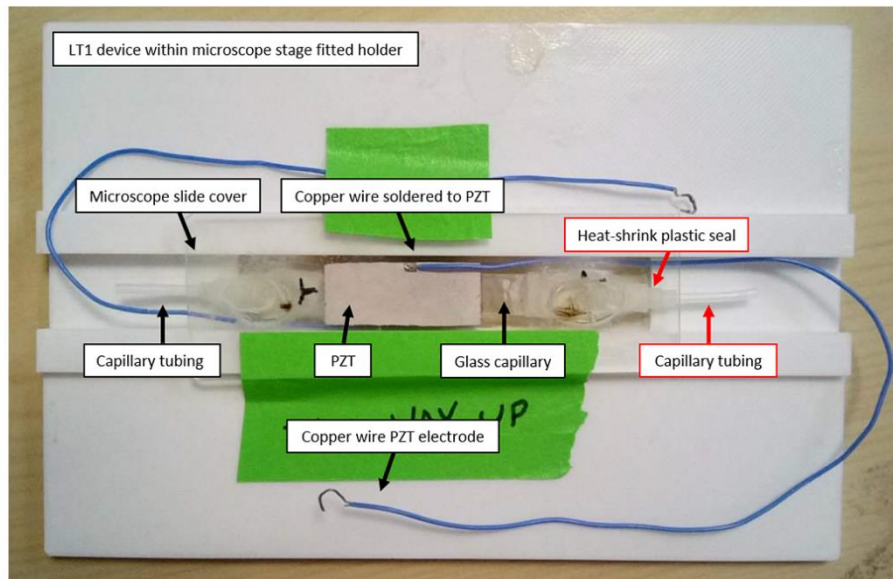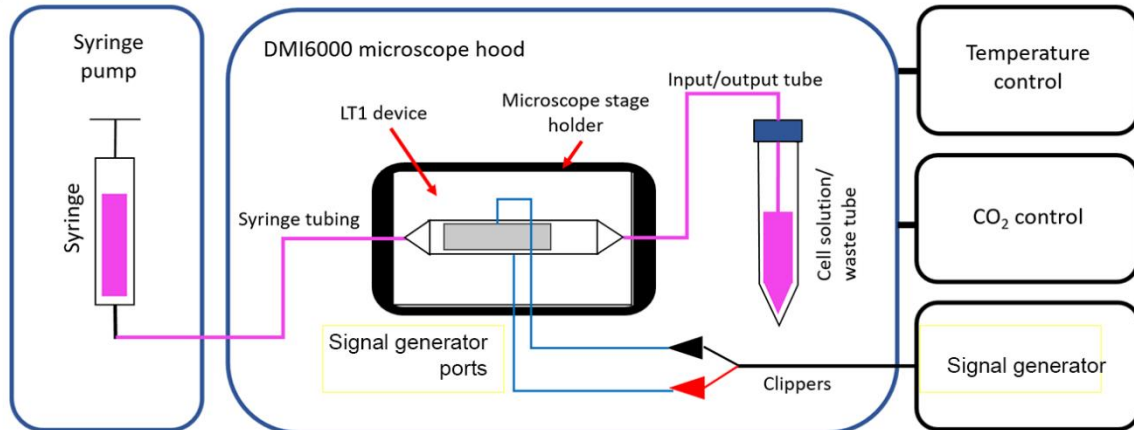
Figure 3.3.1.1 Newly developed LT device design allows visualisation of BECs while levitating.
[A] Labelled image of developed LT1 device. The PZT is 25 mm in length and creates a larger 45 µL PZT volume for BEC sheet creation. Both ends of the device are attached to 0.1 mm capillary tubing, sealed with heat-shrink plastic. The device sits within a microscope stage-fitted holder with a viewing window to allow visualisation below the PZT volume. [B] Diagram of the experimental set-up. Temperature and CO_2 control units keep the microscope hood environment at 37°C, 5% CO_2. The PZT is connected to the signal generator via copper wire electrodes and clippers. Single BECs are aspirated into the device via capillary tubing using a syringe of GM (held within a pump), and falcon tube of cell suspension.

3.3.2 Determining the frequency sweep required for LT1 device operation

For 2D planar levitation, the correct acoustic signal was needed. PZT impedance to an alternating electric current (AC) of increasing frequency (MHz) was measured using an oscilloscope. Readings were taken while loaded with deionised water (dH_2O) as a fluid medium, and while empty. To allow easier analysis of this data, the Spectrograph software was then used to calculate the susceptance and conductance [Bjorn Hammarstrom 2014], which can be described as the susceptibility of the PZT to the AC and it's acoustic output when coupled to the capillary.

A susceptance trough and conductance peak were present with a 2.35 MHz frequency exclusively when using a dH_2O medium (Figure 3.3.2.1). Respective troughs and peaks were of a similar frequency to those of ST devices, and are characteristic of a planar acoustic field within the glass capillary (resonator chamber). To account for secondary acoustic radiation forces after particle loading, LT1 was operated using a 0.1 MHz sweep (2.30 – 2.40 MHz) every 20 ms, and with the same 6.00 V peak-peak signal strength used previously with ST devices.
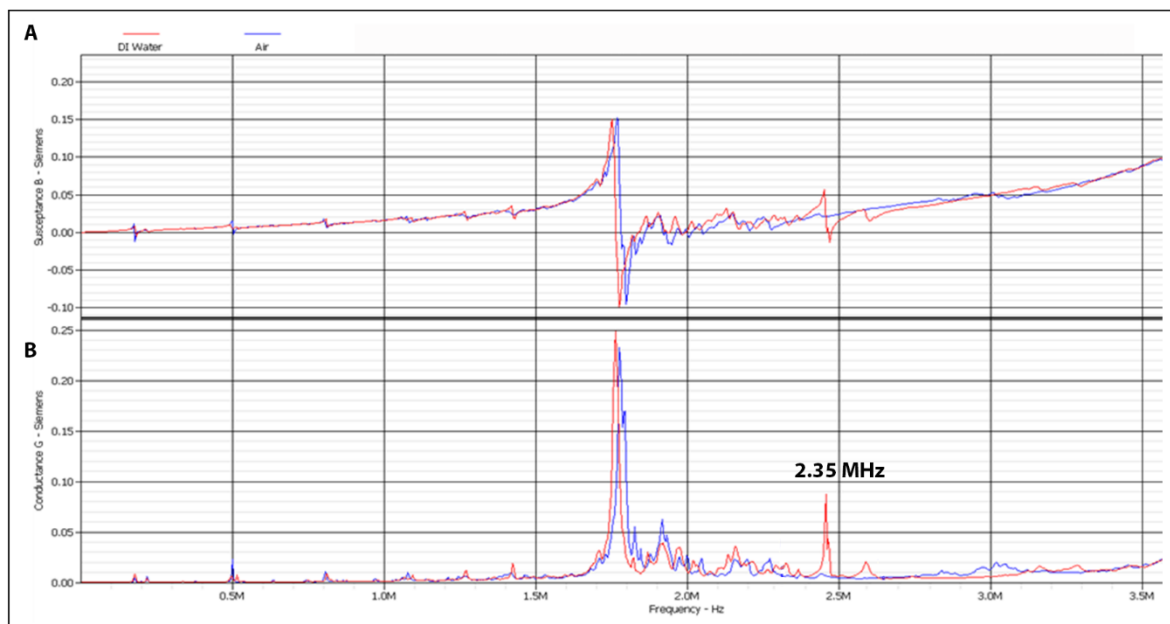
Figure 3.3.2.1 The spectrograph of LT1 device resonance, to determine acoustic signal frequency required for 2D planar levitation.
Susceptance of the LT1 device PZT to 0 - 3.5 MHz frequencies were measured using an oscilloscope: while loaded with dH_2O as a fluid medium, or empty. PZT conductance was calculated using susceptance readings. [A] Susceptance spectra showing a trough at 2.35 MHz when LT1 was loaded with dH2O (red) but not air (air). [B] Conductance spectra showing a peak at 2.35 MHz with dH2O but not air. Respective peaks and troughs at 2.35 MHz signal suggest the creation of a 2D planar USWF.

3.3.3   LT1 device operation test using FLUO-labelled beads

Before using live cells, acoustic strength and device optics were tested using 10 µM GFP-labelled (FLUO) beads. LT1 was conditioned with 1X PBS then placed securely within the microscope stage before aspirating 90 µL of a 2.0 x 10^6 /mL FLUO-bead solution. Images of the PZT-volume were acquired using the GFP-channel over 10 minute's levitation. A tile scan at 5x magnification shows beads successfully loaded across the whole PZT-volume, areas of high bead concentration exhibit GFP-background fluorescence (Figure 3.3.3.1A). Single images at 10x magnification show individual beads levitating within the same focal plane, either in narrow lanes (Figure 3.3.3.1B, C) or more rounded aggregates (Figure 3.3.3.1D) with limited background fluorescence. After successful levitation and imaging of particles within the PZT volume, live-cells were used for further characterisation of pressure nodes within the PZT-volume and how aggregates form within them.
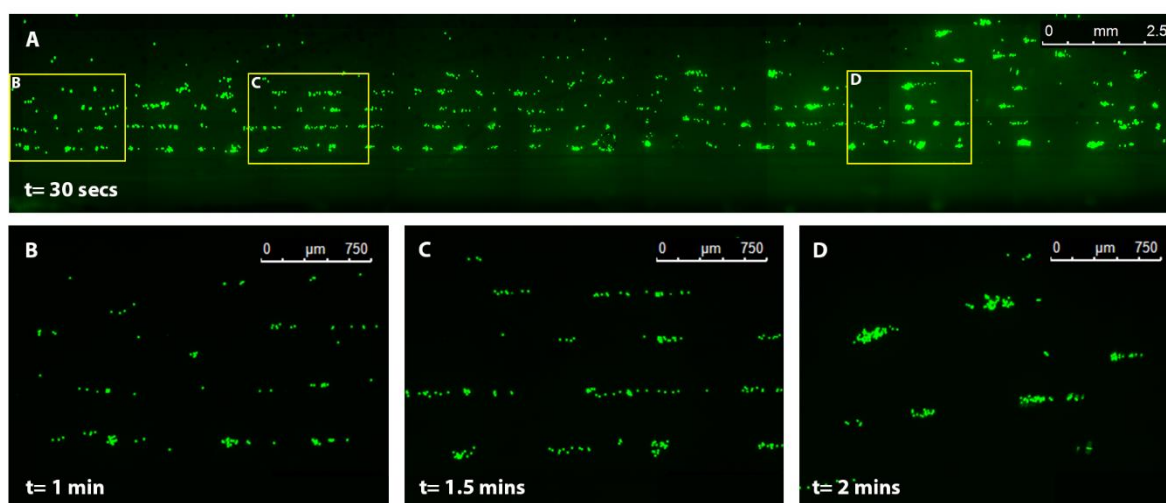
Figure 3.3.3.1 Images of LT1 device operation test using GFP-labelled beads.
With a glass syringe, 90 µL of a 2.0 x 10^6 bead/mL solution was aspirated into the LT1 device with fluorescence images taken over two minutes levitation. [A] 30-second tile scan image showing FLUO-beads across the whole PZT volume and background/auto fluorescence surrounding concentrated beads areas. Yellow rectangles show the location of higher magnification single images [B, C, and D] of FLUO-bead aggregates across the PZT volume.

3.3.4 Characterising aggregate formation within LT1 device pressure nodes

After successful visualisation FLUO-beads levitated within LT1, live cell experiments were performed using BECs. To characterise initial aggregate formation within LT1 pressure nodes: a 2.0 x 10^6 cells/mL 16HBE solution was prepared and pre-loaded with Hoechst33342 live-nuclear stain. The LT1 device was conditioned with equilibrated GM using the syringe pump, then placed within the microscope hood. To load 180,000 single BECs into the device: 90 μL of a 2.0 x 10^6 cells/mL suspension was aspirated via the capillary tube.

Cell nuclei were brought into focus as they entered the left side of the PZT volume using the DAPI-FLUO channel, and videos acquired 10-60 seconds after cell loading (Figure 3.3.4.1.1). BECs remained in focus as they entered the PZT volume, which confirmed they were levitating within a planar pressure node but were divided into narrow lines, suggesting areas of higher acoustic force (lateral nodes) created by acoustic streaming within the device. Within a few seconds of flow forces subsiding, BECs aggregated in either direction at select points within lateral nodes.

From 10-20 seconds central aggregates at the left side of the device were seen merging bi-laterally (Figure 3.3.4.1A), due to secondary acoustic forces created by the presence of cells. At the centre of the device evidence for the bilateral merging of aggregates is seen, but the interplay of acoustic forces appears in equilibrium (Figure 3.3.4.1B). At the far end of the device, several lateral node aggregates have merged bilaterally and begun reshaping into a more rounded aggregate as secondary forces continue transforming the node (Figure 3.3.4.1C).

After 5 minutes levitation, a tile scan image shows evidence of further bilateral merging of the central aggregates, and more rounded aggregates either end of the PZT volume (Figure 3.3.4.1D). Fluorescence tile scan images were converted to Greyscale using the ImageJ software to visualise smaller aggregates better. The entire length of the PZT volume contains multiple rows of peripheral aggregates that have not merged bi-laterally and remain <50 μM in width, and are therefore undesirable for BEC sheet cultures (Figure 3.3.4.1E).
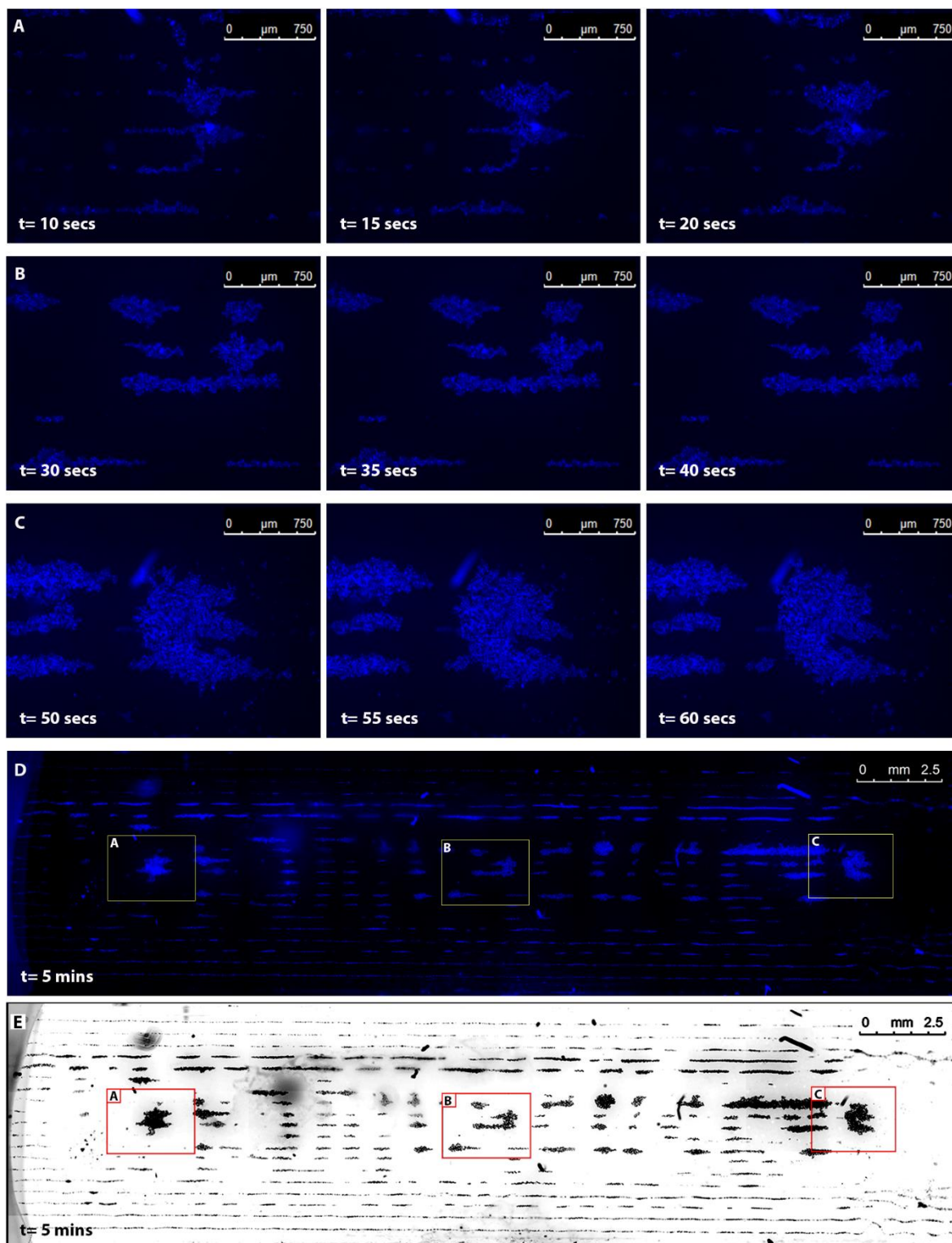
Figure 3.3.4.1 Fluorescence imaging of initial BEC aggregate formation within the LT1 device.
To load the LT1 device with 180,000 single BECs, a 2.0 x 10⁶ cells/mL suspension was pre-loaded with Hoechst33342 nuclear stain (blue), then 90 μL aspirated. Fluorescence videos and images were acquired immediately after loading across the PZT volume. [A] Bilateral merging of BEC aggregates (left). [B] Merged aggregates now static (centre). [C] Large, rounded aggregate reshaping within its node (right). [D] Tile scan image of PZT volume after 5 minutes levitation showing location of BEC aggregates and therefore pressure nodes. [E] Greyscale image of 5-minute tile scan to better visualise narrow peripheral aggregates. Yellow and red rectangles show the location of acquired videos.

54

BECs were levitated without GM perfusion for 30 minutes, followed by 90 minutes of 2 µL/min perfusion to remove unwanted single BECs and keep BEC aggregates well fed. Tile scan images were acquired at regular intervals from 30-minutes (Figure 3.3.4.2A) to 120-minutes levitation (Figure 3.3.4.2B), then converted to Greyscale.

After 30 minutes multiple large BEC sheets 200-800 µM in size were seen across the centre of the device surrounded by smaller central node clusters (Figure 3.3.4.2C), which then merge bilaterally and with the direction of flow for two hours to become larger still (Figure 3.3.4.2D).

Distinct peripheral aggregates were also present after 30 minutes and have remained static (Figure 3.3.4.2E). Peripheral aggregates resist flow forces and remain largely unchanged after two hours levitation with perfusion (Figure 3.3.4.2F), this can largely be attributed to parabolic flow dynamics within the capillary where flow forces are strongest towards the centre and weakest toward the internal surfaces, as well as acoustic streaming.

Peripheral nodes pose a challenge to BEC sheet creation: neither merged aggregates into larger BEC sheets or removed via GM perfusion. It was possible that central lateral nodes were at capacity, allowing cells to enter the weaker peripheral nodes upon device entry.
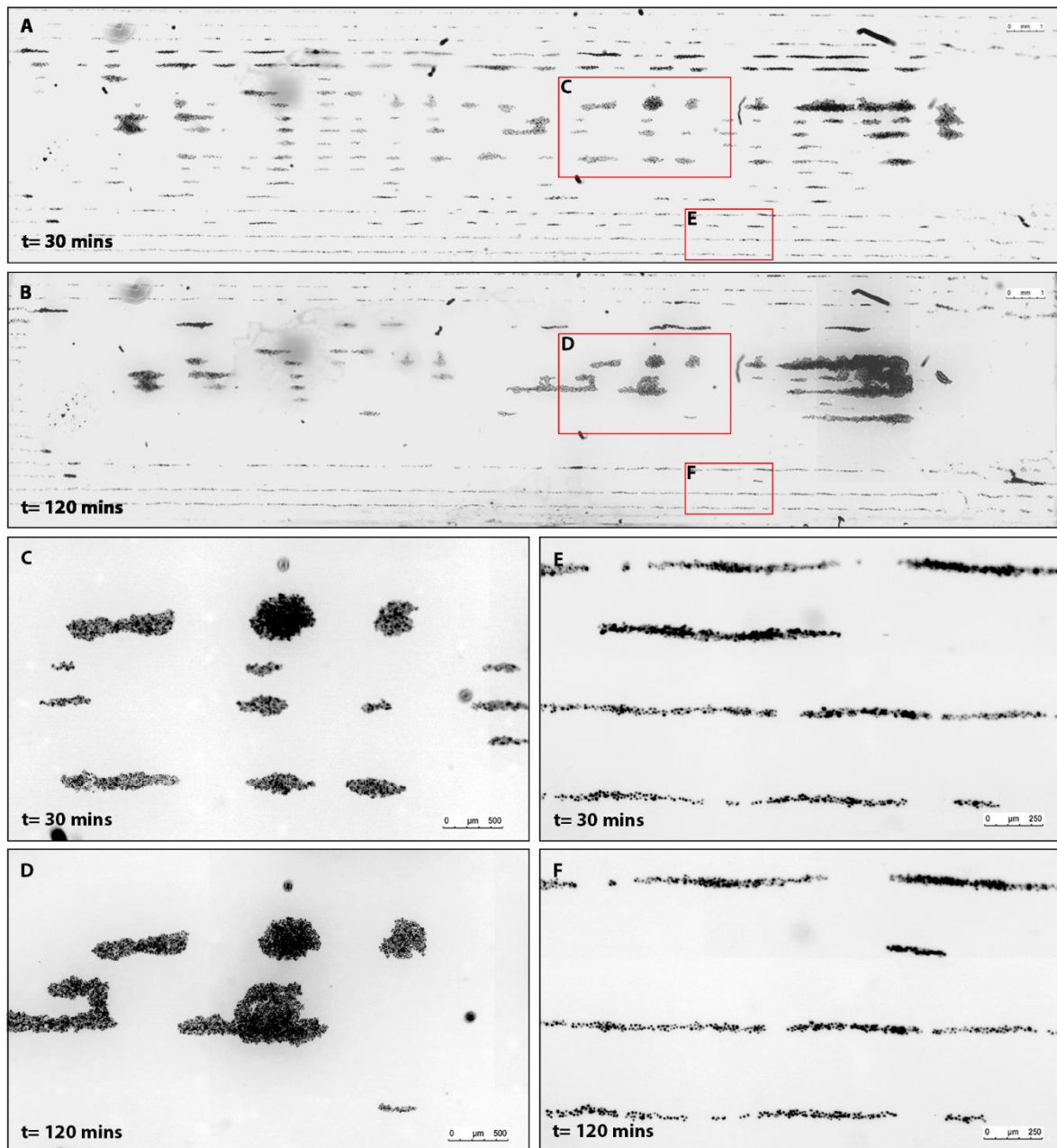
Figure 3.3.4.2 Fluorescence imaging of BEC aggregate formation over two hours levitation within the LT1 device.

To load the LT1 device with 180,000 single BECs, a 2.0 x 10^6 cells/mL suspension was pre-loaded with Hoechst33342 nuclear stain (blue), then 90 µL aspirated. [A] Tile scan image after 30 minutes before perfusion start. [B] Tile scan image after 120 minutes levitation. Red rectangles show the location of snapshot images. [C] 30-minute snapshot of large central aggregates. [D] 120-minute snapshot of merged central aggregates. [E] 30-minute snapshot showing multiple rows of peripheral aggregates. [F] 120-min snapshot of largely unmoved peripheral aggregates.

3.3.5 Reducing cell number to prevent LT1 pressure node over-loading

LT1 device central pressure nodes were overloaded with 180,000 BECs. Thus, the cell-loading solution density was reduced from 2.0 to 1.5 x 10^6 cells/mL to load 135,000 BECs instead. BECs were levitated for two hours with 2 µL/min GM perfusion after a 30-minute static phase. Tile scan images acquired using the DAPI-FLUO channel, then converted to Greyscale using the ImageJ software as before.

After 10 minutes levitation peripheral nodes remained clear, aggregates were seen exclusively in central nodes, split into nine parallel rows either end of the PZT volume (Figure 3.3.5.1A). After two hours levitation with perfusion, aggregates converged to create sheets greater than 50 µM length and width (Figure 3.3.5.1B). Due to flow force-mediated sheet migration and merging, BEC sheets are smaller at the syringe-end of the PZT volume (Figure 3.3.5.1C, D), compared to sheets at the loading end (Figure 3.3.5.1E, F).

This loading technique was repeated with four separate experiments and imaged after 5 or 10 minutes of loading. For two experiments, BECs remained entirely outside of the peripheral nodes (data not shown). However, there was a noticeable disparity between the total number of cells levitating within the PZT volume between these two experiments. Another two levitation experiments (imaged within 5 minutes of loading) appeared to have a comparable number of BECs levitating within PZT volume, but both had a small population of BECs levitating within peripheral nodes (data not shown).

After preventing most peripheral node aggregate formation using a reduced cell number (removing all peripheral node aggregates might not be achievable or necessary), further variables were investigated to provide more reliable BEC sheet formation within central nodes.
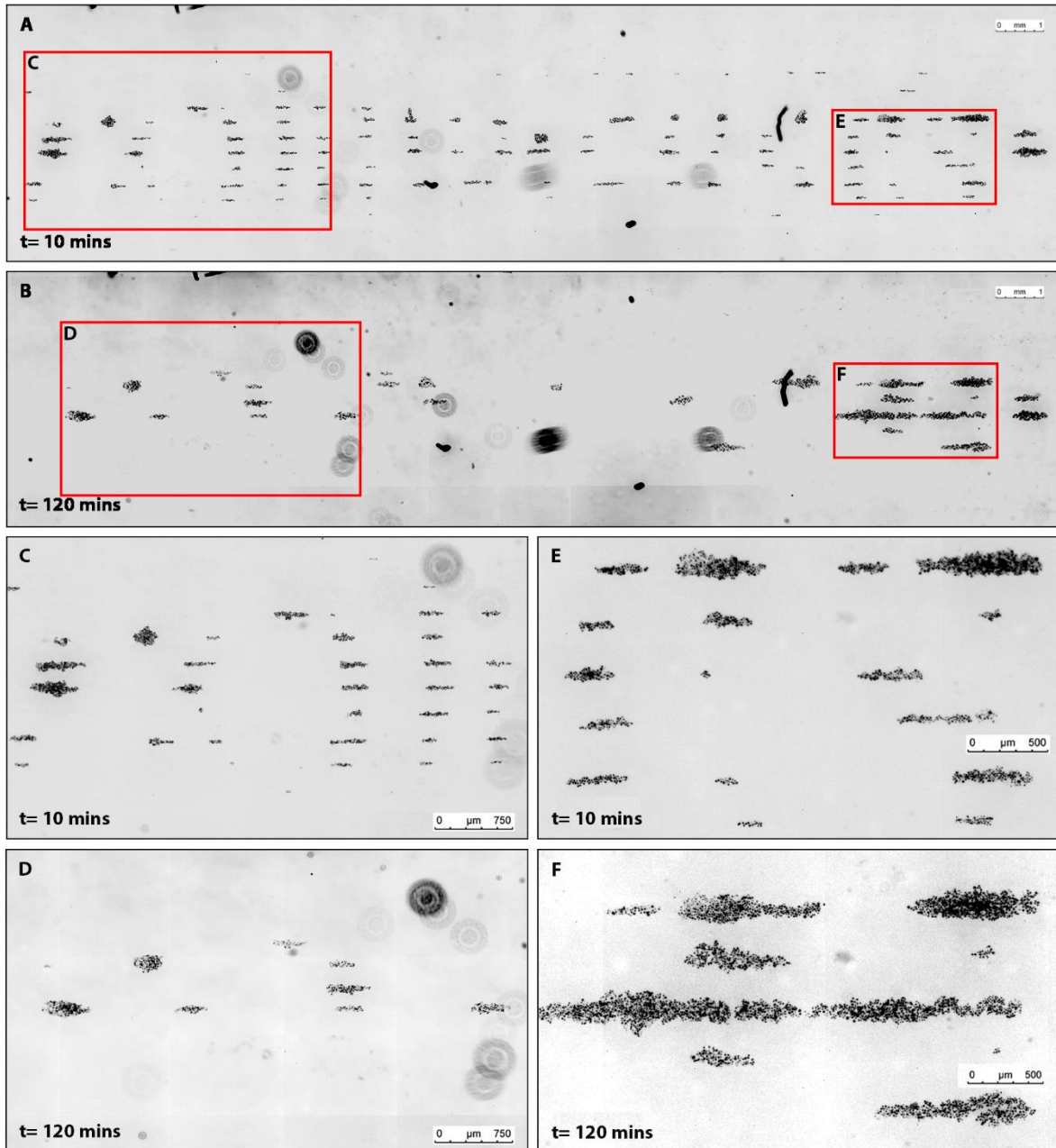
Figure 3.3.5.1 Fluorescence imaging shows reducing BEC number prevents peripheral node aggregate formation within the LT1 device.
To load the LT1 device with 135,000 single BECs, 90 µL of a Hoechst pre-loaded, 1.5 x 10^6 cells/mL suspension was aspirated. BECs were levitated for two hours with GM perfusion after a 30-minute static phase. Fluorescence tile scan images were acquired after [A] 10 minutes, and [B] 120 minutes levitation, then converted to greyscale. Red rectangles show the location of snapshot images. [C] 30-minute and [D] 120-minute images show the bi-lateral merging of central aggregates left side of the PZT and the absence of peripheral node aggregates. [E] 30-minute and [F] 120-minute images right side of the PZT show lateral and bi-lateral merging, and transit of central BEC aggregates across the PZT volume.

3.3.6 Investigating effect of static phase length on BEC sheet formation

Static phase length and its effect on BEC sheet formation were next investigated. Static phase length was reduced periodically from 30 minutes to 30 seconds, in favour of keeping BECs supplied with fresh GM as soon as possible after loading. Static phase levitation experiments were performed on separate days. Tile scan images were acquired over two hours and used to measure the length, width, and number of BEC sheets (Figure 3.3.6.1/2).

The 30-minute static phase experiment shown previously (Figure 3.3.5.1) provided 91 aggregates that merged steadily into 25 aggregates over two hours (30 min static). The first 15-minute static phase experiment provided desirable BEC aggregates within central nodes, which converged into a singular ~4 mm aggregate and six others after two hours levitation with perfusion (15 min static_1). An experimental repeat provided a much smaller number of aggregates which merge more evenly from 19 to 8 aggregates of similar size (15 min static_2).

Two 5-minute static phase experiments had similar BEC aggregate number and distribution after 10 minutes levitation (60 and 61) but were again highly variable after two hours with flow. For one experiment, the number of aggregates approximately halved from 60 to 31 of similar size (5 min static_1). Whereas all 61 aggregates of the repeat experiment merged into a singular aggregate 3,290 x 893 µM in size (5 min static_2).

Lastly, the 30-second static phase experiment provided 35 BEC aggregates immediately after loading. Interestingly, aggregates did not merge evenly or into a single aggregate after two hours levitation. Instead, aggregates became more rounded and moved with the direction of flow across the PZT volume (30 sec static).

Flow-mediated-aggregate merging was highly variable and irrespective of static phase length. Levitating BECs without perfusion could potentially increase consistency of BEC sheet formation after two hours, by removing flow-forces and aggregate drag forces as a factor of BEC sheet merging. However, it was possible that GM perfusion maintained BEC sheet viability, and could not be removed from the protocol.
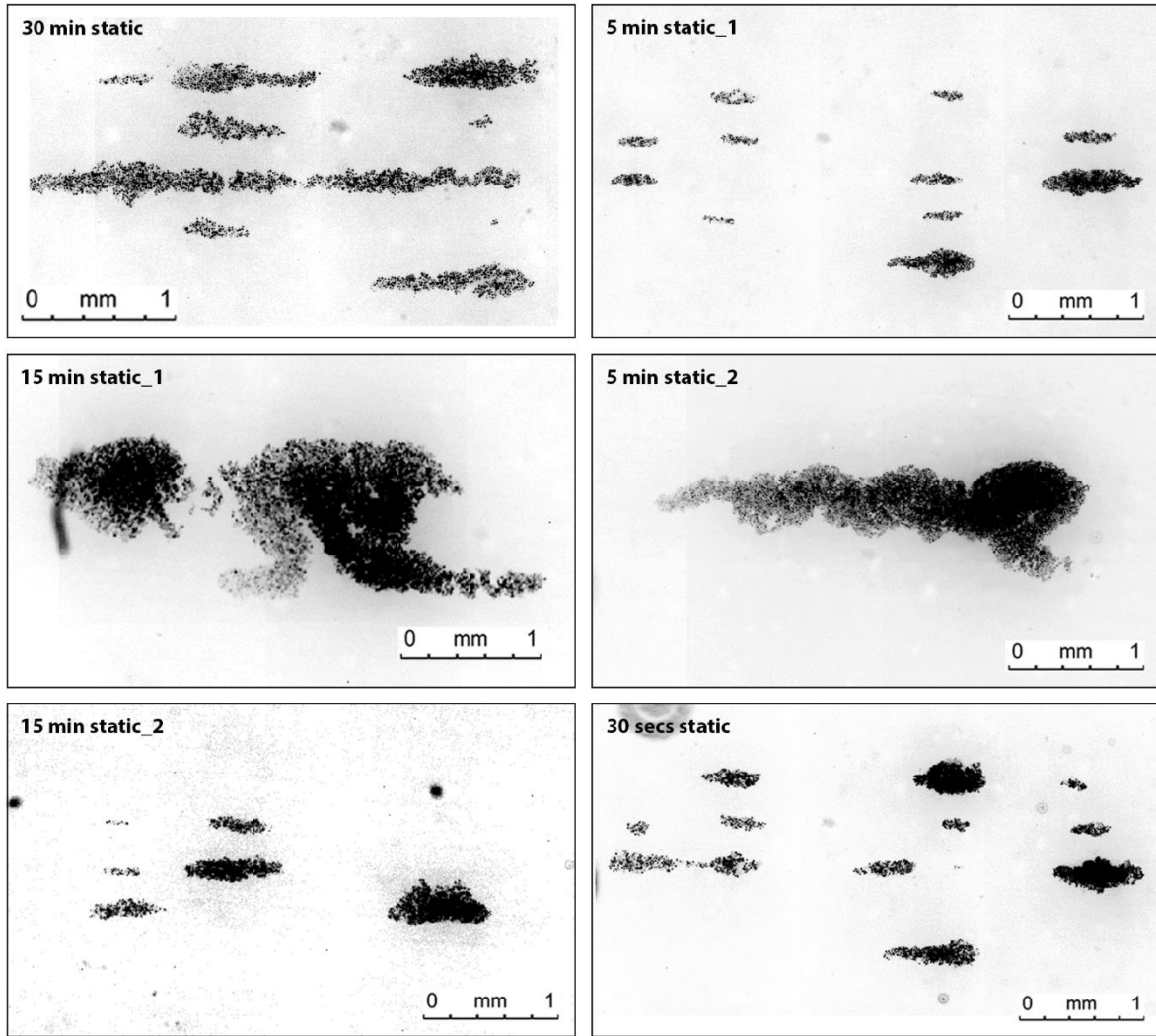
Figure 3.3.6.1 Fluorescence imaging shows variable BEC aggregate formation after two hours levitation within the LT1 device.
BECs were levitated for two hours within the LT1 device using either a 30-minute (n=1), 15-minute (n=2), 5-minute (n=2), or 30-second (n=1) static phase before 2µL/min GM perfusion. Fluorescence images acquired right side of the PZT then converted to greyscale, show variable BEC aggregate formation after two hours irrespective of static-phase length due to lateral and bi-lateral merging.

60
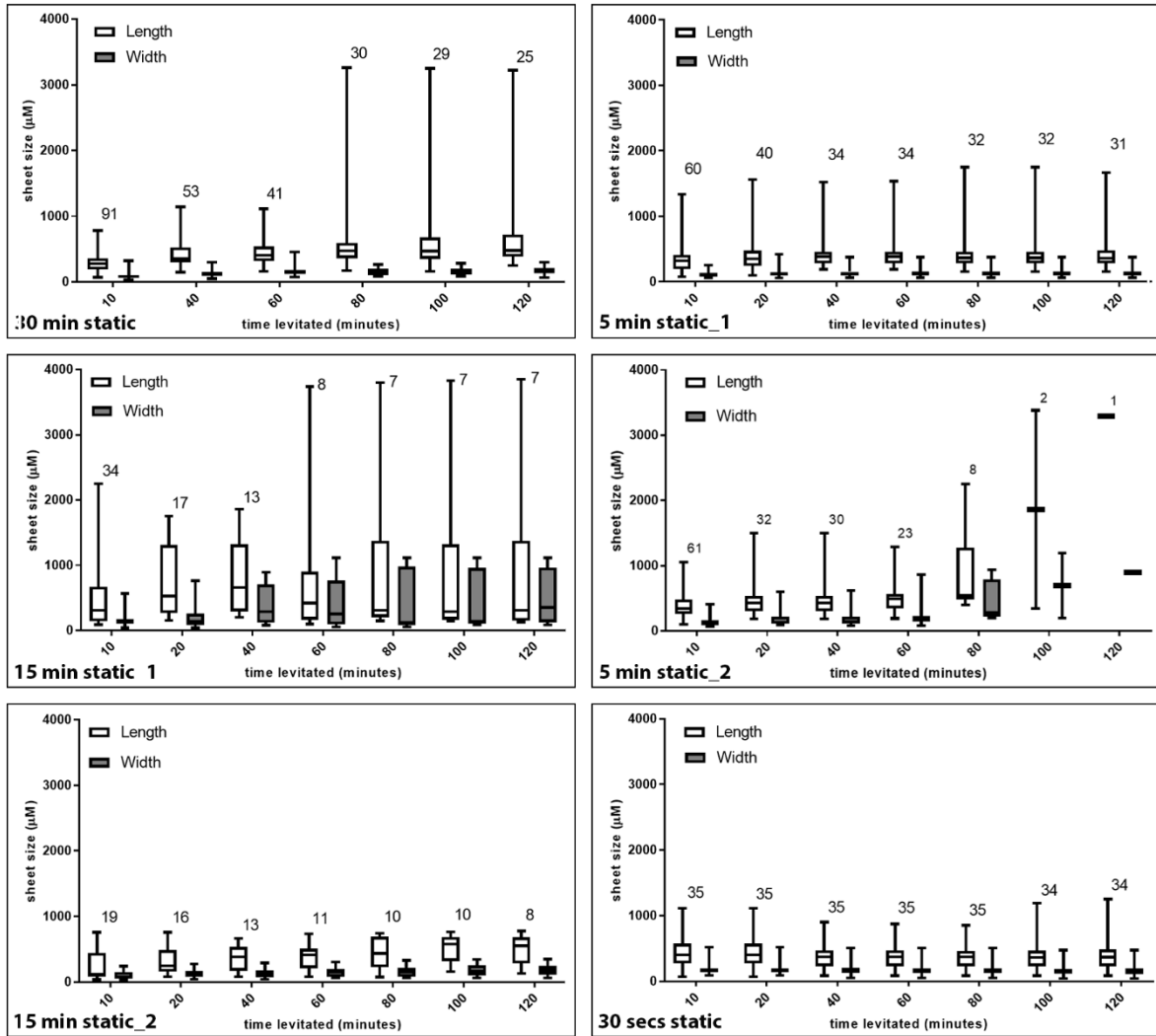
Figure 3.3.6.2 Graphs show variable BEC aggregate formation after two hours levitation within the LT1 device.
BECs were levitated for two hours within the LT1 device using either a 30-minute (n=1), 15-minute (n=2), 5-minute (n=2), or 30-second (n=1) static phase, before 2µL/min GM perfusion. Aggregate number, length, and width was measured using fluorescence tile scan images. Neither initial aggregate formation, or bilateral merging correlated between replicate experiments: either forming a singular large BEC sheet or remain as multiple smaller sheets. Box and whiskers denote the median and inter-quartile range of BEC sheet length and width. Numbers above show total BEC sheet number.

3.3.7 Reduced signal generator strength increases BEC sheet viability

BEC aggregate viability while levitating was investigated using plasma membrane-impermeable NucGreen viability dye (Invitrogen, UK). For all static phase experiments, NucGreen was added to equilibrated GM, then used for LT1 conditioning, suspending Hoechst-loaded BECs, and GM perfusion while levitating. Both NucGreen positive and negative nuclei were imaged while levitating in the PZT volume over two hours. Single BEC controls were also seeded onto collagen and imaged after two hours without levitation.

For all static phase experiments (including immediate GM perfusion) NucGreen staining increased steadily over two hours (Figure 3.3.7.1A) and appeared more prevalent than single BEC controls (Figure 3.3.7.1B). It was possible that acoustic force-GM protein interactions led to LT1 device over-heating, and steadily reduced the viability of BEC sheets while levitating.

To increase BEC sheet viability reducing the acoustic signal strength was explored. Three replicate experiments were performed using a 4.24 V signal, calculated as a 30% reduction in acoustic force. For two experiments, NucGreen positive nuclei incidence increased gradually over time but was comparable to seeded single BEC controls (Figure 3.3.7.1C, D). For the third experiment, NucGreen staining was greater than single BEC controls. NucGreen nuclei incidence was minimal but became moderate and strong either end of the PZT after two hours (data not shown).

BEC sheet viability was quantitated for both the 6 V and 4.24 V immediate perfusion experiments. Using tile scan images, NucGreen positive nuclei were counted at 40-minute intervals and calculated as a percentage of total Hoechst positive nuclei. Compared to the 6.0 V experiment (with immediate perfusion), NucGreen staining was reduced using a 4.24 V signal at each time point and was less than half after two hours levitation (Figure 3.3.7.2B).

Potential adverse effects of reducing device signal strength and BEC aggregate formation were also considered. Fortunately, BEC sheet populations were comparable in size and number to 6.0 V experiments; after two hours levitation with immediate perfusion (Figure 3.3.7.3).

Overall, levitating BECs with the reduced 4.24 V signal decreased NucGreen dye uptake, but did not explain the sudden onset of dye uptake with one experiment. For further investigation, viability dye needed to be added to BEC sheets after seeding but capillary tubing either end of the LT1 device prevented this. Therefore a device which allows both BEC sheet visualisation while levitating and seeding was needed.
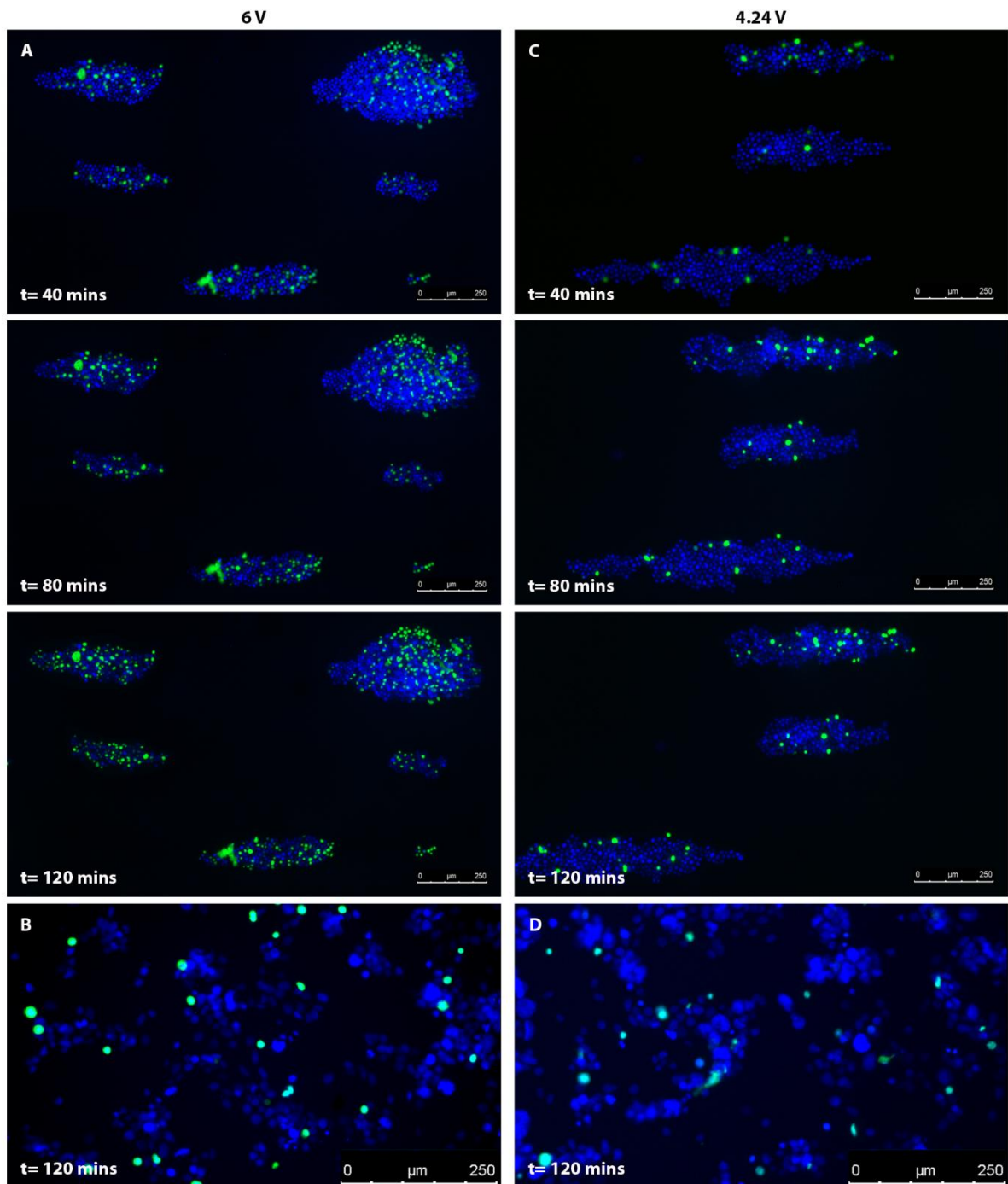
Figure 3.3.7.1 Fluorescence images show BEC sheet viability dye uptake when levitated using a 4.24 V signal strength within the LT1 device.

For viability analysis, single BECs were pre-loaded with Hoechst33342 (blue) and suspended in NucGreen GM. BECs were levitated for two hours within LT1 using either a 6.0 V (n=1) or 4.24 V signal (n=3) with immediate NucGreen GM perfusion. Non-levitated single BECs were seeded onto collagen as controls. [A] Fluorescence images of 6.0 V experiment show NucGreen staining of BEC sheets increases rapidly and is much greater than non-levitated control BECs [B] after two hours. [C] Fluorescence images representative of three 4.24 V experiments show relatively reduced NucGreen staining after two hours, that was more comparable to non-levitated control BECs [D].
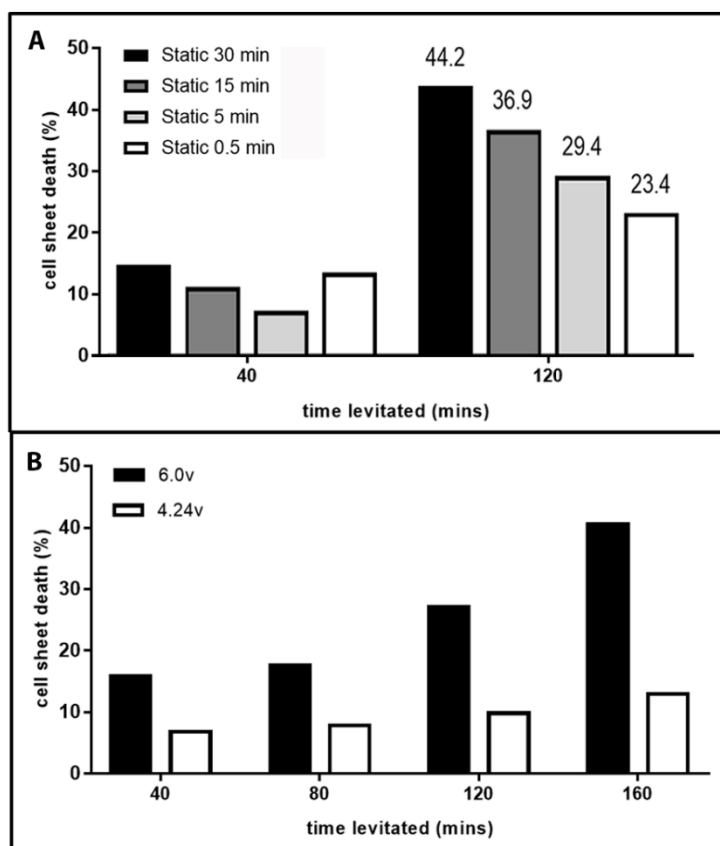
Figure 3.3.7.2 Immediate growth media perfusion and 4.24 V signal strength reduces BEC sheet uptake of NucGreen dye uptake after two hours levitation within the LT1 device.
BECs of variable static phase and reduced voltage experiments were levitated with GM containing NucGreen dye for viability analysis. Fluorescence imaging was used to count the number of non-viable BECs, and calculate them as a percentage of the total population. [A] Graph showing increased BEC sheet viability after two hours using shorter static phase before GM perfusion. Bars represent singular 30-minute and 30-second static phase experiments; and duplicate 15-minute and 5-minute experiments. [B] Graph shows increased BEC sheet viability after two hours levitation using 4.24 V acoustic signal. Bars represent a singular 6.0 V and triplicate 4.24 V experiments.
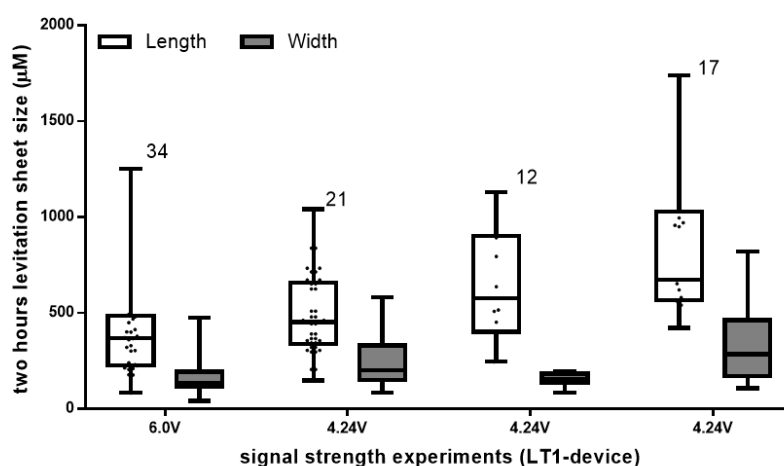
Figure 3.3.7.3 BEC sheet formation after two hours levitation using either a 6.0 V or 4.24 V signal.
Graph showing the total number and size of BEC sheets created after two hours levitation with immediate GM perfusion, for both 6.0 V and 4.24 V acoustic signal experiments. Box and whiskers denote the mean and inter-quartile range. Numbers show the total number of BEC sheets.

64

3.4 Open-tipped large transducer device development

To be able to seed created BEC sheets, a second large-PZT device (LT2) was developed.

3.4.1 Modified LT2 design allows both BEC sheet visualisation and seeding

Equipped with a single tubing end for syringe coupling and an open-end for single BEC loading/BEC sheet seeding (Figure 3.4.1.1A). A removable plastic holder was created with dimensions 75 × 25 × 100 mm, and fit within the microscope-stage glass slide holder. Devices were loaded by submerging the open end in a cell suspension and aspirating single BECs, then placing within the plastic holder and aspirating 90 µL, before inserting into the plastic holder, with attached lid and carefully placing on the microscope stage (Figure 3.4.1.1B).
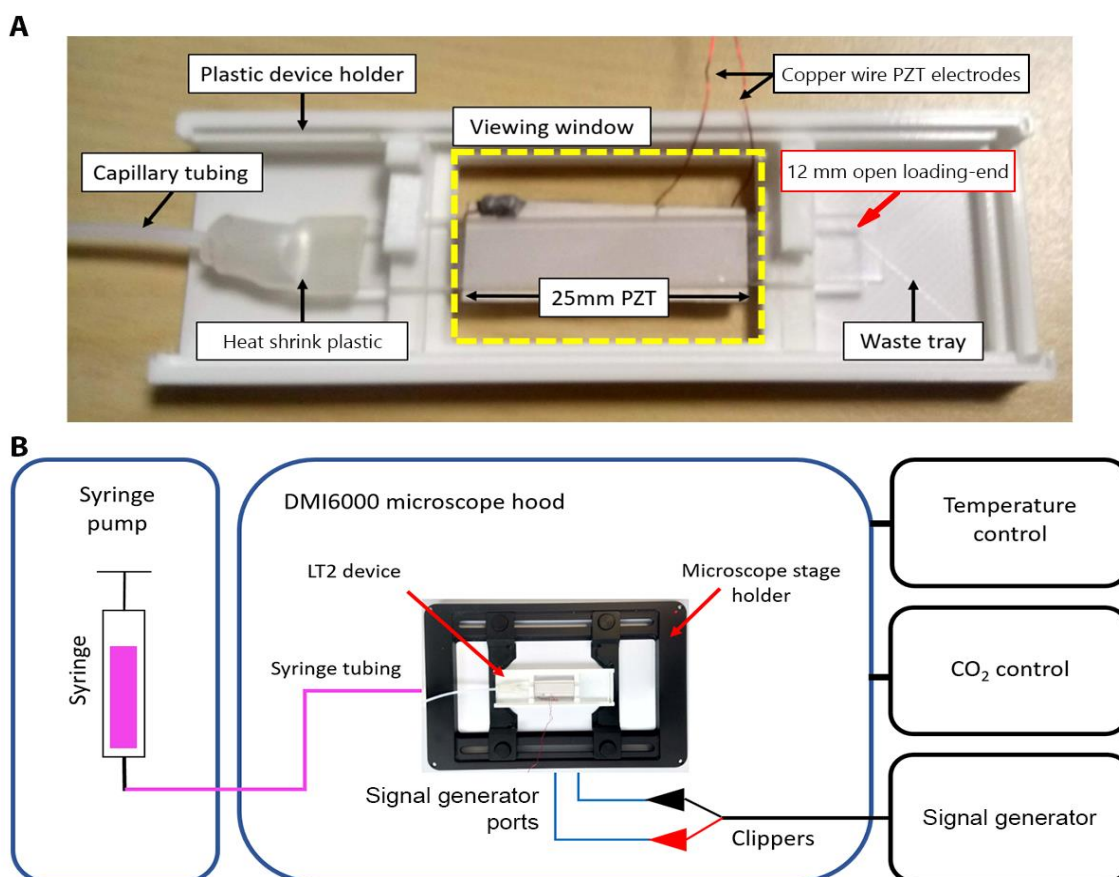
Figure 3.4.1.1 Newly developed LT2 device design allows seeding of created BEC sheets.
[A] Image of developed LT2 device with labelled features. A single end of the device is attached to 0.1 mm capillary tubing, sealed with heat-shrink plastic. The other end of the device is open-tipped for single BEC loading from a 24-well plate, and subsequent BEC sheet seeding. The device sits within a removable, microscope stage-fitted holder with a viewing window, and waste tray to collect perfused GM. [B] Schematic of the experimental set-up for LT2 device levitation experiments within the microscope hood. Temperature and CO_2 control units keep the microscope hood environment at 37°C, 5% CO_2. The PZT is connected to the signal generator via copper wire electrodes and clippers.

3.4.2 Aberrant acoustic pattern with LT2 device

The LT2 device was operated at 4.24 V peak-peak with a 2.39-2.49 MHz frequency sweep to capture its unique resonance spectra. After BEC loading lateral acoustic forces appeared much weaker than LT1, and after 10 minutes, all BECs remain within initial lateral nodes (Figure 3.4.2.1A). Central and peripheral BEC aggregates instead merged exclusively with the direction of 2 µL/min flow, and after two hours were located towards the PZT volume edge, or settled outside of the PZT volume. BECs levitated without flow, again showed very little/no lateral merging over two hours. Lateral pressure nodes were small, distinct, and arranged into an irregular diamond across the PZT volume flanked by peripheral nodes (Figure 3.4.2.1B).
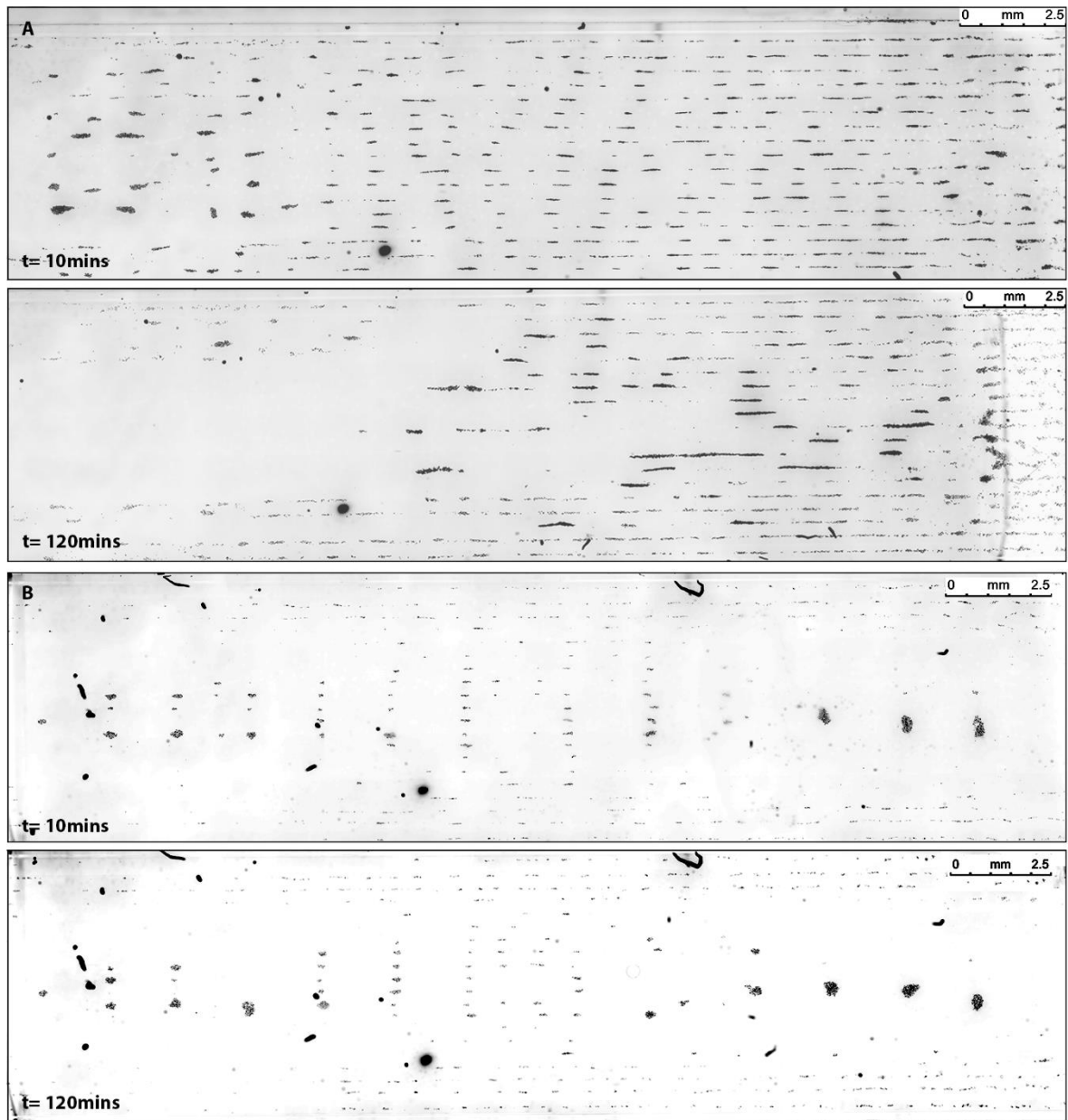
Figure 3.4.2.1 Fluorescence imaging of aberrant BEC aggregate formation within the LT2 device with and without growth media perfusion.
BECs were levitated for two hours using the LT2 device with and without immediate 2 µL/min GM perfusion. Fluorescence images were acquired after 10 and 120 minutes levitation, then converted to greyscale. [A] With flow, BEC aggregates only merge laterally or exit the PZT volume over two hours. [B] Without flow, BEC aggregates remain static and do not merge bilaterally after two hours.

3.4.3 Investigation of BEC membrane sonoporation while levitating

Despite the aberrant acoustic pattern shown previously, NucGreen dye sonoporation was explored using the LT2 device. BECs were levitated with/without NucGreen dye present (on separate days), using a 4.24 V signal output and immediate 2 μL/min GM perfusion after loading. After two hours, levitated BEC sheets were seeded into a collagen-coated 24-well plate containing 400 μL of GM, by immersing the open device tip then perfusing 100 μL of GM over 30 seconds, in addition single BEC controls were seeded after two hours in suspension.

Immediate DAPI-FLUO channel tile scan images, from the NucGreen sonoporation experiments, showed multiple BEC sheets settled either edge of the well (Figure 3.4.3.1A, D), or overlaid towards the centre (Figure 3.4.3.1B, C). A large population of single BECs and fibre contaminants were also present after seeding.

BEC sheets were allowed to settle for 45 minutes before adding NucGreen dye added to unstained wells. After an hour, whole-well tile scan images were taken using both the DAPI-FLUO and GFP-FLUO channels (Figure 3.4.3.2).

BEC sheets levitated with NucGreen GM contained an indistinct, dichotomous population of NucGreen positive nuclei: some were strongly stained and others more diffusely, such that membrane integrity remained ambiguous (Figure 3.4.3.2A, B). Cells were kept away from direct light and not imaged until after seeding so photobleaching was not responsible. More probable is sonoporation and the creation of micro-pores within plasma membrane of cells whilst levitatiing, allowing small amounts of NucGreen dye to cross the plasma membrane of a cell which was still intact, albeit temporarily more porous.

BEC sheets that were levitated without NucGreen GM also exhibited dichotomous staining, even when NucGreen was added one hour after seeding (Figure 3.4.3.2D, E): whether these nuclei were considered strongly or diffusely stained was another obstacle.

Conversely, the single BEC controls contained a small discrete population of NucGreen positive nuclei, and their viability was clear (Figure 3.4.3.2C). Additionally, NucGreen fluorescence intensity was only slightly reduced between the 3-hour and 15-minute incubation samples (Figure 3.4.3.2F).

Though this confirms the occurrence of sonoporation, it suggests a lasting effect on their plasma membrane post-levitation. How long BECs need to recover from sonoporation before accurate viability staining can be done, is not yet known and can be determined at a later date. After these experiments viability analysis was put on hold, so that the issue of BEC sheet seeding without single BECs present could be addressed.
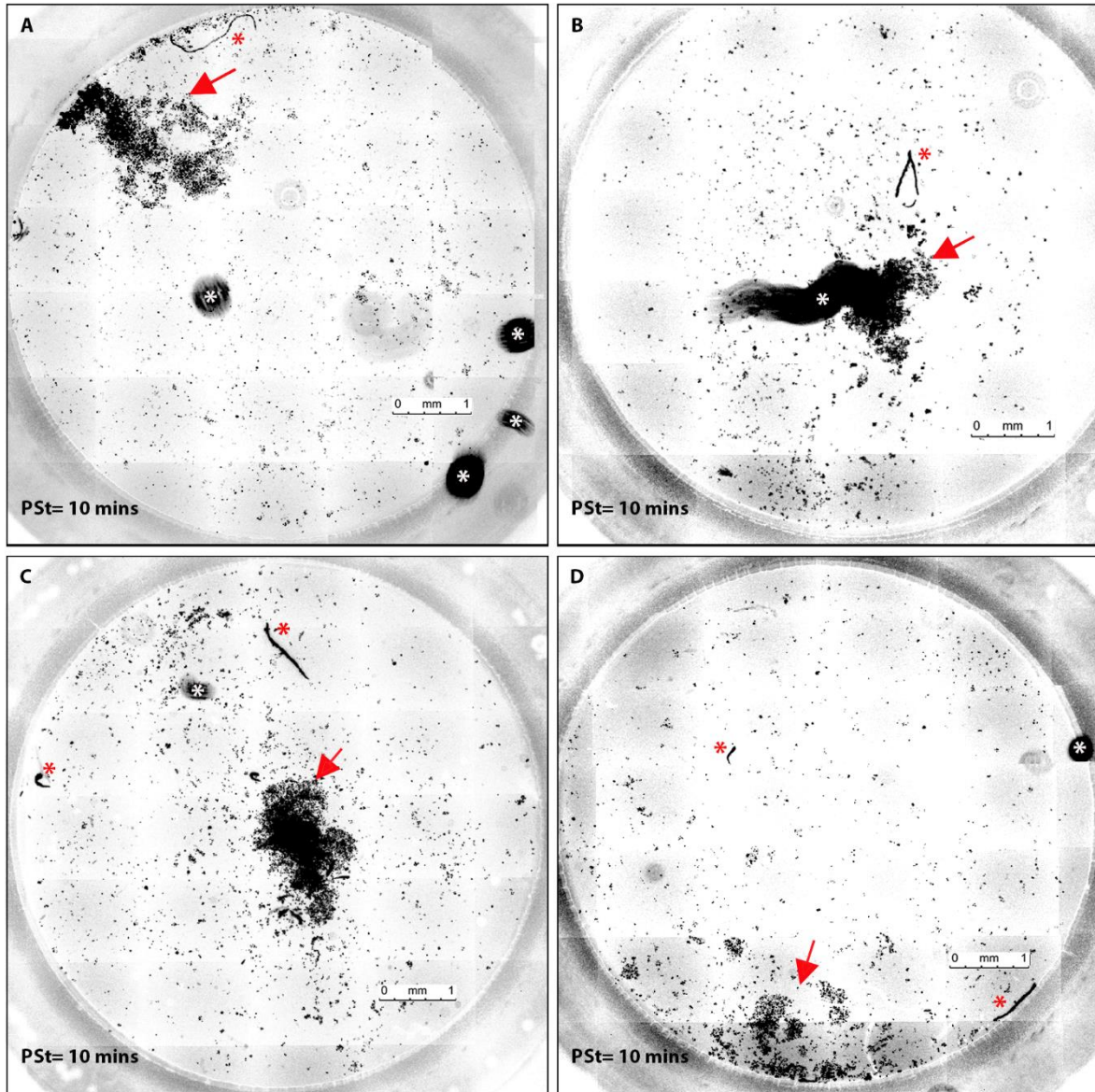
Figure 3.4.3.1 Fluorescence imaging of seeded BEC sheets levitated for two hours without growth media perfusion using the LT2 device.
BECs were levitated for two hours using the LT2 device without GM perfusion, then seeded onto collagen-coated wells. Fluorescence images were acquired after 10 minutes, then converted to greyscale (n=4). For Exp.1 and 4 BEC sheets were seeded toward the edge of the well. For Exp.2 and 3 BEC sheets were overlaid in the centre. Single BEC presence was high for all four experiments. Red arrows show location of BEC sheets. Red and white asterisks show location of fibres in and out of focus.

69
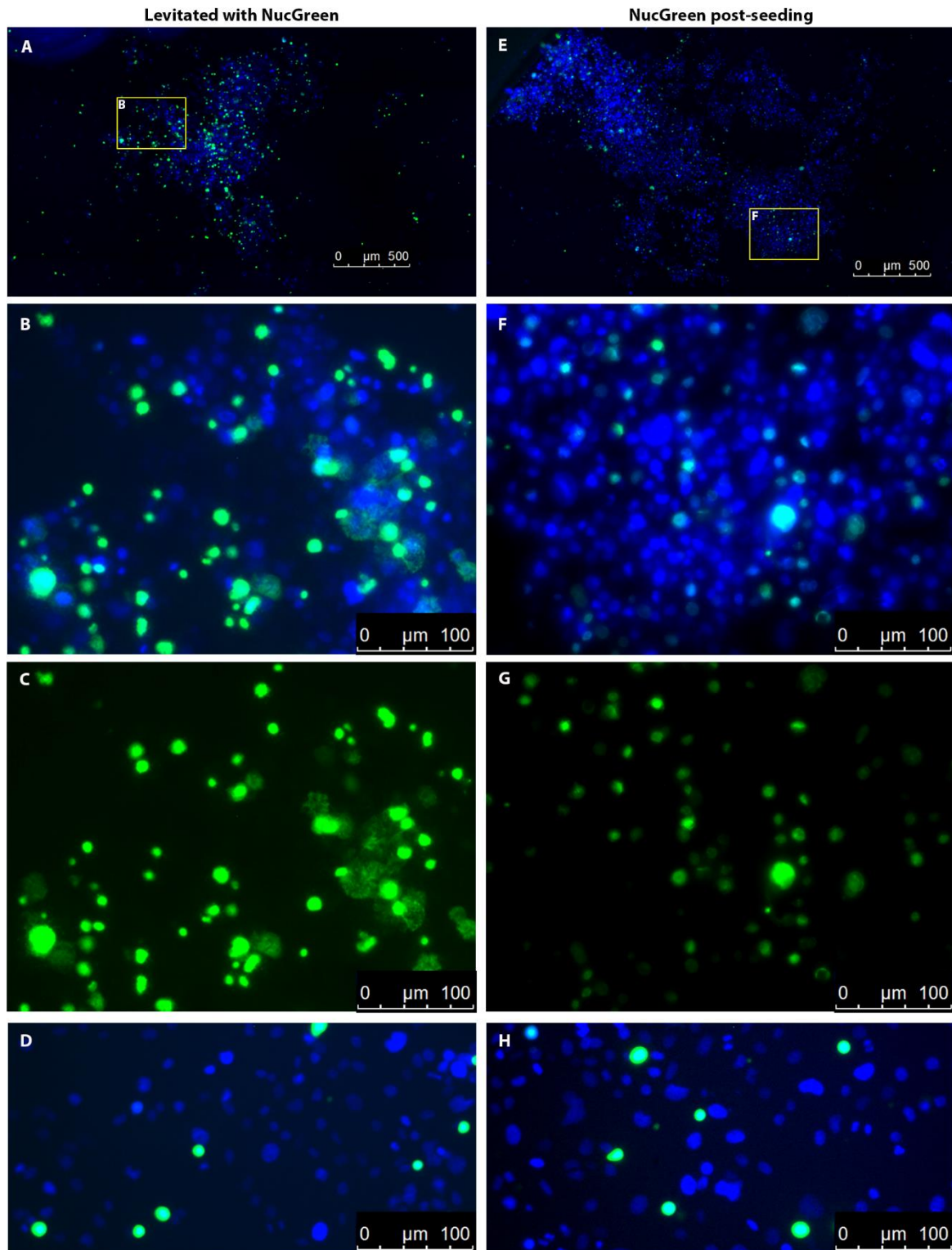
Figure 3.4.3.2 Fluorescent images show differentiated NucGreen staining of BEC sheets when levitated for two hours using LT2 device.
Images are representative of four two-hour levitation experiments, acquired 80 minutes after seeding. [A] Hoechst pre-loaded BEC sheets levitated with NucGreen GM present. Rectangle inset denotes the higher magnification image showing a large differentiated NucGreen population with [B] and without [C] Hoechst population. [D] Single BEC control shows distinct NucGreen population.
[E] Hoechst pre-loaded BEC sheets levitated without NucGreen GM present. Rectangle inset denotes higher magnification image showing a small differentiated NucGreen population with [F] and without [G] Hoechst population. [H] Single BEC control shows distinct NucGreen population.

70

3.4.4 Mapping resonance pattern of newly fabricated LT3-6 devices

Four new devices (LT3-6) of identical design were developed to determine if the LT2 acoustic streaming pattern was atypical, and measure the extent of AF device variability. Using dH_2O as an acoustic medium, oscilloscope readings provided a unique susceptance trough and conductance peak for each device between the 2.465 – 2.550 MHz region, and characteristic of planar acoustic field creation (Figure 3.4.4.1). Initial data suggested variability between these newly developed AF devices would be low. Tailored 0.1 MHz frequency sweeps were then used for live BEC levitation experiments.
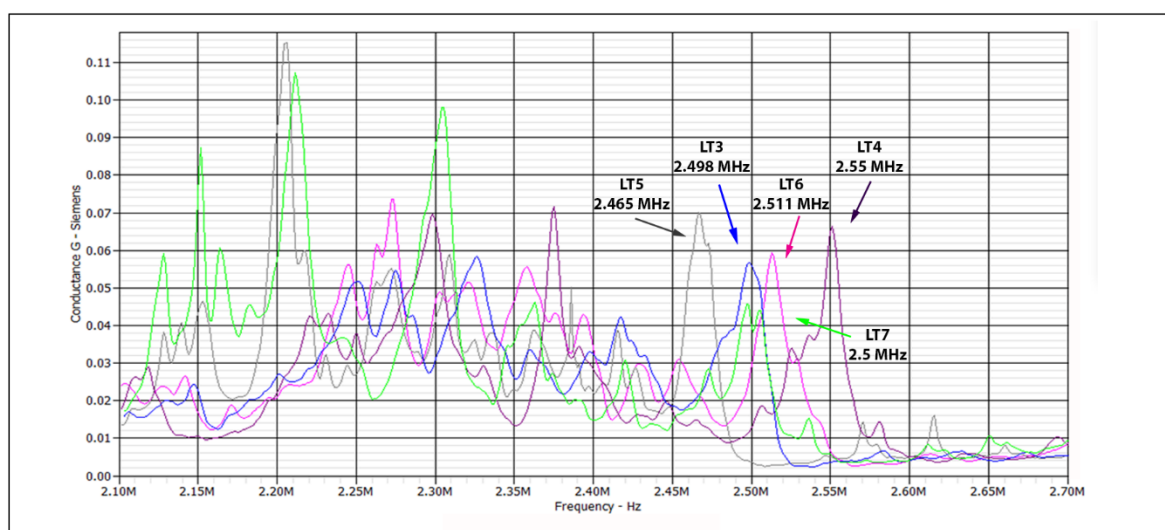
Figure 3.4.4.1 Resonant spectrographs of LT3-6 devices, while loaded with dH_2O, used to determine acoustic signal frequencies required for levitation.
Susceptance of the LT3-6 devices to a 2.1 – 2.70 MHz frequency range was measured using an oscilloscope with dH_2O loaded as a fluid medium. PZT conductance was calculated using susceptance readings. Conductance peaks between 2.465 – 2.550 MHz suggested the creation of acoustic fields required for 2D planar levitation, within each device.

3.4.1 Similar acoustic pattern with newly fabricated LT3-6 devices

Each device was operated at 4.24 V peak-peak, and Hoechst333342 pre-loaded cells were levitated without flow for 10 minutes (Figure 3.4.1.1). Tile scan images showed more desirable acoustic streaming and much larger aggregates present with each new device than LT2, confirming it as abnormal. The LT3 and LT4 devices did levitate some sheets on a slightly different plane to others, but the LT5 and LT6 devices held all BEC sheets within a more precise plane. Therefore, the LT5 device was used for further investigation, and the LT6 device was used for validation of results.
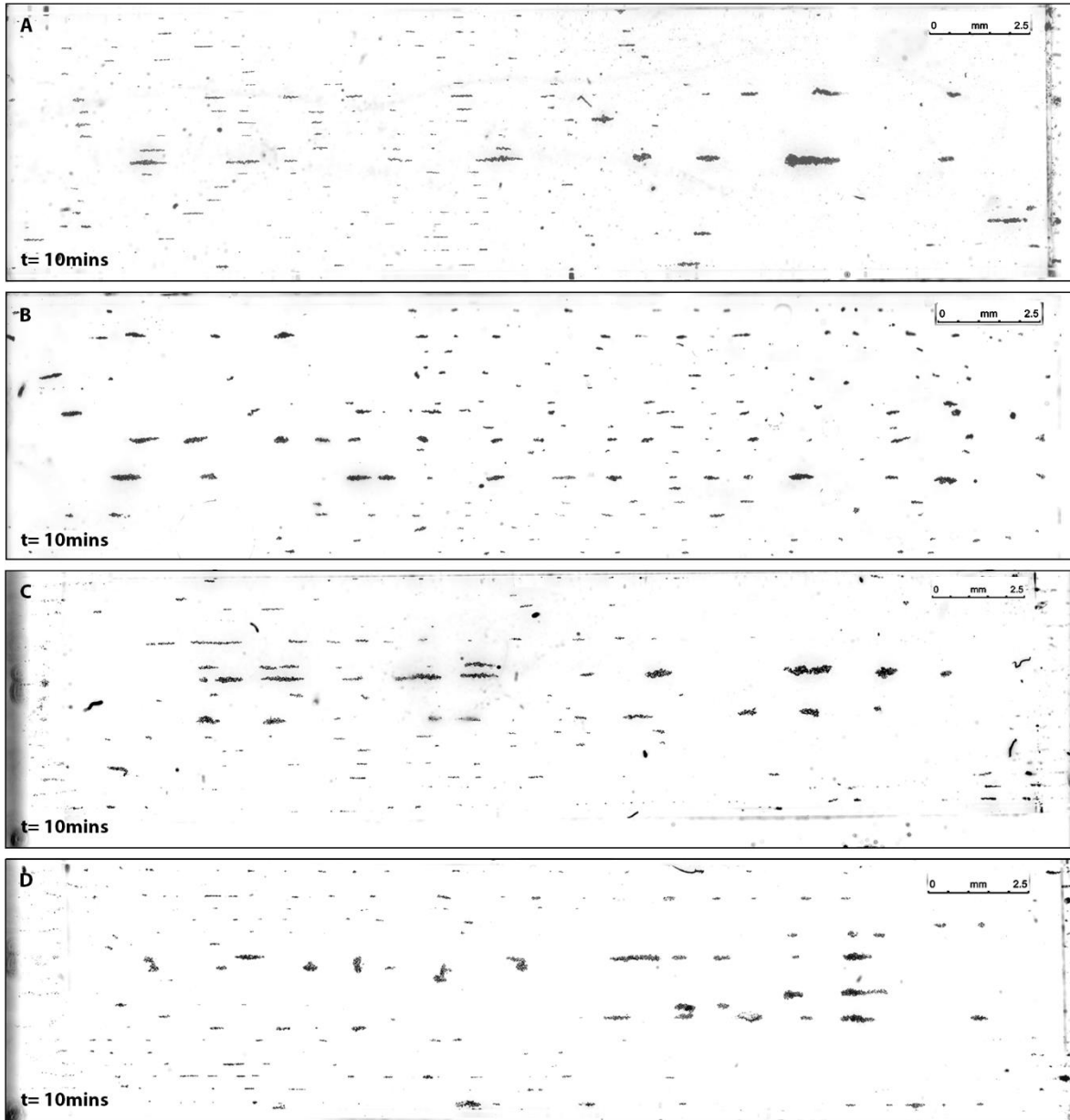
Figure 3.4.1.1 Fluorescence imaging of BEC aggregates levitating within new LT3-6 devices show similar acoustic streaming pattern.
BECs were levitated for 10 minutes using the developed LT3-6 devices without GM perfusion. Fluorescence images were taken, then converted to greyscale. With each device, larger central BEC aggregates were created, and were suggestive of desirable bi-lateral aggregate merging. However, multiple undesirable peripheral node aggregates were also present within each device.

3.4.2 Challenges removing settled BECs and peripheral node aggregates from LT devices while levitating

Though initial LT3-6 device testing shows some lateral merging and desirable BEC aggregate formation, peripheral node aggregates re-emerge. Data acquired using the LT1 device showed removing these aggregates using flow while under operational signal strength was not possible (Figure 3.3.4.2). Additional experiments where different volumes of growth media or 5% CO_2 air were aspirated into the LT3-6 devices post-seeding confirmed that the removal of settled single BECs was not achievable (data not shown).

Loading BECs exclusively into the centre of the PZT volume could circumvent the issue of peripheral node aggregates, but was not possible using the LT device design so further developments to the device design were made.

3.5 Reduced dead volume device development

Four new reduced dead volume devices were developed (RD1-4) to trial a new loading technique where cells are loaded directly into the PZT volume using a flat gel-loading pipet-tip to circumvent the loading volume.

3.5.1 Modified RD device design allows direct injection of BECs into PZT volume

The devices were identical to LT-devices except the PZT was adhered closer toward the open loading end of the capillary, creating a reduced dead volume (RD) and allowing direct-injection of a cell bolus using a flat gel-loading pipette tip with 0.3 mm OD (Figure 3.4.2.1).

Developments were also made to plastic holder design to allow imaging of the 2 mm dead volume. The plastic bottom of the holder design was replaced by a 0.5 mm glass slide, and the second plastic foot was moved to the other side of the PZT next to the other, ensuring that the device remains level while levitating. Counterintuitively, a plastic divider that obstructed visualisation of the dead volume was required with additional epoxy glue surrounding the loading compartment; this was to protect the microscope lens from any potential leaks from the open-end of the device.
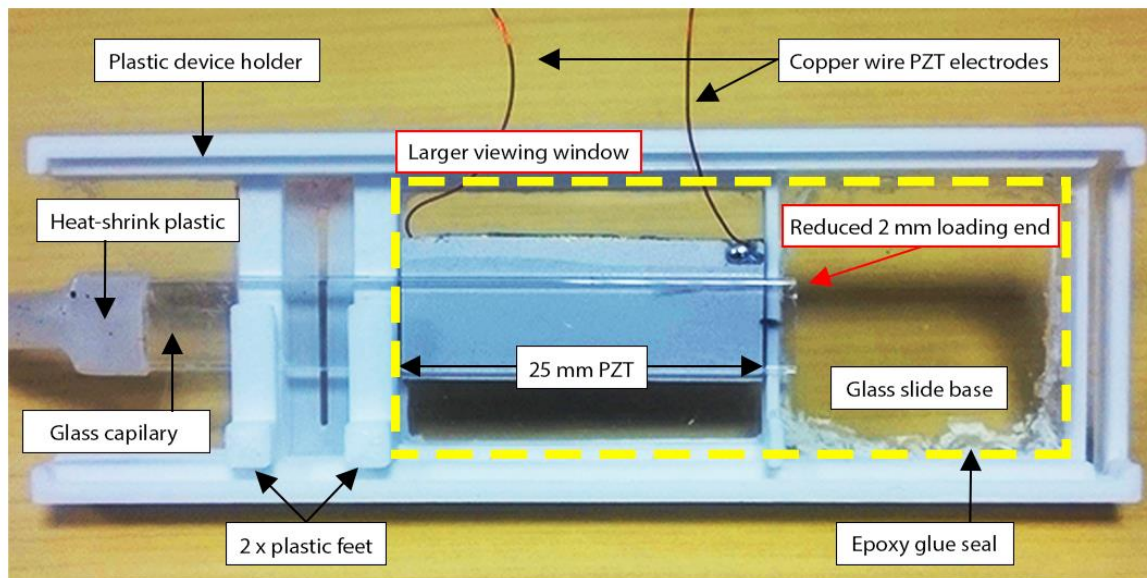
Figure 3.4.2.1 Labelled image of developed RD device and microscope holder design.
The reduced 2mm loading end creates a smaller 3.6 µL loading volume and allows direct-injection of a cell bolus into the PZT volume using a flat gel-loading pipette tip. The opposite end of the device fits securely within two plastic feet of the holder. The glass slide base of the holder allows imaging of both BECs settled within the reduced loading volume, and BECs levitated within the PZT volume. Epoxy glue is used to create a seal around the glass base and protect the microscope. A plastic divider creates a ~1mL compartment used to humidify the device environment.

Glass capillary dimensions

Pipet-tip dimensions

50 mm

23 mm

25 mm PZT volume

2 mm loading end

6 mm

0.3 mm

0.3 mm

38.82 mm

13 mm

51.82 mm
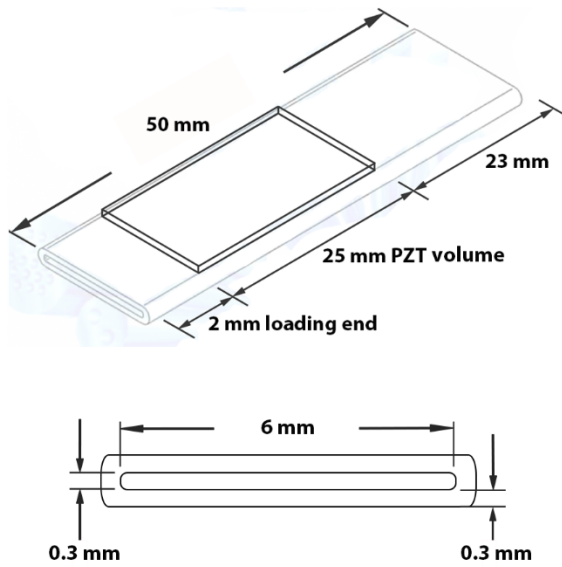
0.3 mm
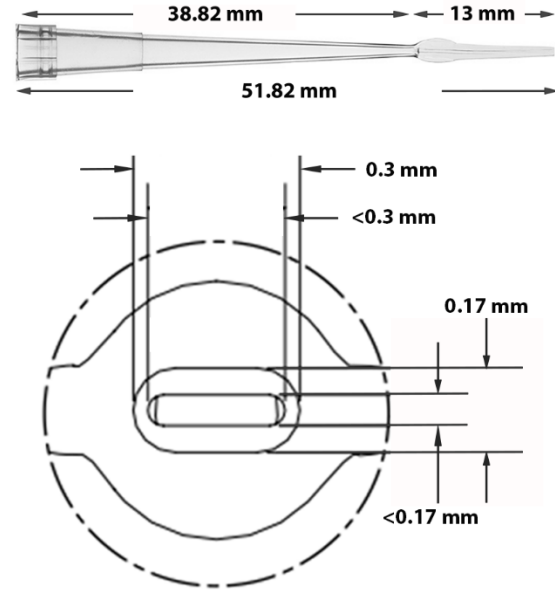
<0.3 mm

0.17 mm

<0.17 mm

Figure 3.4.2.2 Dimensions of RD device and gel-loading pipette tip used for cell bolus injection.
The glass capillary internal dimensions (0.6 x 0.3 mm) allow the insertion of a flat gel-loading pipette tip (0.3 x 0.17 mm). The pipette tip exceeds the loading volume threshold, passing 11 mm into the PZT covered capillary volume. Internal pipette tip dimensions (<0.17 mm) allow safe transit of single BECs.

Before using live BECs and 16HBE GM for direct-injection experiments, injection of a cell bolus was modelled using the desired vehicle with a 1:4 methylene blue dye-glycerol solution and water. Their difference in viscosity will approximate that of a cell bolus and GM and provide a clear image for measuring release and dispersion (Figure 3.4.2.3). The largest volume of a methylene blue-glycerol solution that could safely be injected into the PZT volume was 10 µL and diffused into the loading volume without flow after 30 seconds.

Single release of the dye-bolus was reliable but left behind a "dye-tail" after pipette tip withdrawal. Technique developments included aspirating ~2 µL of solution while slowly removing the pipette tip from the PZT volume, thus preventing dye-tail formation. To prevent pressure node over-loading the possibility of drawing the bolus across the PZT volume was explored by aspirating volumes of dH_2O after loading, at various flow rates (Figure 3.4.2.3). A 10 µL volume of dH_2O aspirated at 50 µL/min sufficiently spread dye across the PZT volume without exceeding it, and was therefore selected for GM aspiration after injecting the 10 µL cell bolus.
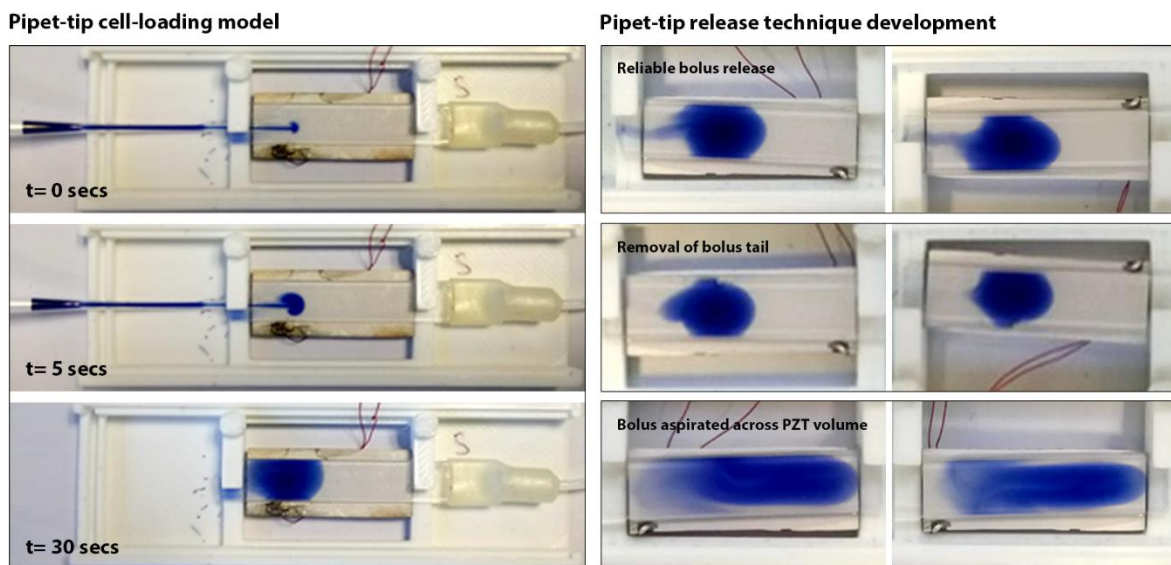
Figure 3.4.2.3 Images of dye-glycerol model for cell bolus loading into RD devices.
Using the 0.3 mm OD pipette tip, a single 10 µL (4:1) dye-glycerol bolus is safely loaded into the RD devices containing dH_2O as a fluid medium. After 30 seconds the dye-bolus remains within the PZT volume. Technique development images show consistent bolus loading, followed by attenuation of the dye-tail present after loading, by withdrawing 2 µL while removing the pipette tip from the PZT volume. Additionally, successful dye dispersion across device PZT volume by aspirating 15 µL of dH_2O at 50 µL/min immediately after loading.

3.5.2 Determining frequency sweep for RD1-4 device operation

As with previous AF device testing, resonance spectra for each RD device was mapped using an oscilloscope with dH_2O as a medium. For RD2, RD3, and RD4 devices single desirable peaks of strong conductance were identified at 2.43, 2.42, and 2.47 MHz respectively. Conversely, the RD1 device had twin conductance peaks at 2.465 and 2.52 MHz (Figure 3.5.2.1). RD2-4 devices were operated using a single, tailored 0.1 MHz frequency sweep, whereas RD1 was temporarily operated using two sweeps until the best could be determined.
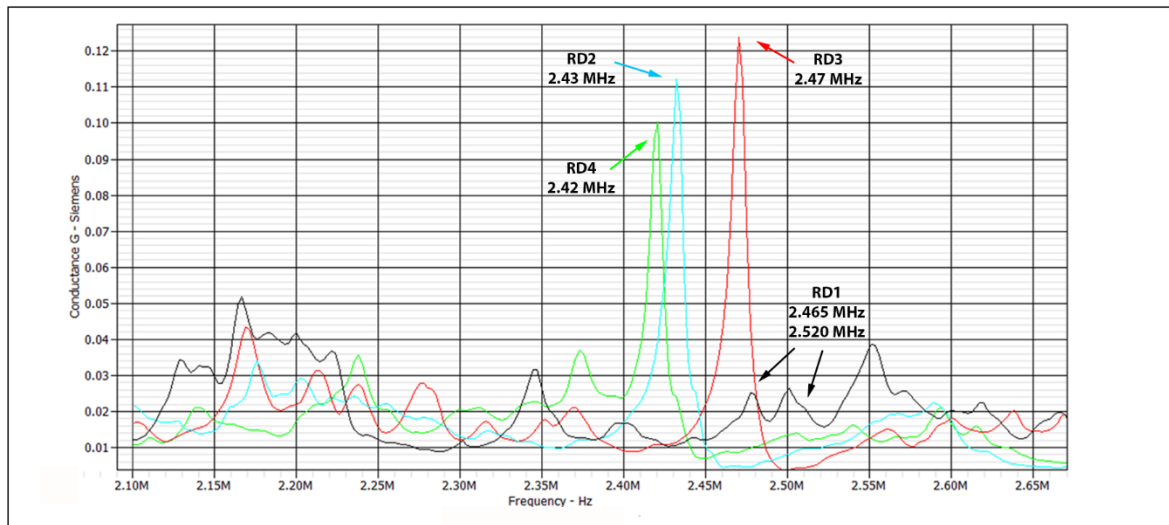

Figure 3.5.2.1 Resonant spectrographs of RD1-4 devices, while loaded with dH₂O, used to determine acoustic signal frequencies required for levitation.
Susceptance of the RD1-4 devices to a 2.1 – 2.45 MHz frequency range was measured using an oscilloscope with dH₂O loaded as a fluid medium. PZT conductance was calculated using susceptance readings. Conductance peaks between 2.420 – 2.520 MHz suggested the creation of acoustic fields required for 2D planar levitation, within each device. The RD2-4 devices have singular peaks of strong conductance, whereas the RD1 device has twin peaks of relatively weaker conductance.

3.5.3 RD2 device operation test using FLUO-labelled beads

Before using live cells, acoustic strength and device optics were tested using GFP-FLUO beads. The RD2 device (with its singular conductance peak) was selected for initial testing. PZT volume tile scan images show the presence of multiple FLUO-bead aggregates that merged between 5 and 10 minutes levitation (Figure 3.5.3.1A, B). Single images, acquired after 10 minutes levitation, confirmed that beads levitated within the same focal plane as increasingly large aggregates across the whole PZT volume (Figure 3.5.3.1C, D, E). After successful levitation and imaging of particles using the developed RD device design, live cell bolus loading experiments could begin.
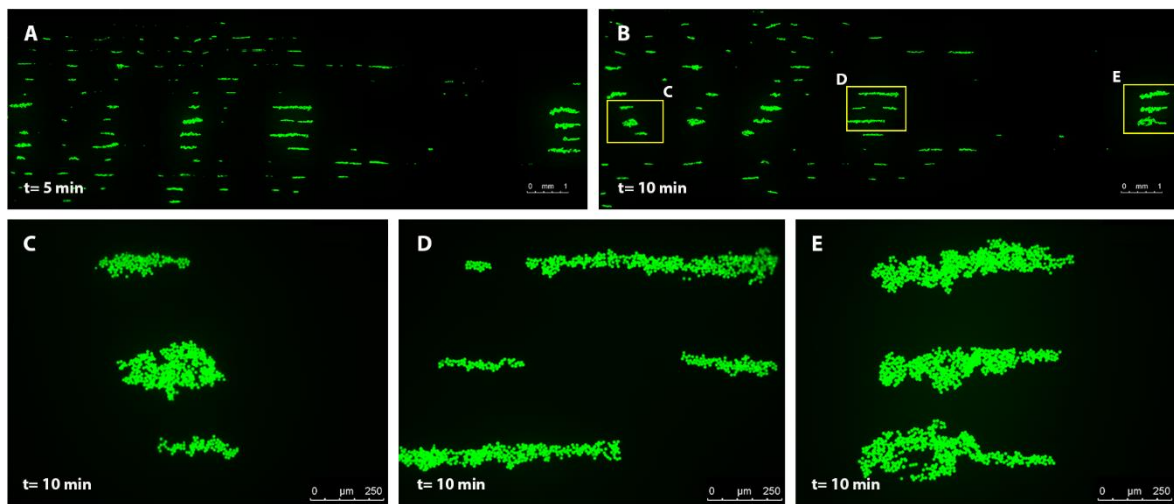
Figure 3.5.3.1 Fluorescence images of RD2 device operation test using GFP-labelled beads.
With a 0.3 mm OD pipette tip. 10 µL of a 2.0 x 10^6 bead/mL solution was injected into the RD2 PZT volume, and fluorescence tile scan images taken after [A] five and [B] ten minutes levitation. Multiple bead aggregates exhibit lateral and bilateral merging within five minutes. Individual images show beads aggregates levitating within a single plane at the [C] left, [D] centre, and [E] right-side of the PZT volume.

3.5.4   Direct injection prevents single BECs from settling in the dead volume

The developed RD device holder and it's extended glass base allowed visualisation of both BECs levitating within, and settled outside of the PZT volume using fluorescence microscopy. Therefore, using direct-injection cell bolus loading to remove settled BEC presence can be investigated.

The RD2 device was first loaded using the original technique of submerged, open-end aspiration. As with previous LT devices: 50 μL of a 1.0 x 10^6 cells/mL solution was aspirated at 300 μL/min to load 50,000 cells. Tile scan images revealed a large number of single BECs settled outside the PZT volume adjacent and gathered near the air-GM meniscus, indicated with a red arrow (

Figure 3.5.4.1).

Another 5.0 x 10^6 cells/mL suspension was prepared for direct-injection cell bolus loading. Using conditions ascertained from the dye-glycerol cell bolus model, a 10 μL bolus of 50,000 cells were first loaded into the flat pipette tip, cleaned with Is-OH, then carefully fed into the RD2 device while operational. The cell bolus was then released either as two 5 μL volumes across the PZT volume for a staggered release or as a single 10 μL volume. Finally, the pipette tip was carefully removed from the device, simultaneously easing the pipet-plunger to withdraw ~2 μL of GM and avoid leaving a "tail" of cells through the loading volume.

With staggered pipette tip release, fewer BECs settled outside of the PZT volume, relative to open-end aspiration, though a large number of BECs were still found within the air-GM meniscus. Single release pipette tip loading provided the fewest settled BECs by a considerably margin, and none held adjacent to the meniscus (

Figure 3.5.4.1). As a result, the single release direct-injection technique was used for further, long-term levitation experiments.
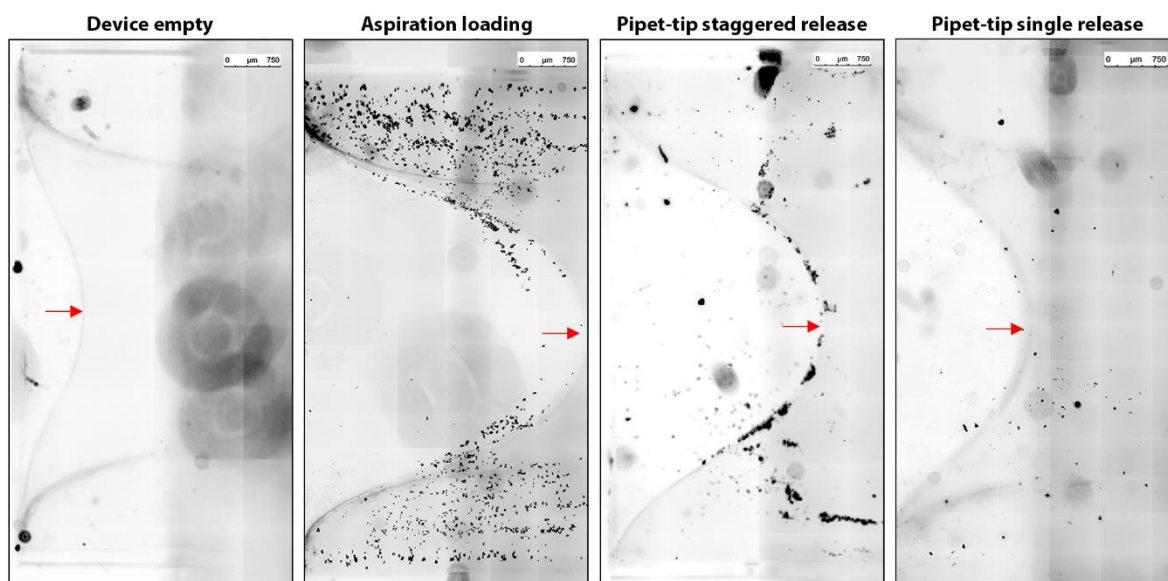
Figure 3.5.4.1 Fluorescence imaging of BECs within RD2 device loading volume after different cell-loading techniques.

The RD2 device was loaded with 50,000 single BECs using either open-end aspiration or direct-injection of a cell bolus into the PZT volume using a 0.3 mm OD pipette tip. Fluorescence images of the loading volume were acquired then converted to greyscale. The largest settled BEC population was seen after aspiration of 50 µL from a 1.0×10^6 cells/mL suspension. Staggered pipette tip release of a cell bolus across the PZT volume produced a moderate single BEC presence with several aggregates trapped within the air-GM meniscus. Single release of a cell bolus produced the fewest single BECs: none were trapped in the meniscus or capillary edge. Red arrows denote location and direction of air-GM meniscus.

3.5.5 Depreciation of RD2 resonance pattern over time

Multiple two, three, and four-hour levitation experiments were performed to optimise levitation time for BEC sheet creation. Fluorescence images acquired after two hours levitation without GM perfusion show depreciation of RD2 bilateral resonant forces over time, possibly due to over-use and PZT burn-out. With the 1st two-hour levitation experiment, lateral and bi-lateral forces merge all levitated BECs into a single aggregate measuring 5.38 x 1.76 mm in length/width with a total area of 5.961 mm^2 (Figure 3.5.5.1). However, with subsequent experiments, bi-lateral merging was reduced, and BECs remained as thin sheets within central nodes. Multiple rows of narrow cell sheets were more susceptible to mechanical damage, and therefore undesirable. Levitating cells for three hours failed to recover bi-lateral merging except for experiment five where all aggregates merged after 170 minutes levitation to create an unstable sheet measuring 4.593 x 1.754 mm, and a total area of 3.644 mm^2. An alternate RD device would be used for further levitation experiments, with increased awareness and consideration of PZT performance between experiments.

2 hour levitation

3 hour levitation
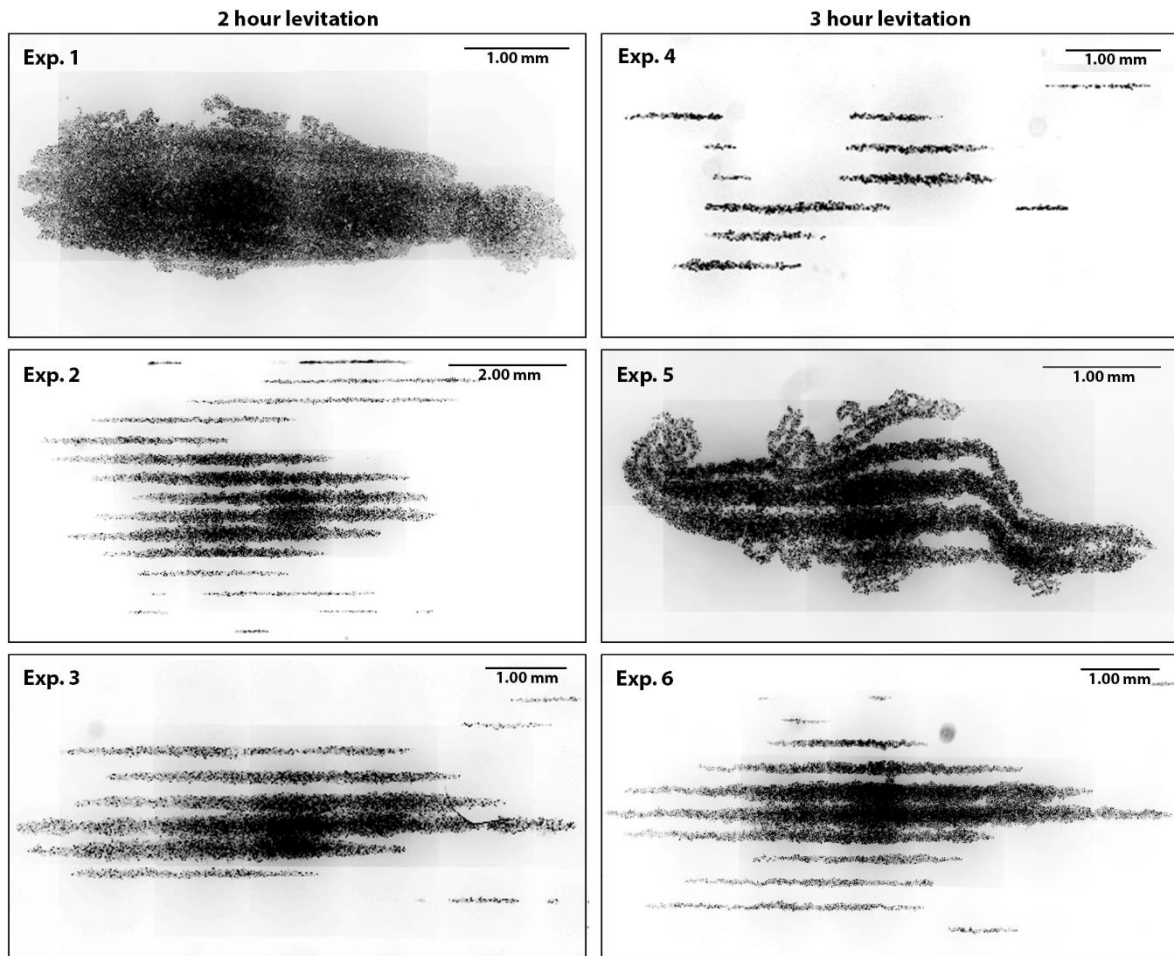
Figure 3.5.5.1 Fluorescence imaging shows depreciation of RD2 bi-lateral acoustic forces.
For six experiments using the RD2 device, a 10 µL, 50,000 single BEC bolus was loaded via single pipette tip release, and levitated for two hours without GM perfusion. Fluorescence images were acquired then converted to greyscale. Single BECs become a single large aggregate with the first experiment due to bi-lateral merging via strong acoustic forces. With subsequent experiments BEC aggregates did not merge bi-laterally and remained distinct due to depreciation of the RD3 PZT form over-use.

3.5.6 RD3 device operation test using FLUO-labelled beads

The RD3 device produced an even stronger conductance peak than RD2, and was a suitable candidate for its replacement, and progressed to GFP-FLUO bead testing. After direct-injection loading of ~50,000 beads, PZT volume tile scans and singular images were acquired over 10 minutes. A one minute image shows all beads in focus and confirms levitation within a singular Z-plane (Figure 3.5.6.1C), as with previous devices. The 5-minute tile scan reveals a large bead aggregate, levitated within a single centre pressure node, suggesting the presence of strong bi-lateral acoustic forces desirable for BEC sheet creation (Figure 3.5.6.1A, D). After 10 minutes, the singular aggregate begins has folded upon itself laterally into a more rounded shape, which is also desirable for sheet creation (Figure 3.5.6.1B, E). Satisfied with the acoustics and optics of the RD3 device, the next challenge was to replicate these results using live cells.
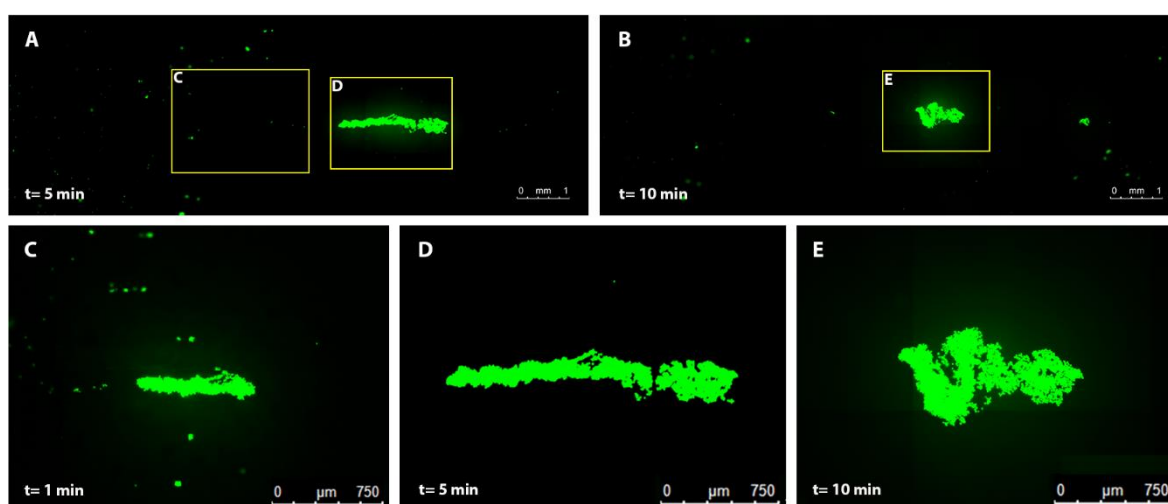
Figure 3.5.6.1 Fluorescence images of RD3 device operation test using GFP-labelled beads.
Using a 0.3 mm OD pipette tip, 10 μL of a 2.0 x 10^6 bead/mL solution was injected into the RD3 PZT volume, and GFP-FLUO tile scan images taken over 10 minutes levitation. [A] Five-minute tile scan image of whole PZT volume showing singular bead aggregate formation in PZT centre. [B] Ten-minute tile scan showing lateral folding of bead aggregate into a more rounded shape. Singular images supporting tile scan data taken after one [C], five [D], and ten minutes [E] respectively.

3.5.7 Desirable BEC sheet merging pattern within RD3 device over two hours levitation

To examine the BEC sheet merging pattern with the RD3 device, four levitation experiments were performed using the direct-injection loading technique, and tile scan images were acquired after two hours levitation (Figure 3.5.7.1). Unlike RD2, the RD3 device held BECs within the same axial and bi-lateral planes. Cells aggregated within a lateral node series traversing the entire PZT length. The lateral merging pattern of BEC sheets was determined by the location and speed of cell bolus injection. For two experiments all single BECs were loaded 11 mm deep into the PZT volume and became singular cell sheets with length/width measurements of 11.79 x 1.69 mm, and 8.52 x 1.06 mm, with cell sheet areas of 13.01 and 5.91 mm^2 respectively. The third experiment also provided a large sheet 10.50 x 1.41 mm, with a smaller sheet measuring 1.44 x 0.83 mm at the opposite end of the PZT volume: with a total surface area of 9.43 mm^2. With the fourth experiment, lateral merging was more distributed. Seven BEC sheets of sufficient size were created measuring 1.96 to 0.24 mm in length, and 0.81 to 0.12 mm in width, with a total surface area of 3.51 mm^2. The variability of these two experiments was attributable to idiosyncrasies with my own pipetting technique, and difficulties working to error margins less than a millimetre.
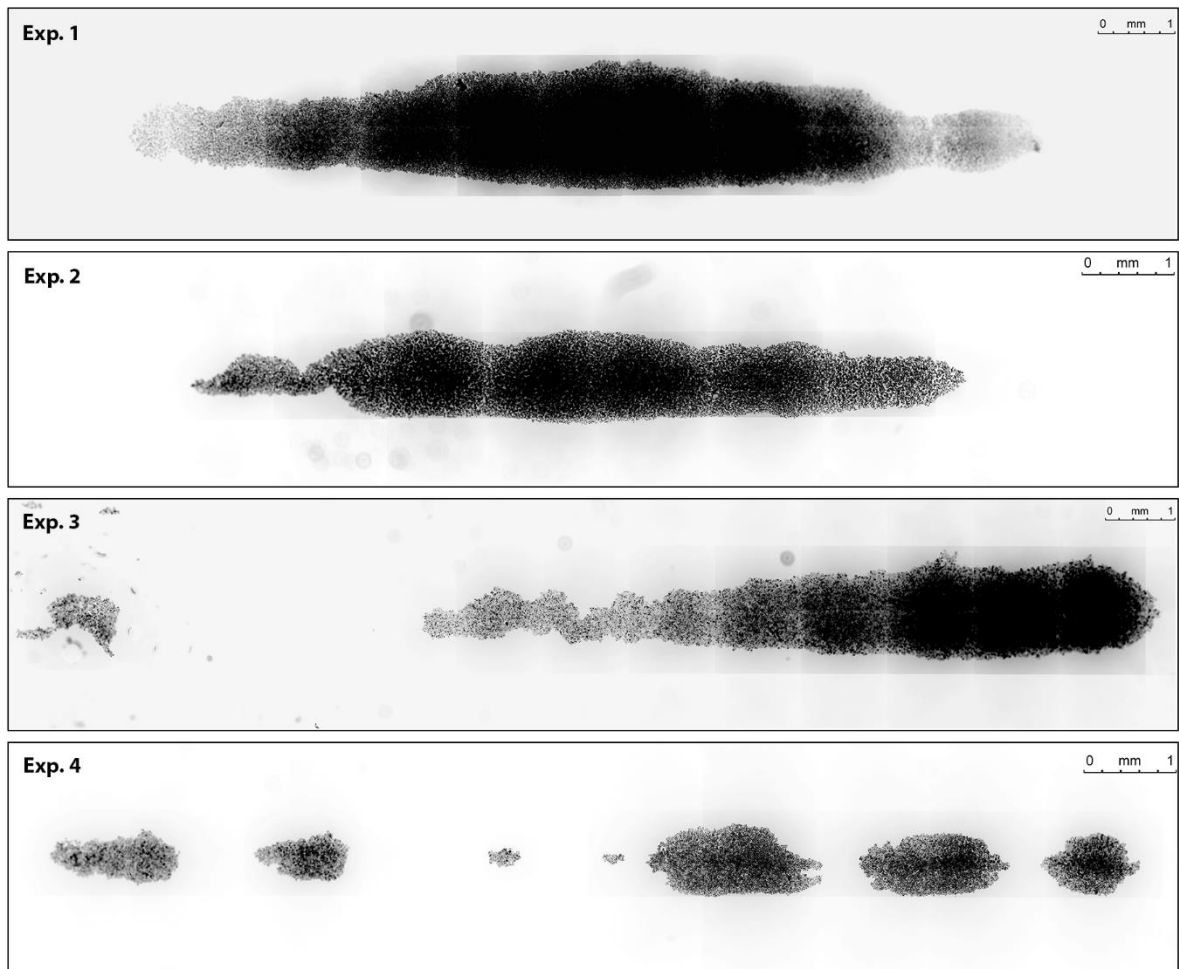
Figure 3.5.7.1 Fluorescence imaging shows desirable BEC sheets within RD3 device after two hours levitation without growth media perfusion.
For four experiments using the RD3 device, a 10 µL, 50,000 single BEC bolus was loaded via single pipette tip release, and levitated for two hours without GM perfusion. Fluorescence images were acquired then converted to greyscale. When loaded precisely, all single BECs form a singular large BEC sheet (exp.1 and 2); with less precision single BECs form multiple large sheets (exp.3 and 4).

3.5.8 Investigating viability of BEC sheets after two hours of acoustic levitation

It was now possible to load 50,000 single BECs into the RD3 device and create a large singular BEC aggregate, or multiple of sufficient size for collective movement and cell sheet behaviour when seeded (theoretically). The next two challenges were removing the sheets safely from the device, and to determine viability of seeded BEC sheets without using membrane permeability-dependent viability dyes.

BEC sheets from the two-hour levitation experiments were seeded onto collagen-coated wells filled with GM after two hours levitation. Non-levitated single BECs were also seeded into wells as a control. To expel the BEC sheets: RD3 was held at ~65° angle with the open-tip submerged in 1-2 mm of the well GM. With the acoustic signal still operational, 100 µL of GM was then perfused at 300 µL/min through the device.

For two experiments, BEC sheets were incubated for one hour at 37°C, 5% CO_2 to settle and adhere to the collagen layer. BEC sheets settled at the edge of each well with minimal mechanical damage or folding (Figure 3.5.8.1). Additionally, no single BECs were present in the well. This was in contrast to the non-levitated controls wells were an unconnected mass of single BECs with no planar or lateral organisation (Figure 3.5.8.1).

GM was carefully removed using a 200 µL pipette tip and withdrawing from the bottom of plate whilst tilted, followed by fixation with 500 µL of (1:1) Acetone: Methanol solution. Another tile scan image was taken to determine whether BEC sheets adhered to the collagen layer, an essential function *in vivo* and a good indicator of collective BEC viability.

It was possible that one hour was insufficient for collagen adhesion, and that two-hour levitated BEC sheets needed longer to recover before they could create sufficient adhesions. For a further two levitation experiments (exp.3 and 4) levitated BEC sheets and non-levitated single BEC controls were allowed to settle for 24 hours at 37°C, 5% CO_2.

The levitated BECs failed to morphologically change, adhere to, or expand across the collagen coated surface. Instead, levitated BECs remained round, were static, and all lost during the fixation protocol (Figure 3.5.8.2). Once again non-levitated single BECs successfully adhered to the collagen-coated surface and appeared to settle after one-hour (Figure 3.5.8.2). Neither physiologically or metabolically active, the levitated BECs can be considered non-viable for cell-sheet engineering purposes. To prevent the sonication and increase viability of BEC sheets the next variable investigated was time levitated before seeding.
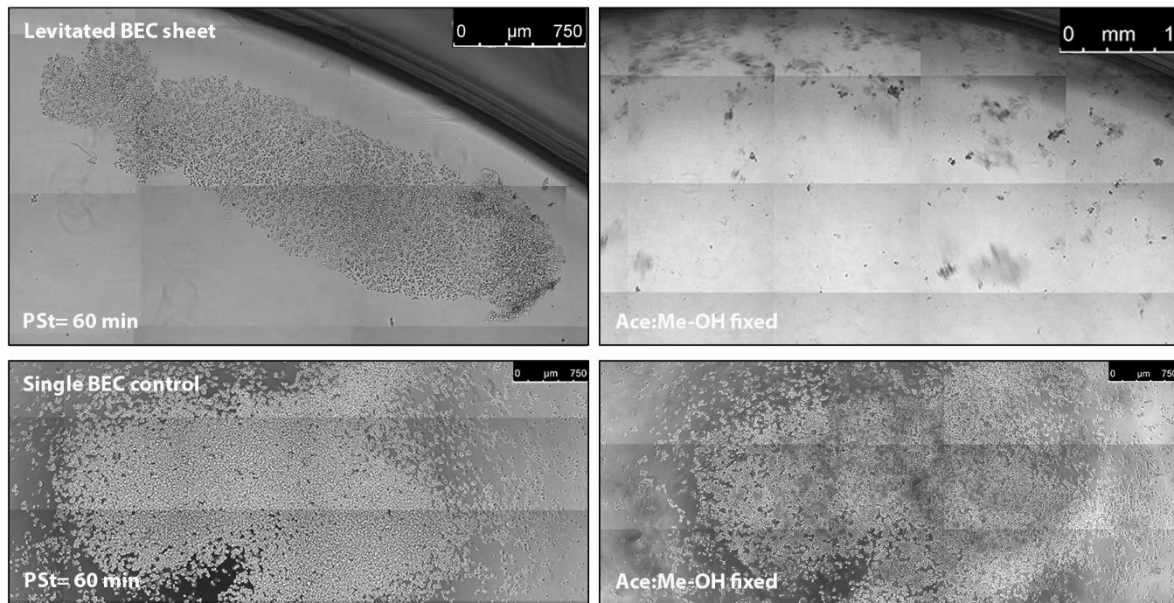
Figure 3.5.8.1 Phase contrast images show BEC sheets levitated for two hours do not adhere to collagen after a one-hour incubation period.
Using the RD3 device: 50,000 single BECs were levitated for two hours without flow then seeded onto collagen-coated wells filled with GM, with non-levitated BECs seeded as controls. BECs were allowed to settle for one hour (37°C, 5%CO_2) before fixation with Acetone: Methanol (1:1) solution. Levitated BEC sheets remain intact when seeded, but fail to adhere, and are lost during alcohol fixation. Whereas non-levitated BECs adhere successfully. Images are representative of two experiments.
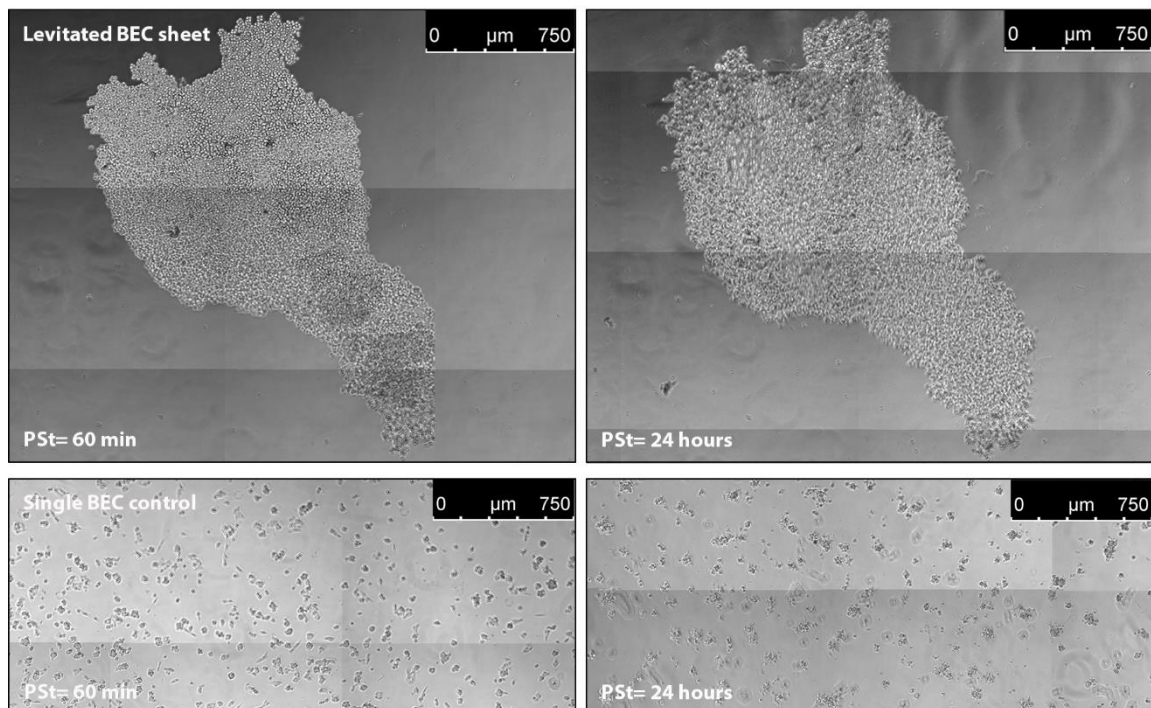
Figure 3.5.8.2 Phase contrast tile scan images show BEC sheets are non-viable after two hours levitation without flow.
Using the RD3 device: 50,000 single BECs were levitated for two hours without flow then seeded onto collagen-coated wells filled with GM. Non-levitated BECs were seeded as controls. BECs were allowed to settle for 24 hours (37°C, 5% CO_2) before fixation with Acetone: Methanol (1:1) solution. Levitated BEC sheets remain intact when seeded, but fail to adhere, grow or expand over 24 hours. Whereas non-levitated BECs adhere and expand.

3.5.9 Unsuccessful BEC sheet formation after 30 minutes levitation

For BEC sheet creation, a shorter levitation period was needed. Levitated BECs needed sufficient time to create adherens junctions and hold together as a sheet without being sonicated irreversibly. Two 30-minute levitation experiments were performed using direct-injection loading and the RD3 device (Figure 3.5.9.1). For one 30-minute levitation, single BECs formed six sheets of similar length (1.69 - 1.18 mm), width 0.78 to 0.46 mm, and surface area (0.75 and 0.31 mm^2). The levitated BEC sheets were then seeded into a collagen-coated well. After ten minutes, BEC sheets were located near the centre, and five had merged with minimal folding during transference. However, after settling for an hour at 37°C, 5% CO_2, approximately half the levitated BECs had dispersed across the well as single BECs. Only a sparse, skeletal, framework of the BEC sheet remained. Fortunately, levitated BECs became less-rounded, successfully adhered to the collagen, and were present after alcohol fixation. With a replicate experiment, a single BEC aggregate 4.64 x 1.28 mm in length/width with a surface area of 3.18 mm^2 was present after 30 minutes. Though when seeded, the aggregate became a single cell suspension immediately upon well entry. Levitated cells successfully adhered to the collagen after settling for an hour, which confirmed cells remained viable after 30 minutes of levitation but created too few adherens junctions to hold together as cell sheets.
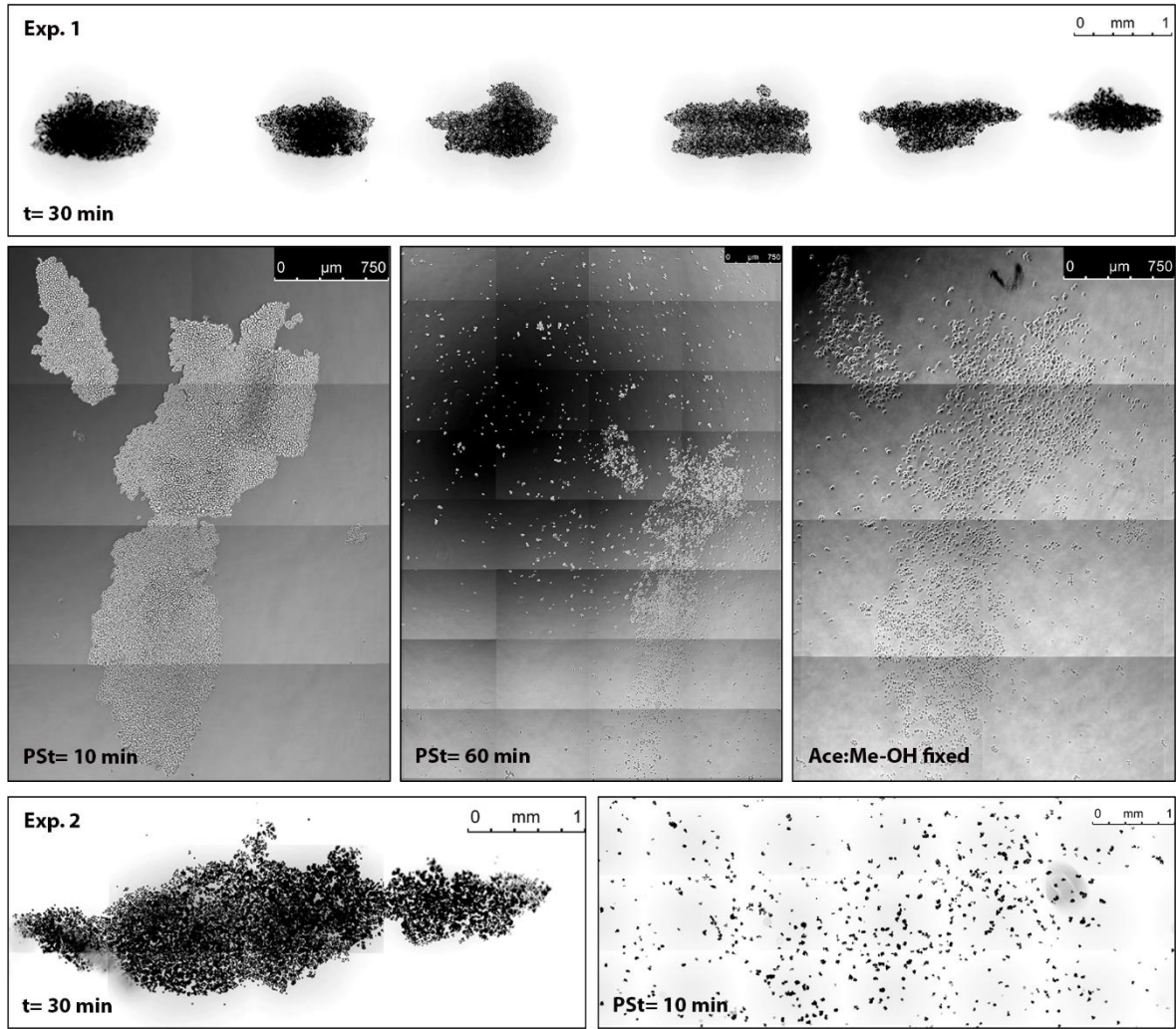
Figure 3.5.9.1 Images show 30-minutes levitation is insufficient for BEC sheet formation.
For two replicate experiments using the RD3 device: 50,000 single BECs were levitated for 30 minutes without flow then seeded onto collagen-coated wells filled with GM, with non-levitated BECs seeded as controls. BECs were allowed to settle for one hour (37°C, 5% CO_2) before fixation with Acetone: Methanol (1:1) solution.

3.5.10 Reducing levitation from two to one hour provides adherent BEC sheets

It was evident that single BECs levitated for two hours become non-viable sheets, and that BECs levitated for 30 minutes did not hold together as sheets. Therefore, a one-hour intermediate levitation period was explored. Five replicate one-hour levitation experiments were performed using the RD3 device with direct-injection cell bolus loading. As with previous experiments, BEC sheet formation was visualised using fluorescence microscopy. The size and number of BEC sheets appeared more variable using a one-hour levitation period instead of two (Figure 3.5.10.1). For experiments two and five, BECs became single sheets measuring 8.55 x 1.87 mm, and 5.44 x 1.265 mm, with surface areas of 10.57 and 4.34 mm^2 respectively. Whereas experiments one, three, and four, yielded multiple BEC sheets of varying proximity to each other. Levitated sheets were all morphologically desirable with individual surface areas between 3.02 and 0.06 mm^2, and total sheet surface areas of 4.50, 5.93, and 4.21 mm^2 respectively. Sheet merging variance caused by manual pipette tip loading was previously minimised by two hours levitation. However, this variance was heightened by incomplete lateral merging after a one-hour levitation period.
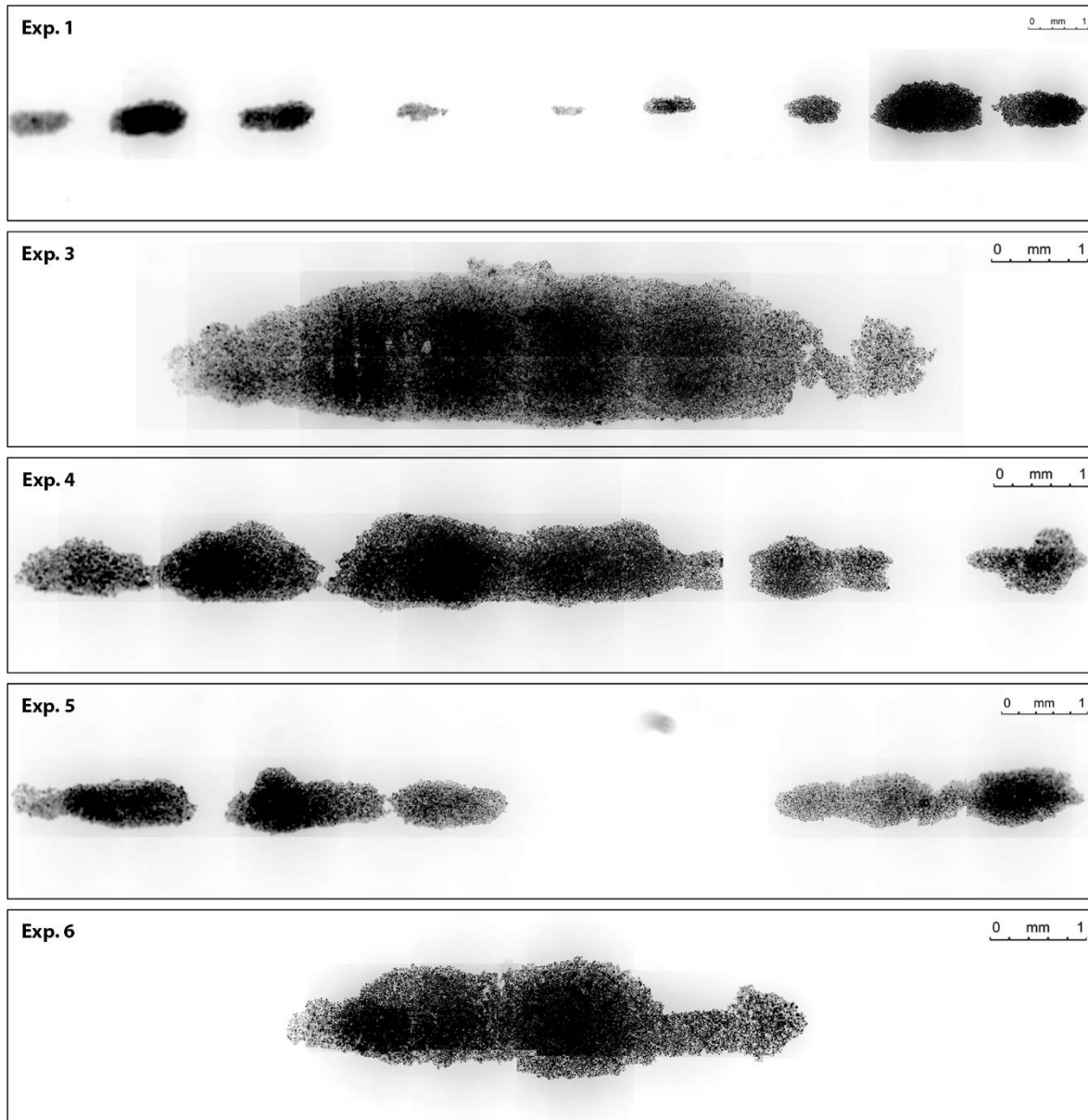
Figure 3.5.10.1 Fluorescence imaging shows desirable BEC sheets within RD3 device after one hours levitation without growth media perfusion.
Five levitation experiments were performed using the direct-injection of a 10 µL, 50,000 cell bolus loading technique. Fluorescence images were acquired after one hour of levitation without flow, then converted to greyscale. When loaded precisely, all single BECs form a singular large BEC sheet (exp.2 and 5); with less precision single BECs form multiple medium to large sheets (exp.1, 3, and 4).

As before, BEC sheets from three replicate one-hour levitation experiments were expelled from the RD3 device and seeded onto collagen-coated wells by perfusing 100 µL of GM at 300 µL/min. Initial images, acquired 10 minutes after seeding showed that BEC sheets remained mostly intact, with some instances of folding, and that single BEC presence was minimal/non-existent (Figure 3.5.10.2). Unfortunately, after settling for one hour (37°C, 5% CO_2) BEC sheets from two experiments came apart in varying degrees, and released a corresponding number of single BECs (exp.1 and 3). Though, for one experiment (exp.4), almost no damage was present after settling. BEC sheet damage was more extensive for all experiments after alcohol fixation; required for IF staining of adherens junctions.

BECs may have failed to adhere to the collagen layer due to geographical or mechanical reasons, instead of physiological. Not all BEC sheets were perfectly planar, and some BECs were not in direct contact with the collagen layer. Additionally, partial collagen adherence may have contributed to more extensive BEC sheet removal; with cells still re-organising themselves before media removal.

A sufficient number of BEC sheets remained intact after alcohol fixation for IF staining of adherens junctions. Therefore, BEC sheets from one experiment were seeded onto a collagen-coated 13 mm glass coverslip to allow fluorescence imaging at higher magnification. BEC sheets were again seeded mostly intact with a very small population of single BECs, which all adhere to the collagen-layer before alcohol fixation (Figure 3.5.10.3). Overall, one hour of levitation allowed BEC sheets to be seeded intact, and maintain sufficient viability for BEC sheet adhesion to collagen.
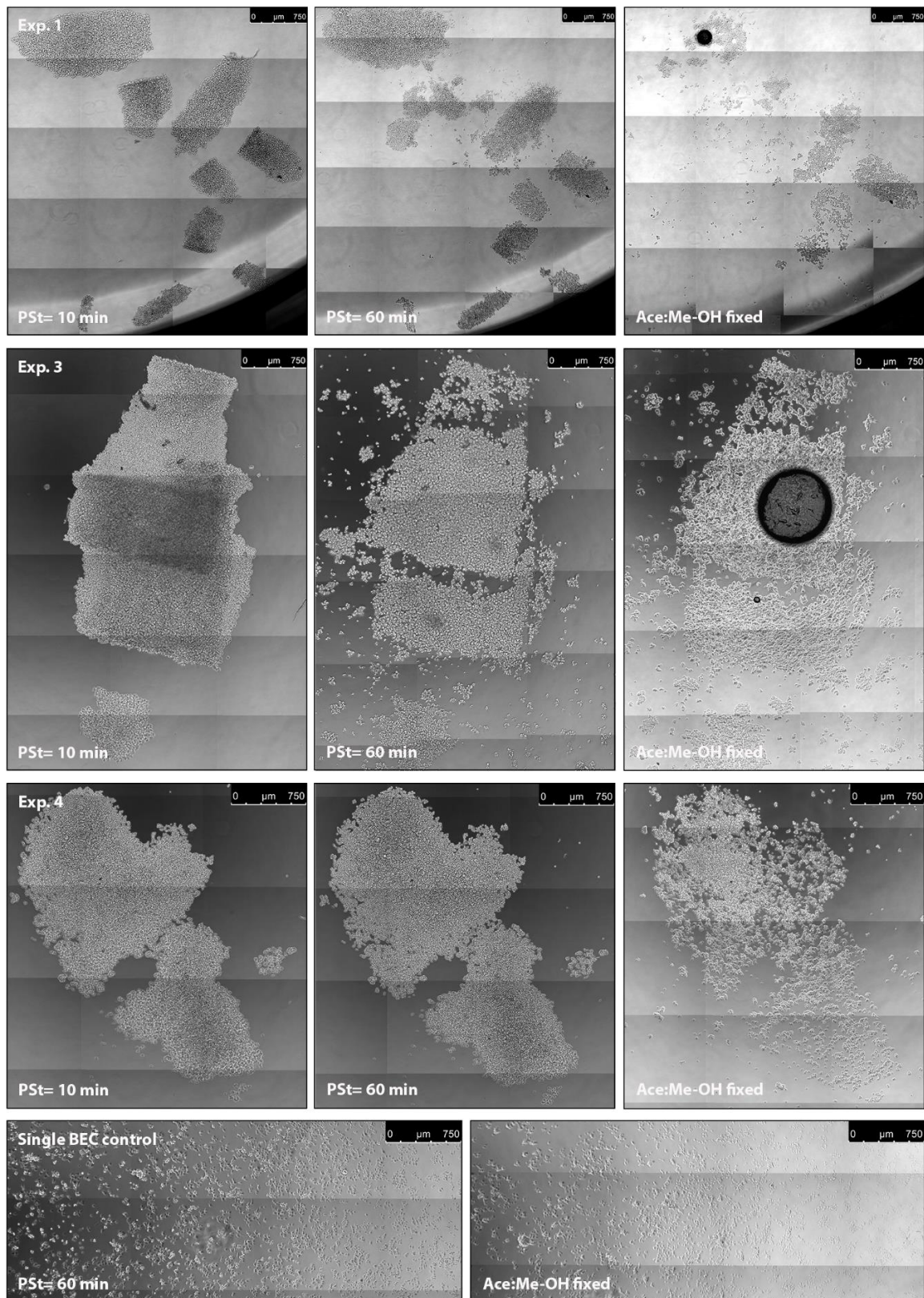
Figure 3.5.10.2 Phase contrast images show successful adherence of BEC sheets levitated for one hour to collagen-coated well.
BEC sheets from three one-hour levitation experiments were seeded onto collagen-coated wells, then fixed with Acetone: Methanol (1:1) solution after one hour. BEC sheets remained mostly intact when seeded with very few single BECs present, BEC sheets were either overlaid or spread across the well. Damage was present with subsequent alcohol fixation. White asterisks show bubbles.
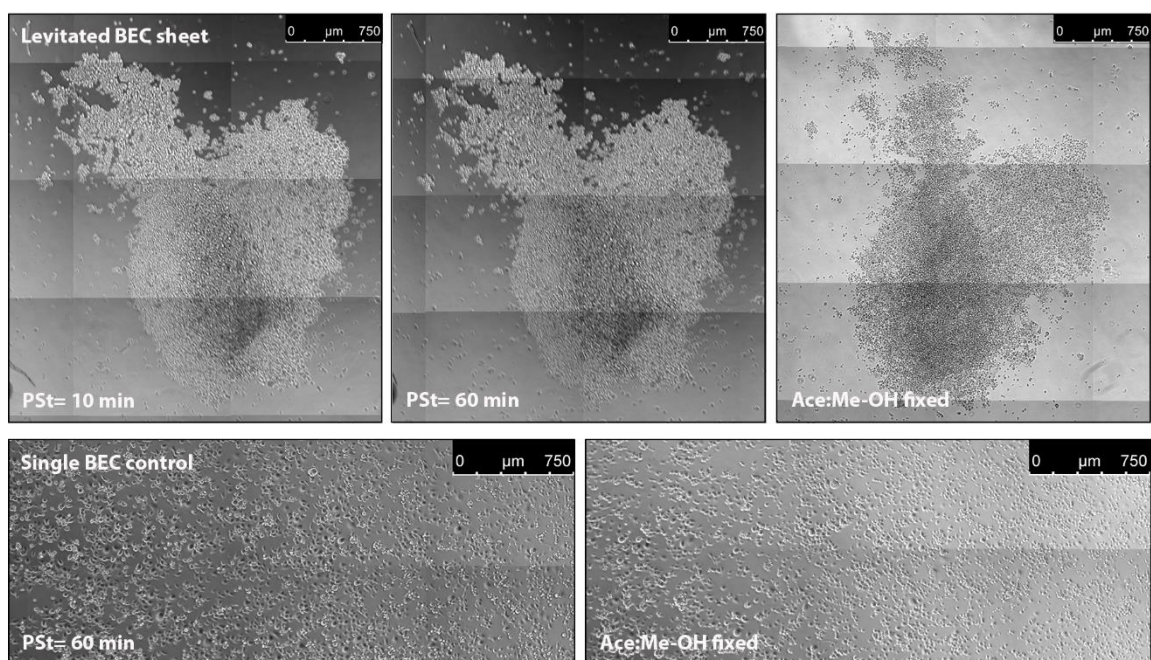
Figure 3.5.10.3 Phase contrast images show successful adherence of BEC sheets levitated for one hour to collagen coated coverslip.
BEC sheets from a single one-hour levitation experiment were seeded onto a collagen-coated coverslip, then fixed with Acetone: Methanol (1:1) solution after one hour. BEC sheets remained mostly intact with few single BECs present, but were overlaid in the centre of the well. Alcohol fixation revealed successful adhesion of BEC sheets and single BEC controls to coverslips.

3.5.11 Visualising BEC sheet adherens junction formation after seeding

Now that it was possible to seed created BEC sheets intact and without a substantial number of single BECs present using the RD3 device, adherens junction formation was investigated. BEC sheets were fixed 60 minutes after seeding using Acetone: Methanol (1:1) solution, then stained with mouse monoclonal E-cadherin to identify adherens junctions.

Rabbit monoclonal β-catenin was used to identify associated actin filament networks within the cell cytoplasm. β-catenin staining was non-specific when added to alcohol-fixed cultures, but highly specific with high fluorescence intensity when added to 4% PFA fixed BEC cultures. However, E-cadherin staining was non-specific with 4 %PFA fixation (data not shown).

With one experiment (exp.4) the tile scan image reveals heterogeneous fluorescence staining within the seeded BEC sheet (Figure 3.5.11.1). Fluorescence intensity was higher towards the centre, and more sparse towards the edges. Single images showed BECs were closely packed together at the sheet centre and organised into a pseudostratified layer: one to two cells deep much like *in vivo*. As a result, BECs have formed adhesions with a greater number of neighbouring BECs.

Towards the sheet edge, BECs were loosely packed together as a 2D planar layer, but with voids and recesses opening within the sheet. As a result, fewer adherens junction were present, and fluorescence intensity was relatively reduced than the BEC sheet centre.

Non-levitated single BEC control wells showed highly specific adherens junction staining. Fluorescence was only present between adjacent cells, of small clusters, and absent with surrounding individual cells.
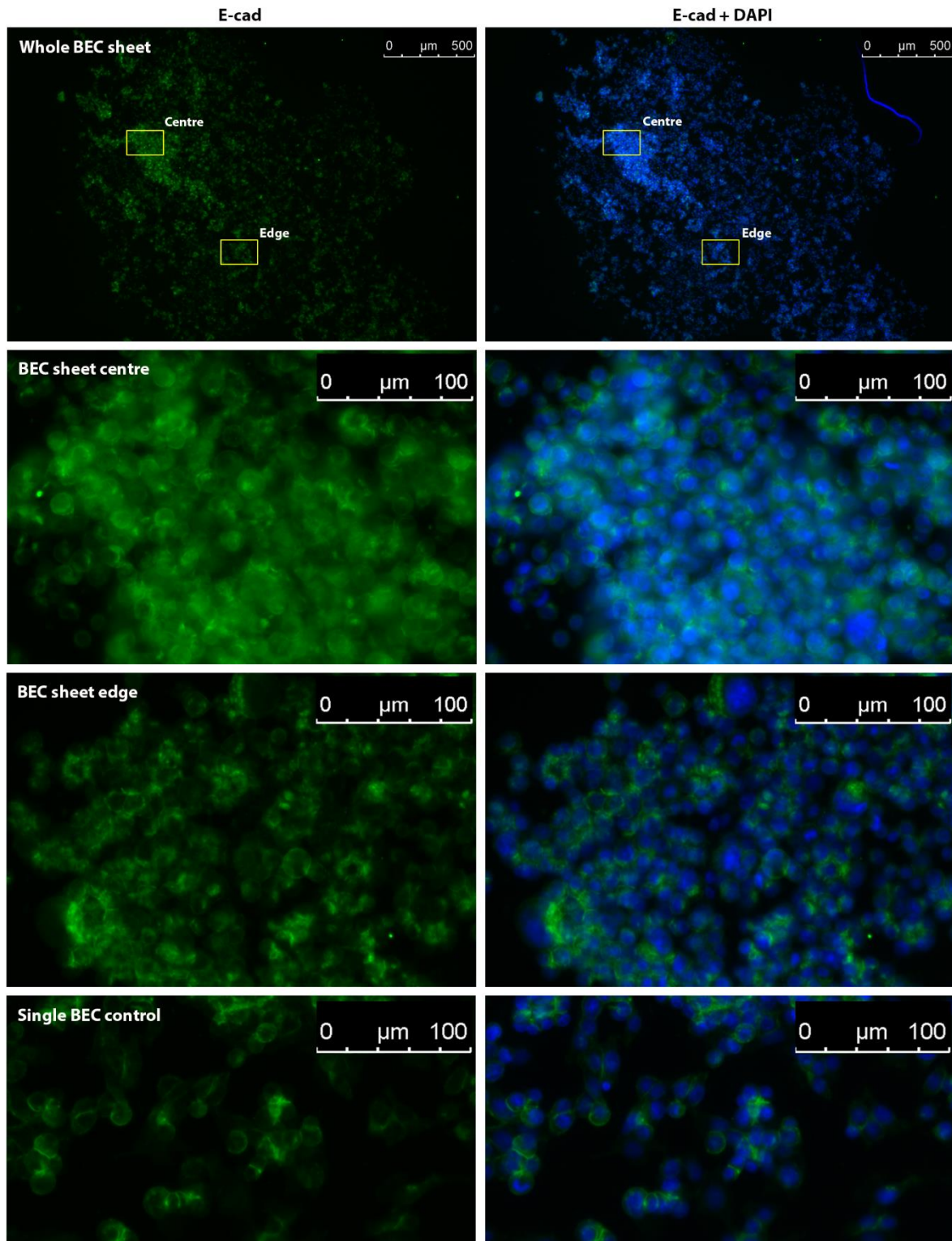
Figure 3.5.11.1 IF staining shows differential adherens junction formation within BEC sheets.
One hour levitated BEC sheets were seeded onto collagen-coated wells, fixed with alcohol and adherens junctions visualised using E-cadherin antibody (green). Nuclei were previously loaded with Hoechst33342 (blue). Towards the centre, BECs appeared pseudostratified and created adhesions with multiple adjacent cells in all directions. BEC sheet edges were 2D planar, but with multiple fissures and fewer adhesions. Single BEC controls were planar with adhesions within small BEC clusters.

Homogeneous adherens staining is also seen with two one-hour levitation experiments. BEC sheet from the third experiment was semi-planar with a high-density of adherins junctions and few cracks. Whereas the fourth experiments BEC sheet was much more sparse and semi-planar Figure 3.5.11.2).

To investigate the density, and orientation of adherens junctions in greater detail, for a single experiment BEC sheet were seeded onto a collagen-coated CS for staining. The intensity and location of the staining between cells were similar to levitated cells. Though, the staggered orientation of the BECs meant all adherens junctions were not in the same focal plane, unlike the single BEC controls (Figure 3.5.11.3).

Overall, IF images supported the idea that BECs were forming appropriate and morphologically accurate adherens junctions while levitating; and that these adhesions were sufficient for BEC sheet creation and subsequent transfer to collagen surfaces.
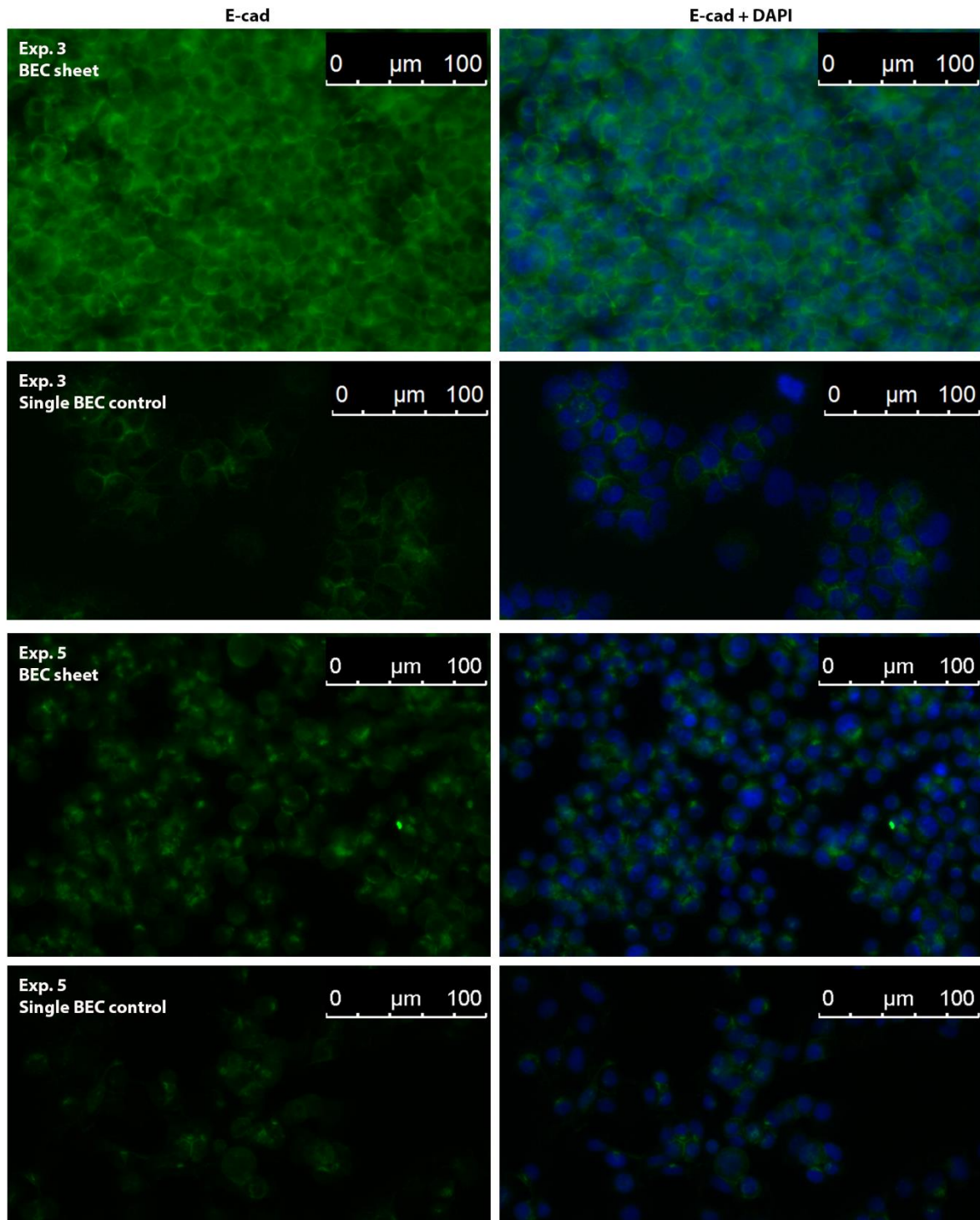
Figure 3.5.11.2 IF staining shows differential adherens junction formation between BEC sheets levitated for one hour.
One hour levitated BEC sheets were seeded onto collagen-coated wells, fixed with alcohol and adherens junctions visualised using E-cadherin antibody (green). Nuclei were previously loaded with Hoechst33342 (blue). For a single experiment BEC sheets appeared pseudostratified and created adhesions with multiple adjacent cells in all directions. For another experiment, BEC sheets were 2D planar, but with multiple fissures and fewer adhesions. All single BEC controls were planar with adhesions within small BEC clusters.
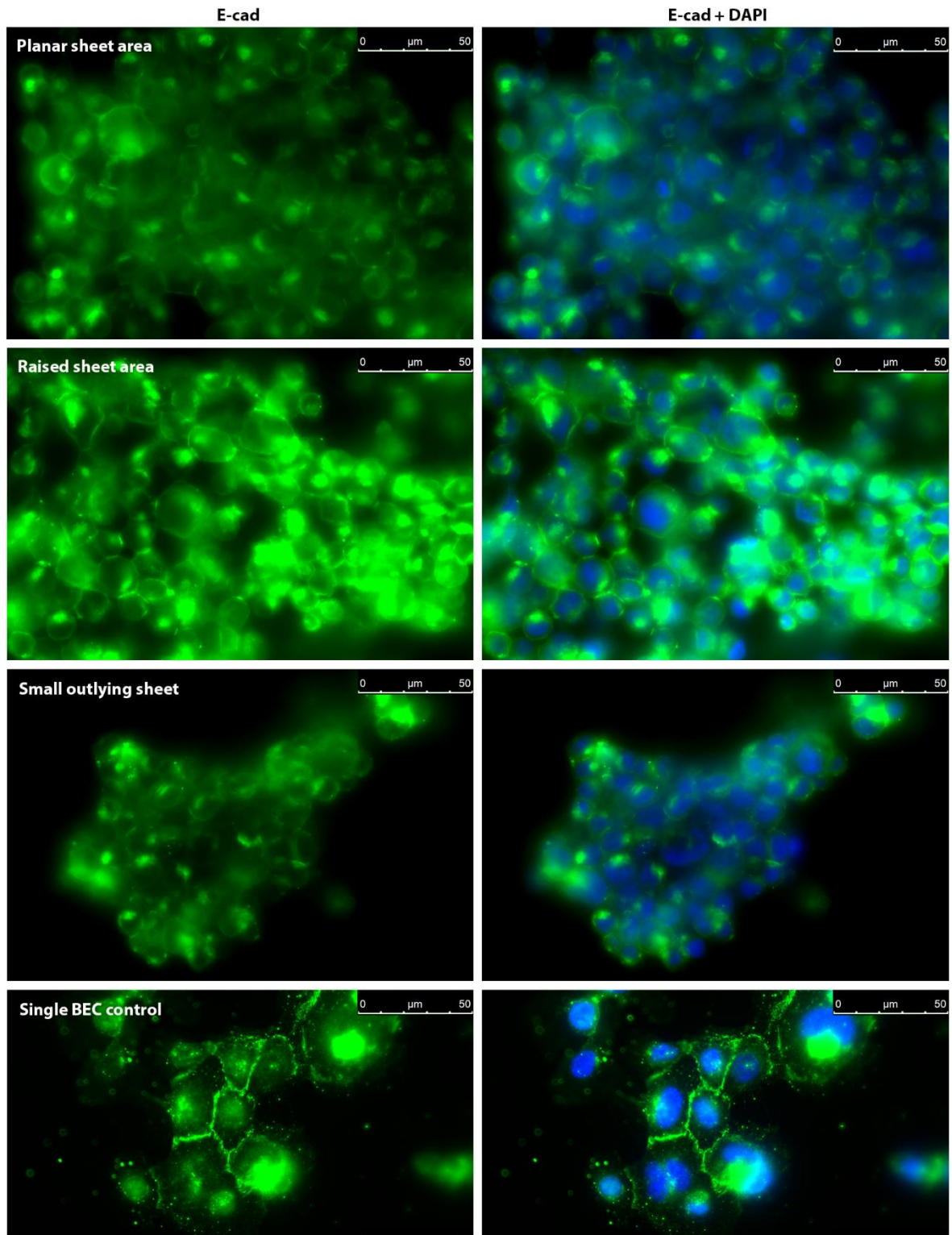
Figure 3.5.11.3 IF staining of adherens junction shows both planar and pseudostratified BEC sheet arrangement.
One hour levitated BEC sheets were seeded onto collagen-coated CS, fixed with alcohol and adherens junctions visualised using E-cadherin antibody (green). Nuclei were previously loaded with Hoechst33342 (blue). Adherens junction arrangement of planar BEC sheet areas was comparable to non-levitated BEC clusters. Raised BEC sheet areas appeared pseudostratified like *in vivo* with irregular junction arrangement. Small outlying sheets exhibited planar junction formation.

100

Chapter 4: General discussion

The purpose of this study was to fabricate novel microfluidic AF devices to generate EC sheets for scaffold-free tissue engineering. Dispensed cell sheets had to satisfy morphological and physiological criteria to be of potential use for 3D tissue graft or research model creation. Developed AF devices must be able to…

1. Create multicellular BEC sheets greater than 50 µM in length and width.
2. Levitate BECs within narrow plane to create BEC sheet monolayers (≤2 cells deep).
3. Maintain viability of BECs (>95%) while levitating inside the device.
4. Levitate BECs steadily enough to create sufficient AJs.
5. Release created BEC sheets without unwanted single cells.

Success or failure using the developed AF devices would expose design limitations, discover new directions for innovation, and help determine the scope of AF technology in the field of cell sheet engineering.

4.1   Morphology of epithelial cell sheets

Levitated cell sheets had to be multi-cellular and planar to ensure sheet layer behaviour and collective movement via plithotaxis. Thus, levitated cell aggregates had to be ≥50 µM in length and width, and no more than two cells in depth. Desirable sheet morphology was achieved by pipette tip loading 50,000 single BECs directly into the PZT volume of the RD3 device. Manual cell bolus increased variability but has potential as a control mechanism (Figure 3.5.10.1).

The precision and flow rate of manually ejecting the cell bolus into the PZT volume determined cell sheet distribution. Cell boluses loaded into fewer lateral nodes of closer proximity became a single BEC sheet, whereas boluses dispersed much further, converged with lateral force gradients or remained distinct due to their size and local force gradient. All levitated sheets exceeded size requirements and had surface areas >0.06 mm^2. Combined sheet surface area was indicative of cell bolus density and was between 4.21 and 5.93 mm^2 for four experiments. The second experiment had an increased cell density and combined sheet area of 10.57 mm^2: either caused by pipetting from a non-homogeneous cell suspension or aberrant pipetting from the suspension. Another contributor to BEC sheet variance was aspirating 2 µL of GM during pipette tip withdrawal to prevent single cell deposition in the loading volume. Aspiration immediately after bolus loading could inadvertently reduce cell density and interfere with bolus dispersal.

Sheet planarity was not measured precisely within the device using Z-stack images due to time constraints. Instead, tilescan images of stained nuclei levitating within the same focal plane were used to assess sheet planarity quickly (Figure 3.5.10.1). Initial images showed that smaller sheets and the edges of larger sheets remained as monolayers, but became increasingly staggered or stratified towards the centre of larger sheets. Fortunately, adherens staining of seeded BEC sheets revealed both planar and complex 3D arrangement of cell-cell adhesions but was not indicative of stratified sheet layers three or more cells deep (Figure 3.5.11.1). Though, cytoskeletal, membrane, or integrin staining with confocal microscopy is needed to confirm this observation.

Initially, the RD2 device provided satisfactory sheets, but with an alternate resonance pattern. Acoustic forces collected cells immediately towards the centre axial and lateral planes as distinct bi-lateral aggregates, which merged slowly over time. PZT degradation led to bi-lateral force depreciation and non-existent bi-lateral merging (Figure 3.5.5.1). Though each levitation device had an individual USWF, the behaviour of USWF pressure nodes could be strongly influenced and potentially normalised by secondary acoustic forces created by the density and distribution of cells within them. LT devices could only be loaded by open tip aspiration, which distributed cells across most device pressure nodes. Cells levitated within peripheral bi-lateral pressure nodes fail to merge bi-laterally and become "static line" aggregates of insufficient width (Figure 3.3.4.2). Whether peripheral node forces were an issue with ST devices is not known due to device design. Pipette tip loading a high density of cells directly into central pressure nodes of RD devices created a stronger bi-lateral force gradient and prevented static line formation. Issues with sheet variability are not limited to AF devices, Dr Tait's static AF device created either a single BEC sheet ~450 μM in size, or multiple smaller sheets[152]. Re-introducing GM perfusion while levitating, but at a further reduced flow rate, could ensure complete lateral merging within the PZT volume over the one hour.

4.2 Viability and functionality of epithelial cell sheets

The viability of levitated cells needed to be comparable to non-levitated cells and kept ≥95%, to allow sufficient adhesion formation and physiological function. It was not possible to quantify cell sheet viability, or consistently measure functionality between ST, LT, and RD device experiments. However, these experiments directed method development and were suggestive of viable cell sheet creation. Preliminary work using the ST devices included measuring physical barrier formation. BEC sheets levitated for two hours using a 6 V peak-peak signal were cultured on collagen-coated transwells up to 18 days. BEC sheets were able to grow, expand and create a physical barrier, demonstrating that levitated cells remained both viable and functional (Figure 3.2.4.1). BEC sheet barrier formation was slower than non-levitated single cell counterparts due to increasingly co-operative movement via plithotaxis (Figure 3.2.4.2).

The NucGreen viability dye was only used with the LT devices. Cells levitated with 6.0 V peak-peak signal showed intense and differential NucGreen staining over time caused either by cavitation, heat-shock death, or reversible sonoporation of the plasma membrane (Figure 3.3.7.1). LT devices were operated using a 2.4 – 2.5 MHz frequency sweep, which followed Wiklund's guidelines of 1-10 MHz to make cavitation less likely, but not impossible[124]. NucGreen was consequently used as a measure of membrane porosity instead of viability. Reducing signal strength to 4.24 V peak-peak decreased NucGreen staining; therefore, potential cavitation or heat-shock death (Figure 3.3.7.2). The reduced 4.24 V was used with all subsequent AF devices.

Functionality testing of RD device-created BEC sheets was collagen adherence within an hour of seeding, before fixation with alcohol. BEC sheets able to create integrins and adhere to the collagen gel were functional and therefore viable. BEC sheets washed away with fixation had reduced functionality or viability. BEC sheets levitated for two hours were unable to adhere to collagen after one hour of seeding (Figure 3.5.8.1), or even twenty-four hours for a single experiment (Figure 3.5.8.2). Cells levitated for thirty minutes, adhered to collagen but were not cell sheets (Figure 3.5.9.1). A one hour levitation period showed promising results. The majority of cells within seeded sheets remained adherent, with only a small sub-population of cells removed after alcohol fixation (Figure 3.5.10.2). Poor adherence of these sheets can be attributed to mechanical and kinetic factors, such as limited contact with the collagen gel and partially stratified sheet arrangement.

4.3 The integrity of epithelial cell sheets after transference

The final requirement was maintaining cell sheet integrity when expelled from AF devices, and preventing the release of single cells into wells via mechanical damage or otherwise. Despite extensive device and technique development, it was not possible to seed BEC sheets without a small sub-population of single cells present (Figure 3.5.10.2/3). To reduce single cell release, loading technique, acoustic signal, and GM perfusion were all explored. However, a strong effort was made to keep the seeding technique as a constant between experiments.

AF device tips were submerged in GM before seeding to avoid damaging hydrostatic interactions with the GM meniscus. Perfusing GM through AF devices at 300 µL/min allowed sheets to pass through the loading volume at sufficient trajectory to avoid contact with the internal capillary surface, due to hydrodynamic forces. Holding AF devices at a precise angle while partially submerged at a specific well location proved challenging, and was not precise. In reality, the location of tip submerging was dependent on the shape and fit of the AF device within the well, and held above at a 55° - 85° angle to compensate. ST and LT devices had PZTs adhered far enough from the loading end to rest against the edge of the well and be held steady with one hand. Whereas, RD devices had PZTs adhered just 2 - 3 mm from the open tip and required much more caution. Steeper angles were needed to submerge the device tips but not the PZT or electrodes. RD devices could not rest against the edge of the well while seeding and required two hands to hold steady. For several RD device experiments, multiple cell sheets were over-laid or folded over themselves in the centre of the well, resulting in mechanical damage and single cell release (Figure 3.5.10.2/3). Slight hand tremors or variable device angles likely influenced the location, spread, and integrity of seeded cell sheets, thereby creating an endemic single cell population. If correct, sheet integrity can only be maintained using a new experimental set-up: sheet seeding outside the microscope with capillary device racks as before, or complete automation.

Dr Tait previously established two hours levitation as sufficient for BEC sheet adherens formation[152]. Two-hour levitations using both ST and LT devices intermittently seeded BEC sheets intact and limited by single cells settled in the loading volume. Two-hour levitations using the RD devices provided intact but non-viable cell sheets. Fortunately, a one-hour levitation period yielded some success with the RD3 device. BEC sheets were fully intact within ten minutes of seeding, but fragmented and released a variable number of single cells later (Figure 3.5.10.2/3). Fragmentation and cell release was also seen with RD2 one-hour levitations (data not shown), and would likely be an issue for all RD devices. Increasing the levitation period by ten or twenty minutes may have resolved this issue, but increased cavitation and heat-death risk.

4.4   Challenges using AF devices for cell sheet engineering

Challenges faced during AF device development revealed several limitations of utilising AF technology for cell sheet engineering, and potential obstacles scaling-up production for clinical and research use. The open-tip aspiration loading technique allowed single cells to settle outside of the PZT-covered capillary volume. Settled cells were more resistant to fluidic forces than levitated sheets, but were released during sheet seeding. Whether a small sub-population of single cells is problematic for epithelial cell sheet creation, is dependent on their application, subtype, and resistance of the recipient cell or protein layer to single cell migration.

Dr Tait demonstrated that single ECs prevent the creation of direct-contact EC and fibroblast co-culture models[152], further supported by preliminary MRes data. Moving independently and in 3D, single epithelial cells cause disruption, and contraction of underlying fibroblast layers, regardless of epithelial cell sheet presence. Single EC presence would be less of an issue creating more durable, stratified epithelial tissues such as the epidermis, cornea, oral mucosa, and oesophagus. Extensive adhesion and physical barrier formation means that a confluent EC layer is much more stable than fibroblast, and could potentially support multiple apically seeded EC sheet layers with minimal risk of disruption or contraction by unwanted single cells.

Alternatively, levitated endothelial cell sheets could be seeded onto confluent sub-epithelium or cardiomyocytes, to create direct-contact arterial and myocardial models. The resistance of these recipient cell layers to single cell disruption is not yet known.

As discussed previously, directly injecting a cell bolus into the PZT volume of AF devices successfully reduced single cell presence in the short-term, but introduced variance and increased the potential for human error. Pipette tip loading also adds another layer of complexity to device usage, which in turn makes automation more difficult and scaling up cell sheet production less likely to occur. An alternative loading technique would require the fabrication of a removable device component, which connects 0.1 mm ID capillary tubing the loading end of the capillary, like the LT1 device. Using the tubing cap and a sufficient flow rate, theoretically single cells could be aspirated directly into the PZT volume of AF devices at a trajectory that minimises contact with the glass capillary surface due to fluidic force dynamics. The proposed tubing cap would later be removed to avoid mechanical damage when seeding levitated cell sheets.

AF devices utilising low-cost borosilicate glass capillaries have unique resonant spectra and require tailored acoustic signals to operate, determined by impedance and conductance readings obtained using an oscilloscope. LT devices exhibited the most extensive acoustic force variance, with the LT2 device proving to be fully aberrant. The RD device series were more homogeneous but had distinct lateral/bi-lateral radiation force relationships. Resonant spectra variance is attributed to several factors including slight irregularities in the epoxy glue layer, location and thickness of the electrode solder, and slight differences in the molecular arrangement of both the borosilicate glass capillary and lead-zinc titanate PZT. Automated manufacture could minimise epoxy and solder-derived resonant force variances, but the glass firing and smelting processes cannot control the precise molecular arrangement of products. Though resonance spectra of manufactured AF devices can never be identical, theoretically, the strength and proximity of desirable conductance peaks could be increased. To this end, manufactured AF devices could be operated simultaneously using an acoustic signal of sufficient range; this was partially successful using the ST devices.

With sustained use, the AF device PZTs can depreciate and require further impedance and conductance readings to provide a new acoustic signal. PZTs can also fully depreciate with over-use and no longer be operational (RD2). Oscilloscopes are not commonplace in cell-based research labs. Adjusting AF device frequency sweeps would incur transport costs returning the device to the manufacturer, or require the purchase of additional equipment to do so. Future AF devices would be operated using the minimum peak-peak voltage and levitation time needed for cell sheet creation, to increase the longevity of PZTs. Individual device tailoring adds a layer of complexity other emergent cell sheet technologies do not possess, such as thermo-responsive polymers and polyelectrolyte films.

Developed AF devices provide a novel method for cell sheet retrieval, with great potential for up-scaling. Pipette tip retrieval of a single sheet limits static acoustic devices and many other non-fluidic cell sheet technologies whereas AF devices allow the transfer of multiple larger cell sheets ≤6 mm in width through the capillary channel opening. Though the developed expulsion method still requires optimisation to prevent cell sheet folding, overlaying, and fragmentation.

4.5　Limitations and weaknesses in the study

The present study could not determine the full scope of AF technology for cell sheet engineering, or the full potential of levitated cell sheets due to several limitations. First and foremost, all levitation experiments were performed within the confines of a microscope hood to allow visualisation, which came with logistical and practical challenges. The utmost diligence was needed to prevent gas bubbles accumulating while conditioning the AF device, syringe, and attached capillary tubing with equilibrated GM. The microfluidic system had to be purged with alcohol then re-conditioned to remove any trapped gas bubbles. The experimental microscope hood environment of 37°C, 5% CO_2 meant LT2-6 and RD devices were susceptible to GM evaporation at their loading end, despite efforts to humidify their local environment. Replacing evaporated GM and shifting the air-GM meniscus proved difficult and frequently led to air bubbles requiring alcohol perfusion formation within these AF devices. Gas bubble accumulation and GM evaporation typically occurred while preparing a single cell suspension in the cell culture lab. Additional alcohol purging and re-conditioning with many experiments mean that the length of time levitated cells were in suspension was not consistent between experiments, which may have impacted the functionality and viability of levitated cells. The arrangement of the AF device microfluidic system and levitation equipment limited hand articulation and pipet/device manipulation within the microscope hood. Depth perception was impaired by the plastic hood casing and made worse by dim lighting of the imaging room. Unfortunately, the copper wire electrodes of AF devices were incredibly delicate. Thus, PZT electrodes intermittently sustained damage: either re-soldering to the PZT or unsheathing of additional wire at the signal receiving end. Dr Tait also encountered problems with fragile PZT electrodes using her static acoustic device[152]. Electrode and solder adjustments may have impacted AF device performance and increased AF device variability.

Levitation experiments within the microscope hood were also a high contamination risk for both created cell cultures, and the microscope lens itself. Multiple hood entry points were fully opened during single cell loading and sheet seeding from AF devices. Particles and visible debris were seen in several 24-well cell culture plates after sheet seeding; plate lids were removed for up to 30 seconds while AF devices were carefully orientated for sheet seeding.

Other limitations of the study include low numbers of replicate experiments, minimal quantitative data for statistical analyses. The study was a collaboration between two departments and two experimental approaches to AF device fabrication, testing, and technique development for desirable cell sheet creation. From a cell biologist's perspective, negative data is of equal value to positive and requires multiple replicates to confirm, such as cellular responses to a drug or pathogen challenge which is a highly complex and

temperamental system. Whereas from an acoustical engineer's point of view, negative data is typically less useful but more reliable and derived from materials science and acoustic/kinetic force interactions. Variables are adjusted more frequently to achieve and replicate positive results, such as optimum device resonance or cell trapping. Combining these research philosophies meant replicate experiment number at each stage of device and method development was inconsistent; exacerbated by AF device damage and gas bubble accumulation. Despite these setbacks, results were positive in the final weeks of the project, but time did not allow for sufficient repeats and statistical analyses.

An additional limitation was the extent of epithelial sheet analysis each experiment.

Fluorescence microscopy allowed sheet size and area to be measured using tilescan images while levitating. However, time constraints and limitations of the imaging software prevented Z-stack imaging of sheet planarity while levitating for most experiments. The intact, adherent BEC sheets from the RD3-device still require integrin staining and confocal microscopy to determine whether they are planar or stratified cell layers.

Functional analysis of sheets was inconsistent between device series. MRes data using ST devices included physical barrier analysis of long term cell sheet cultures, whereas sheets levitated using LT and RD devices were alcohol fixated one or twenty-four hours after seeding. Functional analysis of the latter cell sheets was limited to successful adhesion to a collagen-coated surface. NucGreen viability dye could only measure the extent of levitated cell membrane sonoporation; thus, collagen adhesion became a blunt measure of viability also.

E-cadherin staining of cell sheets was not truly representative of cell-cell contact adhesion formation while levitating: seeded sheets required one hour to adhere to the collagen, and would have formed additional adherens junctions with each other before fixation.

4.6   Summary

Static AF devices have previously been used for tissue engineering in several ways such as controlling the spatial organisation of epithelium, endothelium, and fibroblast cells within a hydrogel[145], the creation of 3D hepatocyte spheroids[122] and modifying collagen fibril ultrastructure[146]. Microfluidic AF devices couple AF technology to a microfluidic system, and have successfully been used to create autologous 3D cartilage tissue grafts[151]. A static AF device has previously been used to generate EC sheets by Dr Tait[152,153] but was limited by pipette tip retrieval of a single cell sheet.

This study presents the first successful application of an inexpensive, glass capillary-based AF device for EC sheet creation, with potential for higher EC sheet output and easier sheet handling and transfer via a microfluidic system. Thus, establishing AF levitation amongst a crowded field of emergent cell sheet technologies that warrant further exploration[38]. Developed AF devices were able to levitate single BECs to create viable, planar BEC sheets which satisfied morphological, and functional requirements, such as sufficient cell-cell and cell-ECM adhesion formation for cohesive movement via plithotaxis, and physical barrier formation.

4.7 Device validation

As discussed previously, it was not possible to measure BEC sheet viability using NucGreen dye due to sonoporation of cell membranes, and seeing whether seeded BEC sheets adhere to collagen-coated surfaces was not an accurate alternative. Therefore, another method to determine BEC sheet viability post-levitation is needed.

A way of testing viability is by labelling cells with Bromodeoxyuridine / 5-bromo-2'-deoxyuridine (BrdU) (Abcam, U.K), which is an analogue of thymidine and is incorporated into newly synthesised DNA of replicating cells. These cells can then identified using primary, and fluorescently labelled secondary antibodies. DNA synthesis and continued progression through the cell cycle is a useful indicator for cell viability. If the percentage of BrdU-positive cells in a levitated BEC sheet population remains the same as a non-levitated single BEC population, this would indicate ≥95% viability (expected viability of cells after passage).

Before viability experiments are performed, the length of time BECs are incubated with BrdU labelling solution will need to be optimised. The protocol and an example plate layout for this experiment is shown below. Following this, BECs would be levitated for 45 minutes using the RD3 device (tailored 0.1 MHz frequency sweep and 4.24 V signal strength) to determine the minimum required time for the creation of BEC sheets without significantly reducing viability.

Optimisation of incubation time needed for BrdU labelling of BECs

4.7.1.1   24-well plate layout

[1] 150,000 single 16HBE + ddH$_2$O for 1 hour	[4] 150,000 single 16HBE + ddH$_2$O for 2 hours	[7] 150,000 single 16HBE + ddH$_2$O for 4 hours	[10] 150,000 single 16HBE + ddH$_2$O for 8 hours	[13] 150,000 single 16HBE + ddH$_2$O for 16 hours	[16] 150,000 single 16HBE + ddH$_2$O for 24 hours
[2] 150,000 single 16HBE + BrdU for 1 hour	[5] 150,000 single 16HBE + BrdU for 2 hours	[8] 150,000 single 16HBE + BrdU for 4 hours	[11] 150,000 single 16HBE + BrdU for 8 hours	[14] 150,000 single 16HBE + BrdU for 16 hours	[17] 150,000 single 16HBE + BrdU for 24 hours
[3] 150,000 single 16HBE + BrdU for 1 hour	[6] 150,000 single 16HBE + BrdU for 2 hours	[9] 150,000 single 16HBE + BrdU for 4 hours	[12] 150,000 single 16HBE + BrdU for 8 hours	[15] 150,000 single 16HBE + BrdU for 16 hours	[18] 150,000 single 16HBE + BrdU for 24 hours
[19] 150,000 single 16HBE for secondary Ab control					

4.7.1.2   Method

1. Sterilise and collagen-coat glass coverslips (as described in 2.1.5) then transfer to 24-well plate (as shown in 4.7.1.1).

2. Passage confluent flask of 16HBEs to prepare single cell suspension (as described in 2.1.2).

3. Seed each glass coverslip with 150,000 single 16HBEs (as described in 2.1.5).

4. Incubate 16HBE cells (24 hours, 37°C, 5% CO_2).

5. Prepare 10 mM BrdU stock solution.

6. Dilute BrdU stock solution in 16HBE GM to make 10 µM BrdU labelling solution.

7. Filter the 10 µM BrdU labelling solution through a 0.2 µm filter under sterile conditions.

8. Replace 16HBE GM with 500 µL of 10 µM labelling solution.

9. Incubate 16HBE cells (37°C, 5% CO_2).

10. Fix cells at the appropriate timepoints (as shown in 4.7.1.1) using 500 µL of 4% paraformaldehyde (PFA) solution (15 minutes, 4°C).

11. Rinse cells with 500 µL of 1xPBS three times.

12. Permeabilise the cells using 0.1% Triton X-100 in 1xPBS (30 minutes, RT).

13. Rinse cells with 500 µL of 1xPBS three times.

14. Prepare block buffer solution (1% BSA, 0.1% Tween-20 in 1xPBS)

15. Block cells using 1 mL block buffer (30 minutes, RT).

16. Add 500 µL of BrdU primary antibody (ab8152) diluted in block buffer then incubate (overnight, 4°C).

17. Rinse cells with 500 µL of 1xPBS three times.

18. Add 500 µL of Alexa Flour 594-conjugated secondary antibody diluted 1:200 in block buffer (1 hour, 4°C).

19. Rinse cells with 500 µL of 1xPBS three times.

20. Add one drop of Hoechst 33342 to each well then incubate (15 minutes, 37°C, 5% CO_2).

21. Mount glass coverslips onto microscope slides using Mowiol.

22. Image slides using a fluorescence microscope and count the number of BrdU positive and Hoechst 33342 positive cells the centre of each coverslip.

23. Calculate BrdU positive cells as a percentage of total population for each coverslips to determine optimal incubation time for BrdU labelling.

Investigating viability of BEC sheets after 45 minutes of acoustic levitation within RD3 device using BrdU labelling.

4.7.1.3　Hypothesis:

Levitating BEC cells within RD3 device for 45 minutes using a 4.24V signal strength creates planar cell sheets that are >95% viable.

4.7.1.4　Aims:

Aim 1. Determine minimum levitation period needed for the creation of planar sheets from single 16HBE cell suspension.

Aim 2. Use BrdU staining to determine viability of 16HBE cells after levitation within RD4 device for 45 minutes using a 4.24 V signal strength.

Aim 3. Determine validity of RD4 device design for planar cell sheet creation.

4.7.1.5　24-well plate layout

[1] 50,000 single 16HBE + ddH$_2$O	[3] 50,000 single 16HBE + 10 µM BrdU	[5] 50,000 levitated 16HBE + 10 µM BrdU
[2] 50,000 single 16HBE + ddH$_2$O	[4] 50,000 single 16HBE + 10 µM BrdU	[6] Remaining levitated 16HBE + 10 µM BrdU

4.7.1.6　Method

1. Sterilise and collagen-coat glass coverslips (as described in 2.1.5) and arrange them in 24-well plate (as shown above).
2. Passage confluent flask of 16HBEs (as described in 2.1.2) to prepare 1.5 x10^6 single cell suspension.
3. Pre-load cell suspension with Hoechst33342 nuclear stain (as described in 2.3.3).
4. Seed coverslips with 50,000 single cell controls then incubate (37°C, 5% CO$_2$).
5. Within the microscope hood, directly inject a 10 µL bolus of 50,000 cells into the PZT volume of the RD3 device using a flat pipet-tip and single-release technique (as described in 3.5.4).
6. Levitate cells using tailored frequency sweep/signal (45 minutes, 37°C, 5% CO$_2$).
7. Acquire tilescan images of whole PZT volume whilst cells are levitated.
8. Seed levitated cell sheets into wells (as described in 3.5.8) and visualise using bright field and DAPI-FLUO channels
9. Incubate cells (24 hours, 37°C, 5% CO$_2$).
10. Prepare BrdU labelling solution (as described in 4.7.1.2).

112

11. Replace 16HBE GM with 500 µL of 10 µM labelling solution and incubate for optimal length of time (37°C, 5% CO_2).

12. Stain coverslips with primary and secondary antibodies and mount coverslips onto glass slides (as described in 4.7.1.2)

13. Image slides using a fluorescence microscope to calculate percentage viability of levitated cell sheets and non-levitated single cell controls.

Analysis

To measure the number and size and the extent of damage the BEC sheets sustain when seeded, brightfield and DAPI-FLUO channel tilescan images immediately before, one and 24 hours after seeding will be analysed using ImageJ software.

Viability of levitated BEC sheets and single BEC control populations will be assessed using Hoechst33342 and BrdU labelling, which will be visualised with a fluorescence microscope using the DAPI-FLUO and Cy5-FLUO channels, respectively. Representative images for each slide will be acquired at 5-40x magnification. The assessor will be blinded to the time point, and the percentage of BrdU positive cells in each population will be calculated. Non-levitated single BECs will be used as a control for viable cells (typically ≥95% confluent after passage).

The experiment will be performed three times to allow statistical analysis of BrdU populations using a one-way ANOVA with Tukey's multiple comparison test to determine whether 45 minutes levitation significantly affects the population of BrdU positive cells, and therefore the viability of BECs.

4.7.2 Conclusions

If a small population of BECs do not form cell-cell contact adhesions while levitating for 45 minutes and are released as single BECs into wells, then the experiment will be repeated a further three times using a one-hour levitation period. If the population of single BECs persists, then the RD device design cannot be used for BEC sheet creation and will require further development.

If BrdU staining shows significantly reduced viability after 45 minutes (or one hour) of acoustofluidic levitation, the RD4 device will be tested in further experiments. If problems with BEC sheet viability persist, this will also elicit further RD device development.

However, if results are positive and the RD3 device reliably produces BEC sheets of sufficient size and viability (without single BECs present), further experiments can be performed using RD devices to determine morphology and functionality of seeded BEC sheets.

4.8   Future work

Utilising AF devices for cell sheet creation requires further method development to increase cell sheet integrity, and to prevent them overlaying or folding when seeded. Replicate experiments are needed in order to perform statistics on the sheet area and depth. Z-stack confocal images could be acquired to quantify the level of cell overlaying. In addition transmission electron microscope (TEM) imaging can be used to analyse TJ formation. Both aforementioned imaging techniques would also allow the depth of the cells to be measured. Once the morphology of cells has been confirmed, functional studies need to be performed on the cells. Examples of these include but are not limited to, TER measurements of long term cultures to assess barrier properties, western blots of cell-specific markers (e.g. T5) and staining of integrins, desmosomes and F-actin.

Future studies should also consider levitating multiple epithelial or endothelial cell subtypes and create stratified epithelial sheet layer constructs to demonstrate the versatility of AF devices for tissue creation. If successful, levitated sheet constructs have enormous potential as autologous tissue grafts for transplant, or complex tissue models for disease research.

When comparing tissue constructs created using AF devices against other scaffold-free technologies (i.e. thermo-responsive polymers), investigators should be blinded to the device used in order to eliminate any unconscious bias. For morphological analysis, the identity of tissue constructs mounted onto glass slides could be erased and coded by another lab member. For functional analysis, confluent tissue constructs created in transwells could be rearranged within a plate and again coded by another lab member before measuring TER and therefore barrier formation.

Bibliography

1. Alberts B, Bray D, Hopkin K, et al. *Essential cell biology*. 2nd ed: Garland Science; 2004.

2. Norden C. Pseudostratified epithelia - cell biology, diversity and roles in organ formation at a glance. *Journal of Cell Science* 2017;130(11):1859-63.

3. Gerritsen J. Series: Basic Sciences: Host defence mechanisms of the respiratory system. *Paediatric Respiratory Reviews* 2000;1(2):128-34.

4. Sadati M, Qazvini NT, Krishnan R, et al. Collective migration and cell jamming. *Differentiation* 2013;86(3):121-25.

5. Fletcher DA, Mullins D. Cell mechanics and the cytoskeleton. *Nature* 2010;463(7280):485-92.

6. Chalut KJ, Paluch EK. The Actin Cortex: A Bridge between Cell Shape and Function. *Developmental Cell* 2016;38(6):571-73.

7. Gumbiner B. Cadherins: a family of Ca2+ dependent adhesion molecules. *Trends in Biochemistry Scinece* 1998;13(3):670-78.

8. Miller PW, Clarke DN, Weis WI, et al. The Evolutionary Origin of Epithelial Cell-Cell Adhesion Mechanisms. In: Bennett V (ed.) *Functional Organization of Vertebrate Plasma Membrane*; 2013 p267-311.

9. Green KJ, Jones JCR. Desmosomes and hemidesmosomes: Structure and function of molecular components. *Faseb Journal* 1996;10(8):871-81.

10. Garrod D, Chidgey M, North A. Desmosomes: Differentiation, development, dynamics and disease. *Current Opinion in Cell Biology* 1996;8(5):670-78.

11. Adair BD, Xiong J-P, Maddock C, et al. Three-dimensional EM structure of the ectodomain of integrin αVβ3 in a complex with fibronectin. *The Journal of cell biology* 2005;168(7):1109-18.

12. Delon I, Brown NH. Integrins and the actin cytoskeleton. *Current Opinion in Cell Biology* 2007;19(1):43-50.

13. Aijaz S, Balda MS, Matter K. Tight junctions: molecular architecture and function. *International review of cytology* 2006;248:261-98.

14. Tsukita S, Tstlkita S. Occludin: a novel integral membrane protein localizing at tight junctions. *J Cell Biol* 1993;123(6 Pt 2):17771788.

15. Fanning AS, Jameson BJ, Jesaitis LA, et al. The tight junction protein ZO-1 establishes a link between the transmembrane protein occludin and the actin cytoskeleton. *Journal of Biological Chemistry* 1998;273(45):29745-53.

16. Feldman GJ, Mullin JM, Ryan MP. Occludin: Structure, function and regulation. *Advanced Drug Delivery Reviews* 2005;57(6):883-917.

17. Kostrewa D, Brockhaus M, D'Arcy A, et al. X-ray structure of junctional adhesion molecule: structural basis for homophilic adhesion via a novel dimerization motif. *The EMBO journal* 2001;20(16):4391-98.

18. Günzel D, Alan S. Claudins and the modulation of tight junction permeability. *Physiological reviews* 2013;93(2):525-69.

19. Schmidt S, Friedl P. Interstitial cell migration: integrin-dependent and alternative adhesion mechanisms. *Cell Tissue Res* 2010;339(1):83-92.

20. MW. K. The Medical Biochemistry Page. 2016. <span style="font-size:11.0ptmso-bidi-font-size:10.0ptmso-bidi-language:AR-SA">http://themedicalbiochemistrypage.org/extracellularmatrix.php#fibronectin. (accessed28/07/2016).

21. Wise SG, Weiss AS. Tropoelastin. *Int J Biochem Cell Biol* 2009;41(3):494-7.

22. Weber GF, Bjerke MA, DeSimone DW. A Mechanoresponsive Cadherin-Keratin Complex Directs Polarized Protrusive Behavior and Collective Cell Migration. *Developmental Cell* 2012;22(1):104-15.

23. Trepat X, Fredberg JJ. Plithotaxis and emergent dynamics in collective cellular migration. *Trends in Cell Biology* 2011;21(11):638-46.

24. Serra-Picamal X, Conte V, Vincent R, et al. Mechanical waves during tissue expansion. *Nature Physics* 2012;8(8):628-U66.

25. Angelini TE, Hannezo E, Trepat X, et al. Glass-like dynamics of collective cell migration. *Proceedings of the National Academy of Sciences of the United States of America* 2011;108(12):4714-19.

26. Wu PH, Gilkes DM, Wirtz D. The Biophysics of 3D Cell Migration. In: Dill KA (ed.) *Annual Review of Biophysics, Vol 47*; 2018 p549-67.

27. Physiology Aa. *Epithelial tissue*. http://anatomyandphysiologyi.com/epithelial-tissue/ (accessed 11.06.2018).

28. Strauss O. The role of retinal pigment epithelium in visual functions. *Ophthalmologe* 2009;106(4):299-304.

29. Strzyz PJ, Matejcic M, Norden C. Heterogeneity, Cell Biology and Tissue Mechanics of Pseudostratified Epithelia: Coordination of Cell Divisions and Growth in Tightly Packed Tissues. In: Jeon KW (ed.) *International Review of Cell and Molecular Biology, Vol 325*; 2016 p89-118.

30. Hong KU, Reynolds SD, Watkins S, et al. Basal cells are a multipotent progenitor capable of renewing the bronchial epithelium. *American Journal of Pathology* 2004;164(2):577-88.

31. Duffield JS, Lupher M, Thannickal VJ, et al. Host responses in tissue repair and fibrosis. *Annual Review of Pathology: Mechanisms of Disease* 2013;8:241-76.

32. Hallstrand TS, Hackett TL, Altemeier WA, et al. Airway epithelial regulation of pulmonary immune homeostasis and inflammation. *Clinical Immunology* 2014;151(1):1-15.

33. Nicholas B, Skipp P, Mould R, et al. Shotgun proteomic analysis of human-induced sputum. *Proteomics* 2006;6(15):4390-401.

34. Zakeri A, Yazdi FG. Toll-like receptor-mediated involvement of innate immune cells in asthma disease. *Biochimica et Biophysica Acta (BBA) - General Subjects* 2017;1861(1, Part A):3270-77.

35. Greene CM, McElvaney NG. Toll-like receptor expression and function in airway epithelial cells. *ARCHIVUM IMMUNOLOGIAE ET THERAPIAE EXPERIMENTALIS-ENGLISH EDITION-* 2005;53(5):418.

36. Huston DP, Liu YJ. Thymic stromal lymphopoietin: A potential therapeutic target for allergy and asthma. *Current Allergy and Asthma Reports* 2006;6(5):372-76.

37. Li MX, Ma J, Gao YB, et al. Cell sheet technology: a promising strategy in regenerative medicine. *Cytotherapy* 2019;21(1):3-16.

38. Kirby GS, Michelmore A, Smith LE, et al. Cell sheets in cell therapies. *Cytotherapy* 2018;20(2):169-80.

39. Segers VFM, Lee RT. Biomaterials to Enhance Stem Cell Function in the Heart. *Circulation Research* 2011;109(8):910-22.

40. Ratner D. Skin grafting - From here to there. *Dermatologic Clinics* 1998;16(1):75-+.

41. Wolfe J, R. A new method of performing plastic operations. *The British Medical Journal* 1875.

42. Rheinwald JG, Green H. SERIAL CULTIVATION OF STRAINS OF HUMAN EPIDERMAL KERATINOCYTES - FORMATION OF KERATINIZING COLONIES FROM SINGLE CELLS. *Cell* 1975;6(3):331-44.

43. Oconnor NE, Mulliken JB, Banksschlegel S, et al. GRAFTING OF BURNS WITH CULTURED EPITHELIUM PREPARED FROM AUTOLOGOUS EPIDERMAL-CELLS. *Lancet* 1981;1(8211):75-78.

44. Yang J, Yamato M, Kohno C, et al. Cell sheet engineering: Recreating tissues without biodegradable scaffolds. *Biomaterials* 2005;26(33):6415-22.

45. Vacanti JP. BEYOND TRANSPLANTATION - 3RD ANNUAL MIXTER,SAMUEL,JASON, LECTURE. *Archives of Surgery* 1988;123(5):545-49.

46. Langer R, Vacanti JP. TISSUE ENGINEERING. *Science* 1993;260(5110):920-26.

47. Vacanti CA, Vacanti JP. The science of tissue engineering. *Orthopedic Clinics of North America* 2000;31(3):351-+.

48. MacNeil S, Shepherd J, Smith L. Production of Tissue-Engineered Skin and Oral Mucosa for Clinical and Experimental Use. *3d Cell Culture: Methods and Protocols* 2011;695:129-53.

49. Bhargava S, Patterson JM, Inman RD, et al. Tissue-engineered buccal mucosa urethroplasty - Clinical outcomes. *European Urology* 2008;53(6):1263-71.

50. Kim HS, Song XJ, de Paiva C, et al. Phenotypic characterization of human corneal epithelial cells expanded ex vivo from limbal explant and single cell cultures. *Experimental Eye Research* 2004;79(1):41-49.

51. Jonas JB, Cheung CMG, Panda-Jonas S. Updates on the Epidemiology of Age-Related Macular Degeneration. *Asia-Pacific Journal of Ophthalmology* 2017;6(6):493-97.

52. Singh S, Woerly S, McLaughlin BJ. Natural and artificial substrates for retinal pigment epithelial monolayer transplantation. *Biomaterials* 2001;22(24):3337-43.

53. Alexander P, Thomson HAJ, Luff AJ, et al. Retinal pigment epithelium transplantation: concepts, challenges, and future prospects. *Eye* 2015;29(8):992-1002.

54. Ong CS, Nam L, Ong K, et al. 3D and 4D Bioprinting of the Myocardium: Current Approaches, Challenges, and Future Prospects. *Biomed Research International* 2018.

55. Roth GA, Johnson C, Abajobir A, et al. Global, Regional, and National Burden of Cardiovascular Diseases for 10 Causes, 1990 to 2015. *Journal of the American College of Cardiology* 2017;70(1):1-25.

56. Munos B. Lessons from 60 years of pharmaceutical innovation. *Nature Reviews Drug Discovery* 2009;8(12):959-68.

57. Asthma UK. *Asthma facts and statistics*. https://www.asthma.org.uk/about/media/facts-and-statistics (accessed 01/08/2016).

58. Holgate ST, Arshad HS, Roberts GC, et al. A new look at the pathogenesis of asthma. *Clinical Science* 2010;118(7-8):439-50.

59. Brown HM, Storey G, George WHS. BECLOMETHASONE DIPROPIONATE - NEW STEROID AEROSOL FOR TREATMENT OF ALLERGIC ASTHMA. *British Medical Journal* 1972;1(5800):585-&.

60. Swindle EJ, Davies DE. Artificial airways for the study of respiratory disease. *Expert review of respiratory medicine* 2011;5(6):757-65.

61. Birgersdotter A, Sandberg R, Ernberg I. Gene expression perturbation in vitro - A growing case for three-dimensional (3D) culture systems. *Seminars in Cancer Biology* 2005;15(5):405-12.

62. Cukierman E, Pankov R, Yamada KM. Cell interactions with three-dimensional matrices. *Current Opinion in Cell Biology* 2002;14(5):633-39.

63. Griffith LG, Swartz MA. Capturing complex 3D tissue physiology in vitro. *Nature Reviews Molecular Cell Biology* 2006;7(3):211-24.

64. Nelson CM, Bissell MJ. Of extracellular matrix, scaffolds, and signaling: Tissue architecture regulates development, homeostasis, and cancer *Annual Review of Cell and Developmental Biology*; 2006 p287-309.

65. Knight ZA, Shokat KM. Chemical genetics: Where genetics and pharmacology meet. *Cell* 2007;128(3):425-30.

66. Gura T. Cancer models - Systems for identifying new drugs are often faulty. *Science* 1997;278(5340):1041-42.

67. Reuters. *U.S. to develop chip that tests if a drug is toxic.* http://www.msnbc.msn.com/id/4455007/ns/health-health care/-..To5AMnPaixF. (accessed 1st May).

68. Kieburtz K, Olanow CW. Translational experimental therapeutics: The translation of laboratory-based discovery into disease-related therapy. *Mount Sinai Journal of Medicine* 2007;74(1):7-14.

69. Liu Z, Maas K, Aune TM. Comparison of differentially expressed genes in T lymphocytes between human autoimmune disease and murine models of autoimmune disease. *Clinical Immunology* 2004;112(3):225-30.

70. Blume C, Davies DE. In vitro and ex vivo models of human asthma. *European Journal of Pharmaceutics and Biopharmaceutics* 2013;84(2):394-400.

71. Research VM. 3D Cell Culture Market (By Technology: Extracellular Matrices, Bioreactors, Gels, Scaffold Free Platform, and Microchips; By Application: Research, Drug Discovery, Tissue Engineering, Clinical Applications and Stem Cell Biology; By End-User: Research Laboratories & Institutes, Biotechnology and Pharmaceutical Industry and Hospital & Diagnostic Centers; By Geography: North America, Europe, Asia-Pacific and RoW) Global Scenario, Market Size, Outlook, Trend, and Forecast, 2015-2024.: Variant Market Research, 2017:1-120.

72. Michalek J, Pradny M, Dusek K, et al. *Hydrogels in Biology and Medicine*. Prague 6, Czech Republic: Nova Science Publishers; 2010.

73. Lutolf MP. Integration column: artificial ECM: expanding the cell biology toolbox in 3D. *Integrative Biology* 2009;1(3):235-41.

74. Przyborski S. Advanced Cell Culture Technology for Generation of In vivo-like Tissue Models, 2018.

75. Loh QL, Choong C. Three-Dimensional Scaffolds for Tissue Engineering Applications: Role of Porosity and Pore Size. *Tissue Engineering Part B-Reviews* 2013;19(6):485-502.

76. Ronneberger B, Kao WJ, Anderson JM, et al. In vivo biocompatibility study of ABA triblock copolymers consisting of poly(L-lactic-co-glycolic acid) A blocks attached to central poly(oxyethylene) B blocks. *Journal of Biomedical Materials Research* 1996;30(1):31-40.

77. Schakenraad JM, Hardonk MJ, Feijen J, et al. ENZYMATIC-ACTIVITY TOWARD POLY(L-LACTIC ACID) IMPLANTS. *Journal of Biomedical Materials Research* 1990;24(5):529-45.

78. Sheikh AY, Lin SA, Cao F, et al. Molecular Imaging of bone marrow mononuclear cell homing and engraftment in ischemic myocardium. *Stem Cells* 2007;25(10):2677-84.

79. Zhang M, Methot D, Poppa V, et al. Cardiomyocyte grafting for cardiac repair: Graft cell death and anti-death strategies. *Journal of Molecular and Cellular Cardiology* 2001;33(5):907-21.

80. Dababneh AB, Ozbolat IT. Bioprinting Technology: A Current State-of-the-Art Review. *Journal of Manufacturing Science and Engineering-Transactions of the Asme* 2014;136(6).

81. Green H, Kehinde O, Thomas J. GROWTH OF CULTURED HUMAN EPIDERMAL-CELLS INTO MULTIPLE EPITHELIA SUITABLE FOR GRAFTING. *Proceedings of the National Academy of Sciences of the United States of America* 1979;76(11):5665-68.

82. Hernon CA, Dawson RA, Freedlander E, et al. Clinical experience using cultured epithelial autografts leads to an alternative methodology for transferring skin cells from the laboratory to the patient. *Regenerative Medicine* 2006;1(6):809-21.

83. Yamada N, Okano T, Sakai H, et al. Thermo-responsive polymeric surfaces; control of attachment and detachment of cultured cells. *Die Makromolekulare Chemie.* 1990;11(11).

84. Nithya J, Kumar PRA, Tilak P, et al. Intelligent Thermoresponsive Substrate from Modified Overhead Projection Sheet as a Tool for Construction and Support of Cell Sheets In Vitro. *Tissue Engineering Part C-Methods* 2011;17(2):181-91.

85. Tang Z, Kikuchi A, Akiyama Y, et al. Novel cell sheet carriers using polyion complex gel modified membranes for tissue engineering technology for cell sheet manipulation and transplantation. *Reactive & Functional Polymers* 2007;67(11):1388-97.

86. Nishida K, Yamato M, Hayashida Y, et al. Functional bioengineered corneal epithelial sheet grafts from corneal stem cells expanded ex vivo on a temperature-responsieve cell culture surface. *Transplantation* 2004;77(3):379-85.

87. Madathil BK, Sundaran SP, Kumary TV, et al. Biofunctionalised polycaprolactone fibrous mat as a transfer tool for cell sheet engineering. *Fibers and Polymers* 2017;18(11):2094-101.

88. Ide T, Nishida K, Yamato M, et al. Structural characterization of bioengineered human corneal endothelial cell sheets fabricated on temperature-responsive culture dishes. *Biomaterials* 2006;27(4):607-14.

89. Huang C-C, Liao Z-X, Chen D-Y, et al. Injectable Cell Constructs Fabricated via Culture on a Thermoresponsive Methylcellulose Hydrogel System for the Treatment of Ischemic Diseases. *Advanced Healthcare Materials* 2014;3(8):1133-48.

90. Ito A, Hayashida M, Honda H, et al. Construction and harvest of multilayered keratinocyte sheets using magnetite nanoparticles and magnetic force. *Tissue Engineering* 2004;10(5-6):873-80.

91. Ito A, Takizawa Y, Honda H, et al. Tissue engineering using magnetite nanoparticles and magnetic force: Heterotypic layers of cocultured hepatocytes and endothelial cells. *Tissue Engineering* 2004;10(5-6):833-40.

92. Guillaume-Gentil O, Akiyama Y, Schuler M, et al. Polyelectrolyte coatings with a potential for electronic control and cell sheet engineering. *Advanced Materials* 2008;20(3):560-+.

93. Guillaume-Gentil O, Semenov OV, Zisch AH, et al. pH-controlled recovery of placenta-derived mesenchymal stem cell sheets. *Biomaterials* 2011;32(19):4376-84.

94. Hong Y, Yu M, Weng W, et al. Light-induced cell detachment for cell sheet technology. *Biomaterials* 2013;34(1):11-18.

95. Griffith M, Osborne R, Munger R, et al. Functional human corneal equivalents constructed from cell lines. *Science* 1999;286(5447):2169-72.

96. Bhargava S, Chapple CR, Bullock AJ, et al. Tissue-engineered buccal mucosa for substitution urethroplasty. *Bju International* 2004;93(6):807-11.

97. Yamato M, Utsumi M, Kushida A, et al. Thermo-responsive culture dishes allow the intact harvest of multilayered keratinocyte sheets without dispase by reducing temperature. *Tissue Engineering* 2001;7(4):473-80.

98. von Recum H, Kikuchi A, Yamato M, et al. Growth factor and matrix molecules preserve cell function on thermally responsive culture surfaces. *Tissue Engineering* 1999;5(3):251-65.

99. Nishida K, Yamato M, Hayashida Y, et al. Corneal reconstruction with tissue-engineered cell sheets composed of autologous oral mucosal epithelium. *New England Journal of Medicine* 2004;351(12):1187-96.

100. Shiroyanagi Y, Yamato M, Yamazaki Y, et al. Transplantable urothelial cell sheets harvested noninvasively from temperature-responsive culture surfaces by reducing temperature. *Tissue Engineering* 2003;9(5):1005-12.

101. Shiroyanagi Y, Yamato M, Yamazaki Y, et al. Urothelium regeneration using viable cultured urothelial cell sheets grafted on demucosalized gastric flaps. *Journal of Urology* 2004;171(4):460-60.

102. Kushida A, Yamato M, Isoi Y, et al. A noninvasive transfer system for polarized renal tubule epithelial cell sheets using temperature-responsive culture dishes. *European Cells and Materials* 2005;10:23-30.

103. Hirose M, Kwon OH, Yamato M, et al. Creation of designed shape cell sheets that are noninvasively harvested and moved onto another surface. *Biomacromolecules* 2000;1(3):377-81.

104. Hasegawa M, Yamato M, Kikuchi A, et al. Human periodontal ligament cell sheets can regenerate periodontal ligament tissue in an athymic rat model. *Tissue Engineering* 2005;11(3-4):469-78.

105. Akizuki T, Oda S, Komaki M, et al. Application of periodontal ligament cell sheet for periodontal regeneration: a pilot study in beagle dogs. *Journal of Periodontal Research* 2005;40(3):245-51.

106. Shimizu T, Yamato M, Isoi Y, et al. Fabrication of pulsatile cardiac tissue grafts using a novel 3-dimensional cell sheet manipulation technique and temperature-responsive cell culture surfaces. *Circulation Research* 2002;90(3):E40-E48.

107. Shimizu T, Sekine H, Yang J, et al. Polysurgery of cell sheet grafts overcomes diffusion limits to produce thick, vascularized myocardial tissues. *Faseb Journal* 2006;20(1):708-+.

108. Rangarajan A, Hong SJ, Gifford A, et al. Species- and Cell Type-Specific Requirements for Cellular Transformation (vol 6, pg 171, 2004). *Cancer Cell* 2013;24(3):394-98.

109. Pampaloni F, Reynaud EG, Stelzer EHK. The third dimension bridges the gap between cell culture and live tissue. *Nature Reviews Molecular Cell Biology* 2007;8(10):839-45.

110. Mroue R, Bissell MJ. Three-dimensional cultures of mouse mammary epithelial cells. *Methods in molecular biology (Clifton, N.J.)* 2013;945:221-50.

111. Sato T, Clevers H. Growing Self-Organizing Mini-Guts from a Single Intestinal Stem Cell: Mechanism and Applications. *Science* 2013;340(6137):1190-94.

112. Lancaster MA, Renner M, Martin C-A, et al. Cerebral organoids model human brain development and microcephaly. *Nature* 2013;501(7467):373-+.

113. Kim JB. Three-dimensional tissue culture models in cancer biology. *Seminars in Cancer Biology* 2005;15(5):365-77.

114. Atiyeh BS, Costagliola M. Cultured epithelial autograft (CEA) in burn treatment: Three decades later. *Burns* 2007;33(4):405-13.

115. Meana A, Iglesias J, Del Rio M, et al. Large surface of cultured human epithelium obtained on a dermal matrix based on live fibroblast-containing fibrin gels. *Burns* 1998;24(7):621-30.

116. Bruus H, Dual J, Hawkes J, et al. Forthcoming Lab on a Chip tutorial series on acoustofluidics: Acoustofluidics-exploiting ultrasonic standing wave forces and acoustic streaming in microfluidic systems for cell and particle manipulation. *Lab on a Chip* 2011;11(21):3579-80.

117. Glynne-Jones P, Boltryk RJ, Hill M. Acoustofluidics 9: Modelling and applications of planar resonant devices for acoustic particle manipulation. *Lab on a Chip* 2012;12(8):1417-26.

118. Evander M, Nilsson J. Acoustofluidics 20: Applications in acoustic trapping. *Lab on a Chip* 2012;12(22):4667-76.

119. Hill M, Townsend RJ, Harris NR. Modelling for the robust design of layered resonators for ultrasonic particle manipulation. *Ultrasonics* 2008;48(6-7):521-28.

120. Ankrett DN, Carugo D, Lei JJ, et al. The effect of ultrasound-related stimuli on cell viability in microfluidic channels. *Journal of Nanobiotechnology* 2013;11.

121. Bazou D, Kuznetsova LA, Coakley WT. Physical enviroment of 2-D animal cell aggregates formed in a short pathlength ultrasound standing wave trap. *Ultrasound Med Biol* 2005;31(3):423-30.

122. Bazou D, Coakley WT, Hayes AJ, et al. Long-term viability and proliferation of alginate-encapsulated 3-D HepG2 aggregates formed in an ultrasound trap. *Toxicology in Vitro* 2008;22(5):1321-31.

123. Bazou D. Biochemical properties of encapsulated high-density 3-D HepG2 aggregates formed in an ultrasound trap for application in hepatotoxicity studies. *Cell Biology and Toxicology* 2010;26(2):127-41.

124. Wiklund M. Acoustofluidics 12: biocompatibility and cell viability in microfluidic acoustic resonators (vol 12, pg 2018, 2012). *Lab on a Chip* 2012;12(24):5283-83.

125. Suslick K. Sonochemistry. *Science* 1990;247:1439-45.

126. Lentacker I, De Cock I, Deckers R, et al. Understanding ultrasound induced sonoporation: Definitions and underlying mechanisms. *Advanced Drug Delivery Reviews* 2014;72:49-64.

127. Nyborg WL. Biological effects of ultrasound: Development of safety guidelines. Part II: General review. *Ultrasound in Medicine and Biology* 2001;27(3):301-33.

128. Marmottant P, Hilgenfeldt S. Controlled vesicle deformation and lysis by single oscillating bubbles. *Nature* 2003;423(6936):153-56.

129. Carstens.El. BIOLOGICAL EFFECTS OF ULTRASOUND. *Ieee Transactions on Sonics and Ultrasonics* 1974;SU21(1):74-74.

130. Miller DL, Thomas RM, Frazier ME. ULTRASONIC CAVITATION INDIRECTLY INDUCES SINGLE-STRAND BREAKS IN DNA OF VIABLE CELLS-INVITRO BY THE ACTION OF RESIDUAL HYDROGEN-PEROXIDE. *Ultrasound in Medicine and Biology* 1991;17(7):729-35.

131. Zhou Y, Shi JY, Cui JM, et al. Effects of extracellular calcium on cell membrane resealing in sonoporation. *Journal of Controlled Release* 2008;126(1):34-43.

132. Mitragotri S. Innovation - Healing sound: the use of ultrasound in drug delivery and other therapeutic applications. *Nature Reviews Drug Discovery* 2005;4(3):255-60.

133. Qin P, Han T, Yu ACH, et al. Mechanistic understanding the bioeffects of ultrasound-driven microbubbles to enhance macromolecule delivery. *Journal of Controlled Release* 2018;272:169-81.

134. Wang M, Zhang Y, Cai C, et al. Sonoporation-induced cell membrane permeabilization and cytoskeleton disassembly at varied acoustic and microbubble-cell parameters. *Scientific Reports* 2018;8.

135. Burgess MT, Porter TM. CONTROL OF ACOUSTIC CAVITATION FOR EFFICIENT SONOPORATION WITH PHASE-SHIFT NANOEMULSIONS. *Ultrasound in Medicine and Biology* 2019;45(3):846-58.

136. Horsley H, Owen J, Browning R, et al. Ultrasound-activated microbubbles as a novel intracellular drug delivery system for urinary tract infection. *Journal of Controlled Release* 2019;301:166-75.

137. Huang SH, Ren Y, Wang X, et al. Application of Ultrasound-Targeted Microbubble Destruction-Mediated Exogenous Gene Transfer in Treating Various Renal Diseases. *Human Gene Therapy* 2019;30(2):127-38.

138. Snipstad S, Sulheim E, Davies CD, et al. Sonopermeation to improve drug delivery to tumors: from fundamental understanding to clinical translation. *Expert Opinion on Drug Delivery* 2018;15(12):1249-61.

139. Lee JH, Moon H, Han H, et al. Antitumor Effects of Intra-Arterial Delivery of Albumin-Doxorubicin Nanoparticle Conjugated Microbubbles Combined with Ultrasound-Targeted Microbubble Activation on VX2 Rabbit Liver Tumors. *Cancers* 2019;11(4).

140. Wang Y, Bi K, Shu JX, et al. Ultrasound-controlled DOX-SiO2 nanocomposites enhance the antitumour efficacy and attenuate the toxicity of doxorubicin. *Nanoscale* 2019;11(10):4210-18.

141. Wischhusen J, Padilla F. Ultrasound Targeted Microbubble Destruction (UTMD) for Localized Drug Delivery into Tumor Tissue. *Irbm* 2019;40(1):10-15.

142. Dalecki D, Comeau ES, Raeman CH, et al. Guiding tissue regeneration with ultrasound in vitro and in vivo. In: George T, Dutta AK, Islam MS (eds.) *Micro- and Nanotechnology Sensors, Systems, and Applications Vii*; 2015.

143. Garvin KA, Hocking DC, Dalecki D. Controlling the spatial organisation of cells and extracellular matrix proteins in engineered tissues using ultrasound standing wave fields. *Ultrasound in Medicine and Biology* 2010;36(11):1919-32.

144. Garvin KA, Dalecki D, Hocking DC. VASCULARIZATION OF THREE-DIMENSIONAL COLLAGEN HYDROGELS USING ULTRASOUND STANDING WAVE FIELDS. *Ultrasound in Medicine and Biology* 2011;37(11):1853-64.

145. Garvin KA, Dalecki D, Yousefhussien M, et al. Spatial patterning of endothelial cells and vascular network formation using ultrasound standing wave fields. *Journal of the Acoustical Society of America* 2013;134(2):1483-90.

146. Garvin KA, VanderBurgh J, Hocking DC, et al. Controlling collagen fiber microstructure in three-dimensional hydrogels using ultrasound. *Journal of the Acoustical Society of America* 2013;134(2):1491-502.

147. Evander M, Johansson L, Lilliehorn T, et al. Noninvasive acoustic cell trapping in a microfluidic perfusion system for online bioassays. *Anal Chem* 2007;79(7):2984-91.

148. Hammarstrom B, Evander M, Barbeau H, et al. Non-contact acoustic cell trapping in disposable glass capillaries. *Lab on a Chip* 2010;10(17):2251-57.

149. Hammarstrom B, Nilsson J, Laurell T, et al. Improved washing in immuno-MALDI MS by acoustic trapping. Seattle, USA., 2011.

150. Gupta T, Ghosh R, Ganguly R. Acoustophoretic separation of infected erythrocytes from blood plasma in a microfluidic platform using biofunctionalized, matched-impedance layers. *International Journal for Numerical Methods in Biomedical Engineering* 2018;34(4).

151. Li SW, Glynne-Jones P, Andriotis OG, et al. Application of an acoustofluidic perfusion bioreactor for cartilage tissue engineering. *Lab on a Chip* 2014;14(23):4475-85.

152. A. T. *Development of Multi-layered Models of the Airway Mucosa*. University of Southampton, 2014.

153. Tait A, Glynne-Jones P, Hill AR, et al. Engineering multi-layered tissue constructs using acoustic levitation. *Scientific Reports* 2019;9:11.

154. Hammarstrom B, Laurell T, Nilsson J. Seed particle-enabled acoustic trapping of bacteria and nanoparticles in continuous flow systems. *Lab on a Chip* 2012;12(21):4296-304.

155. Chen Z, You J, Liu X, et al. Biomaterials for corneal bioengineering. *Biomedical Materials* 2018;13(3).

156. A. T. University of Southampton, 2014.

157. Meng J, Roy S. Study of Epithelium Barrier Functions by Real-time TER Measurement. *Bio-protocol* 2016;6(10).

158. Ye L, Martin TA, Parr C, et al. Biphasic effects of 17-beta-estradiol on expression of occludin and transendothelial resistance and paracellular permeability in human vascular endothelial cells. *Journal of Cellular Physiology* 2003;196(2):362-69.